

## Overview and Results From the Mars 2020 Perseverance Rover's First Science Campaign on the Jezero Crater Floor



### Special Section:

The Mars Perseverance Rover  
Jezero Crater Floor Campaign

### Key Points:

- The Mááz and Séítah formations are igneous, with Séítah representing olivine-rich cumulates and Mááz representing separate lava flows
- Crater floor rocks have been variably altered to produce carbonates and other alteration minerals during multiple aqueous episodes
- Post-emplacement processes tilted these rocks near the Mááz-Séítah contact, and erosion produced varied textures and olivine-rich regolith

### Supporting Information:

Supporting Information may be found in the online version of this article.

### Correspondence to:

V. Z. Sun,  
[vivian.sun@jpl.nasa.gov](mailto:vivian.sun@jpl.nasa.gov)






















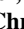



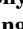
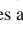




### Citation:

Sun, V. Z., Hand, K. P., Stack, K. M., Farley, K. A., Simon, J. I., Newman, C., et al. (2023). Overview and results from the Mars 2020 Perseverance rover's first science campaign on the Jezero crater floor. *Journal of Geophysical Research: Planets*, 128, e2022JE007613. <https://doi.org/10.1029/2022JE007613>

Received 11 OCT 2022  
Accepted 1 MAY 2023

© 2023 Jet Propulsion Laboratory, California Institute of Technology and The Authors. Government sponsorship acknowledged. This article has been contributed to by U.S. Government employees and their work is in the public domain in the USA.

This is an open access article under the terms of the [Creative Commons Attribution-NonCommercial License](https://creativecommons.org/licenses/by-nc/4.0/), which permits use, distribution and reproduction in any medium, provided the original work is properly cited and is not used for commercial purposes.

Vivian Z. Sun<sup>1</sup> , Kevin P. Hand<sup>1</sup> , Kathryn M. Stack<sup>1</sup>, Ken A. Farley<sup>2</sup>, Justin I. Simon<sup>3</sup> , Claire Newman<sup>4</sup> , Sunanda Sharma<sup>1</sup>, Yang Liu<sup>1</sup>, Roger C. Wiens<sup>5</sup> , Amy J. Williams<sup>6</sup>, Nicholas Tosca<sup>7</sup> , Sanna Alwmark<sup>8,9</sup> , Olivier Beyssac<sup>10</sup> , Adrian Brown<sup>11</sup> , Fred Calef<sup>1</sup> , Emily L. Cardarelli<sup>1</sup> , Elise Clavé<sup>12</sup> , Barbara Cohen<sup>13</sup> , Andrea Corpolongo<sup>14</sup> , Andrew D. Czaja<sup>14</sup> , Tyler Del Sesto<sup>1</sup>, Alberto Fairen<sup>15,16</sup> , Teresa Fornaro<sup>17</sup> , Thierry Fouchet<sup>18</sup> , Brad Garczynski<sup>5</sup>, Sanjeev Gupta<sup>19</sup>, Chris D. K. Herd<sup>20</sup> , Keyron Hickman-Lewis<sup>21,22</sup>, Briony Horgan<sup>5</sup> , Jeffrey Johnson<sup>23</sup> , Kjartan Kinch<sup>8</sup> , Tanya Kizovski<sup>24</sup>, Rachel Kronyak<sup>1</sup> , Robert Lange<sup>1</sup>, Lucia Mandon<sup>18</sup> , Sarah Milkovich<sup>1</sup>, Robert Moeller<sup>1</sup>, Jorge Núñez<sup>23</sup> , Gerhard Paar<sup>25</sup> , Guy Pyrzak<sup>1</sup> , Cathy Quantin-Nataf<sup>26</sup>, David L. Shuster<sup>27</sup>, Sandra Siljestrom<sup>28</sup>, Andrew Steele<sup>13,29</sup> , Michael Tice<sup>30</sup>, Olivier Toupet<sup>1</sup> , Arya Udry<sup>31</sup> , Alicia Vaughan<sup>32</sup>, and Brittan Wogslund<sup>33</sup> 

<sup>1</sup>Jet Propulsion Laboratory, California Institute of Technology, Pasadena, CA, USA, <sup>2</sup>California Institute of Technology, Pasadena, CA, USA, <sup>3</sup>NASA Johnson Space Center, Houston, TX, USA, <sup>4</sup>Aeolis Research, Chandler, AZ, USA, <sup>5</sup>Purdue University, West Lafayette, IN, USA, <sup>6</sup>Department of Geological Sciences, University of Florida, Gainesville, FL, USA, <sup>7</sup>University of Cambridge, Cambridge, UK, <sup>8</sup>Niels Bohr Institute, University of Copenhagen, Copenhagen, Denmark, <sup>9</sup>Department of Geology, Lund University, Lund, Sweden, <sup>10</sup>CNRS, Muséum National d'Histoire Naturelle, Institut de Minéralogie, de Physique des Matériaux et de Cosmochimie, Sorbonne Université, Paris, France, <sup>11</sup>Plancius Research, Severna Park, MD, USA, <sup>12</sup>Centre Lasers Intenses et Applications, CNRS, CEA, Université de Bordeaux, Bordeaux, France, <sup>13</sup>NASA Goddard Spaceflight Center, Greenbelt, MD, USA, <sup>14</sup>Department of Geology, University of Cincinnati, Cincinnati, OH, USA, <sup>15</sup>Centro de Astrobiología (CSIC-INTA), Madrid, Spain, <sup>16</sup>Department Astronomy, Cornell University, Ithaca, NY, USA, <sup>17</sup>INAF-Astrophysical Observatory of Arcetri, Florence, Italy, <sup>18</sup>LESIA, Observatoire de Paris, CNRS, Université PSL, Sorbonne Université, Université Paris Cité, Meudon, France, <sup>19</sup>Imperial College London, London, UK, <sup>20</sup>University of Alberta, Edmonton, AB, Canada, <sup>21</sup>Natural History Museum, London, UK, <sup>22</sup>Dipartimento di Scienze Biologiche, Geologiche e Ambientali, Università di Bologna, Bologna, Italy, <sup>23</sup>Johns Hopkins University Applied Physics Laboratory, Laurel, MD, USA, <sup>24</sup>Brock University, St. Catharines, ON, Canada, <sup>25</sup>Joanneum Research, Graz, Austria, <sup>26</sup>Laboratoire de Géologie de Lyon, Université Lyon, Villeurbanne, France, <sup>27</sup>University of California, Berkeley, Berkeley, CA, USA, <sup>28</sup>RISE Research Institutes of Sweden, Gothenburg, Sweden, <sup>29</sup>Carnegie Institute Washington, Washington, DC, USA, <sup>30</sup>Department of Geology and Geophysics, Texas A&M University, College Station, TX, USA, <sup>31</sup>University of Nevada, Las Vegas, NV, USA, <sup>32</sup>United States Geological Survey, Flagstaff, AZ, USA, <sup>33</sup>University of Tennessee, Knoxville, TN, USA

**Abstract** The Mars 2020 Perseverance rover landed in Jezero crater on 18 February 2021. After a 100-sol period of commissioning and the Ingenuity Helicopter technology demonstration, Perseverance began its first science campaign to explore the enigmatic Jezero crater floor, whose igneous or sedimentary origins have been much debated in the scientific community. This paper describes the campaign plan developed to explore the crater floor's Mááz and Séítah formations and summarizes the results of the campaign between sols 100–379. By the end of the campaign, Perseverance had traversed more than 5 km, created seven abrasion patches, and sealed nine samples and a witness tube. Analysis of remote and proximity science observations show that the Mááz and Séítah formations are igneous in origin and composed of five and two geologic members, respectively. The Séítah formation represents the olivine-rich cumulate formed from differentiation of a slowly cooling melt or magma body, and the Mááz formation likely represents a separate series of lava flows emplaced after Séítah. The Mááz and Séítah rocks also preserve evidence of multiple episodes of aqueous alteration in secondary minerals like carbonate, Fe/Mg phyllosilicates, sulfates, and perchlorate, and surficial coatings. Post-emplacement processes tilted the rocks near the Mááz-Séítah contact and substantial erosion modified the crater floor rocks to their present-day expressions. Results from this crater floor campaign, including those obtained upon return of the collected samples, will help to build the geologic history of events that occurred in Jezero crater and provide time constraints on the formation of the Jezero delta.

**Plain Language Summary** The Mars 2020 Perseverance rover, along with the Ingenuity Helicopter technology demonstration, landed in Jezero crater, Mars on 18 February 2021. Here, we detail results from the first science campaign of the mission, the purpose of which was to explore the enigmatic Jezero crater floor. By the end of the campaign, Perseverance traversed more than 5 km, created seven abrasion patches,

and sealed a total of nine samples and a witness tube for return to Earth. Analysis of the rocks in the crater floor revealed two distinct geologic formations, named the Mááz and Séítah formations. Both formations were determined to be igneous in origin, the former likely from a series of lava flows and the latter formed from a slowly cooling melt or magma body. The composition of the Mááz and Séítah formation rocks also indicate that they experienced significant alteration from water in the past, consistent with Jezero crater having once been filled with water. Results from Perseverance's Jezero crater floor campaign, including those obtained upon return of the collected samples to Earth, will help build the geologic history of Jezero crater and reveal its past habitability.

## 1. Introduction

On 18 February 2021, the Mars 2020 Perseverance rover landed in Jezero crater, Mars (Figures 1a and 1b) and began its prime mission to explore and cache samples from this ancient lacustrine environment. Perseverance landed at Octavia E. Butler (OEB) Landing near the junction between two significant units on the Jezero crater floor (Stack et al., 2020; Sun & Stack, 2020), and about 2 km from the western delta front (Fassett & Head, 2008; Goudge et al., 2015) (Figures 1c and 1d). While the operations teams planned rover commissioning events and the Ingenuity Helicopter technology demonstration over the first 100 sols of the mission, the science team was tasked with planning the exploration of the enigmatic Jezero crater floor in its first science campaign to take place over the first year of the mission.

This paper describes the planning and execution of the Jezero crater floor science campaign. Section 1 introduces Perseverance's payload, mission operations concepts, and activities conducted during the first 100 sols of the mission. Section 2 introduces Jezero crater's geologic context and the pre-landing understanding of the major geologic units and features on the crater floor. The creation of the crater floor campaign plan is described in Section 3, and the chronological narrative of the campaign, as executed by Perseverance and its operations team, is detailed in Section 4. Section 5 summarizes the main science results from the crater floor campaign. A debriefing of the campaign and implications for future investigations at Jezero is described in Section 6, and Section 7 concludes with a summary.

The scope of this paper is primarily focused on the crater floor science campaign, which took place from sols 101 to 379 and is described in detail in Sections 4.1–4.10. For completeness, references are made to observations from the first 100 sols of the mission (Section 1.7) and the drive-focused rapid traverse campaign from the crater floor to the delta (sols 379–410; Section 4.11), but the main science observations and results described therein are from the main science campaign from sols 101 to 379.

### 1.1. Mars 2020 Mission Objectives

The Perseverance rover was designed to build on discoveries made by previous orbital, landed, and rover missions that had established the presence of past habitable aqueous environments across Mars. The Mars 2020 mission takes the next step in Mars exploration, to seek potential signs of past life in a habitable environment and to cache samples for potential return to Earth by future missions. The mission has four objectives (Farley et al., 2020) which are addressed by the suite of instruments on Perseverance (Section 1.2):

- Objective 1—Geology: To understand the geology of its landing site (Jezero crater) by characterizing the primary and secondary processes that emplaced and modified the rock record.
- Objective 2—Astrobiology: To determine whether there existed ancient habitable environments that could have preserved biosignatures, and to search for such biosignatures with the rover payload.
- Objective 3—Sample Caching: To collect and document a suite of scientifically compelling samples, that are representative of the area's geologic diversity, for return to Earth by a future mission.
- Objective 4—Preparation for Human Exploration: To demonstrate new technologies that may support future in situ human exploration of Mars.

### 1.2. Rover Payload

To accomplish its objectives, the Perseverance rover is equipped with seven science instruments, as well as engineering instruments, designed to make scientific observations at various spatial scales (Table 1; Farley

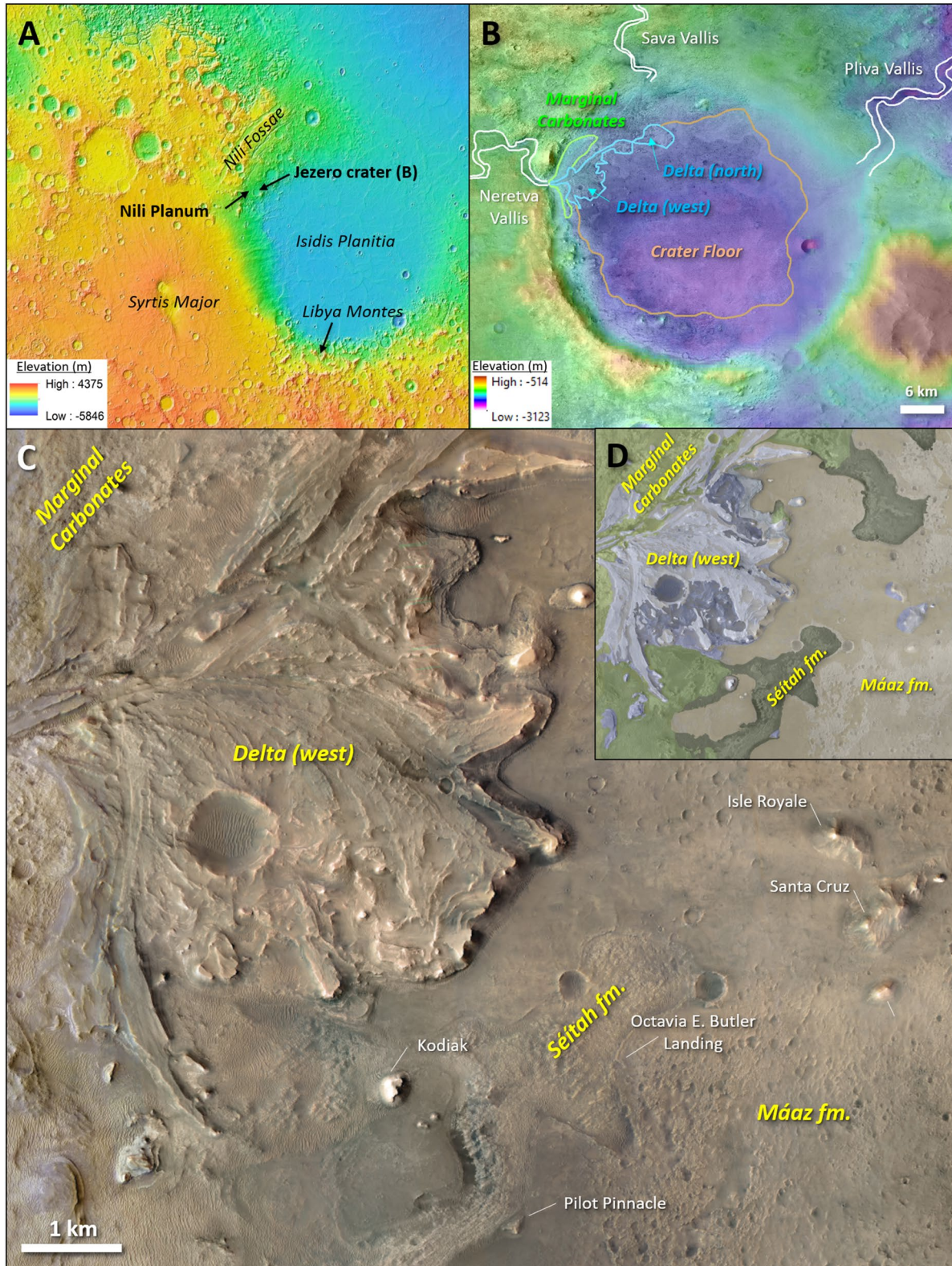


Figure 1.

et al., 2020, Figure 1). We refer the reader to Text S1 in Supporting Information S1 and the references in Table 1 for more information on the rover payload.

*Remote Sensing (RS)* instruments, most of which are on the remote sensing mast (RSM) are intended to be used on an almost daily basis for operations and science observations. These instruments include: Navcam, Mastcam-Z, and SuperCam. These instruments are mounted on the RSM, and so can image nearly any geologic target not obscured by the rover itself. The RS instruments are also routinely used to support atmospheric observations of atmospheric opacity and to search for clouds and dust devils (e.g., Newman et al., 2021). Other instruments that are located on the rover body are Hazcam, RIMFAX, MEDA, and MOXIE.

*Proximity Science (PS)* instruments are mounted on the turret at the end of the robotic arm (RA) and can therefore be placed as close as a few cm from a natural or abraded rock surface for the highest-resolution observations possible using the rover payload. These instruments include SHERLOC, WATSON, and PIXL, and results from these instruments may help confirm or elucidate phases that the RS instruments cannot detect (e.g., Razzell Hollis et al., 2022). However, within the crater floor terrain, these instruments provided limited data unless used on an abrasion surface (Corpolongo et al., 2023). With the added time and power of a prerequisite abrasion activity, PS instruments were typically used to follow up on RS observations or to document characteristics of a rock that will be sampled.

Though not scientific instruments, several engineering subsystems are used to support scientific investigations and operations. The *Sampling and Caching Subsystem* (SCS; Moeller et al., 2020) provides the mechanisms used to abrade rock surfaces and collect rock core and regolith samples. Several elements, such as the corer (used to abrade and core) and the gas dust removal tool (gDRT), are housed on the turret at the end of the RA alongside SHERLOC, WATSON, and PIXL. The rover body houses the adaptive caching assembly (ACA), which uses a sample handling arm (SHA) to manipulate sample tubes and exchange between abrading bits and coring bits housed in the bit carousel (BC). The ACA also ingests filled sample tubes, images them with Cachecam, measures them with a volume probe, and seals the tubes with a hermetic seal. The *Ingenuity Helicopter* (Balarum et al., 2021) was deployed shortly after landing primarily for a 30-sol technology demonstration of the first powered, controlled flight on another planet. After this demonstration, Ingenuity was used to fly ahead of the rover and scout, providing Rover Planners with insights on terrain quality to evaluate ease or difficulty in driving and providing the science team with initial images of upcoming terrains to help determine the most scientifically compelling outcrops to drive to.

The typical workflow was that upon reaching a new rover location, Navcam and Hazcam images were immediately acquired of the rover surroundings and workspace (i.e., the area immediately in front of the rover in which most RS and PS activities are planned). In the next sol's plan, the Navcam and Front Hazcam images were then used to identify and select targets for subsequent targeted RS using Mastcam-Z and SuperCam. The combination of Navcam, Mastcam-Z, and SuperCam observations provided outcrop-scale observations of the local stratigraphy, geologic structures, and chemistry and mineralogy of local rocks and soils along the rover traverse (Objective 1 from Section 1.1). If the RS results were sufficiently compelling for further investigation, or if a decision had been made to sample a particular rock, SHERLOC, WATSON, and PIXL were then deployed to obtain microscopic-scale observations of select targets. The rock surface was usually abraded with an abrading bit in the corer, and then the gDRT was used to clear dust from the abraded surface. SHERLOC, WATSON, and PIXL were then placed close to the rock surface to image and map the highest-resolution chemistry and mineralogy of the target to determine the rock lithology and assess the presence of organics or other potential biosignatures (Objective 2). If sampling the target rock, the corer would then be deployed to collect a sample (Objective 3). As the rover drove, RIMFAX data was acquired, providing a look into the subsurface structure of the terrain even if no other RS observations were acquired. MEDA data was acquired daily to monitor local atmospheric conditions, and MOXIE runs were planned periodically to test the generation of O<sub>2</sub> under different seasonal and temporal conditions (Objective 4).

**Figure 1.** (a) Regional context for Jezero crater and Nili Planum. Data: Mars Orbiter Laser Altimeter (MOLA) elevation (meters) overlaid on MOLA topography. Upper left coordinates are 35.6°N, 59.0°E; lower right coordinates are 5.5°S, 101.1°E. (b) Major geographic regions of Jezero crater (crater floor, deltas, marginal carbonates) and Jezero's inlet (Neretva and Sava Valles) and outlet (Pliva Vallis) channels. Data: MOLA elevation (meters) overlaid on Thermal Emission Imaging System daytime infrared data. Upper left coordinates are 18.94°N, 77.1°E; lower right coordinates are 17.9°N, 78.3°E. (c) Jezero's interior units annotated in yellow text, with local points of interest annotated in white (Perseverance's landing site and possible delta remnants). Data: High Resolution Imaging Experiment color mosaic. (d) Same area as (c), but showing the geologic units as mapped by Stack et al. (2020). All orbital views in this work depict north as up.

**Table 1**  
Summary of the Primary Instruments Used to Achieve Crater Floor Campaign Objectives

Instrument	Abbreviation	Observations and purpose	Instrument references	STOP list documentation (Simon et al., 2023)
Navigation cameras	Navcam	Color stereo imager on the RSM, with $96^\circ \times 73^\circ$ FOV at 0.33 mrad/pixel. Provides context images used for navigation and science targeting with the other science instruments	Maki et al. (2020)	N/A
Hazard Avoidance cameras	Hazcam	Color stereo imager fixed to the front and rear of rover body, with $136^\circ \times 102^\circ$ FOV at 0.46 mrad/pixel. Used for navigation and science targeting in the arm workspace	Maki et al. (2020)	N/A
Cachecam	Cachecam	Color imager within the rover body with spatial scale of 12.5 microns/pixel. Used to document and verify sample processing	Maki et al. (2020)	N/A
Mastcam-Z	Mastcam-Z	Multispectral, stereo imager on the RSM with adjustable zoom and focus. FOV ranges from $25.6^\circ \times 19.2^\circ$ (26 mm focal length, 283 $\mu\text{rad}/\text{pixel}$ ) to $6.2^\circ \times 4.6^\circ$ (110 mm focal length, 67.4 $\mu\text{rad}/\text{pixel}$ ). Multispectral acquires images at 14 unique wavelengths in the 0.4–1.0 $\mu\text{m}$ range. Used for high-resolution landscape imaging, 3D analyses, and documenting compositional variations across landscapes	J. F. Bell et al. (2021), Hayes et al. (2021)	Sample workspace imaging; Multispectral of abrasion borehole and tailings
SuperCam	SuperCam	Multi-technique instrument on the RSM and on the rover body. Provides elemental composition via Laser-Induced Breakdown Spectroscopy (LIBS), mineralogy via Raman, Time-Resolved Luminescence Spectroscopy (TRLS), and visible and near-infrared spectroscopy (VISIR; 379–464 nm, 535–855 nm, 1.3–2.6 $\mu\text{m}$ ), high-resolution color imaging (RMI; $1.08^\circ \times 1.08^\circ$ FOV at 10 $\mu\text{rad}/\text{pixel}$ ), and acoustic recordings (MIC). RMI provides the highest-resolution imaging available from the RSM, albeit in a smaller spatial footprint than Mastcam-Z images	Maurice et al. (2021), Wiens et al. (2020)	SuperCam RMI/LIBS/VISIR/Raman on abrasion patch; SuperCam RMI/LIBS on borehole or tailings
Scanning Habitable Environments with Raman and Luminescence for Organics and Chemicals	SHERLOC	Fluorescence and Raman spectrometer and the Wide Angle Topographic Sensor for Operation and eEngineering (WATSON) on the RA. Provides high-resolution mapping of organics and mineralogy in individual grains in rock targets. The resolution of SHERLOC's Autofocus Context Imager (ACI) is <100 microns per mapping pixel. When placed close to target surfaces, WATSON ( $32.8^\circ \times 31.2^\circ$ – $24.6^\circ \times 23.4^\circ$ FOV at $\sim 300 \mu\text{rad}/\text{pixel}$ ) provides the highest resolution imaging possible from Perseverance's payload	Bhartia et al. (2021)	Full suite WATSON imaging of abrasion patch; pre-drill WATSON imaging of core targets; WATSON imaging of at least one borehole; SHERLOC scan of abrasion patch
Planetary Instrument for X-ray Lithochemistry	PIXL	Micro-X-ray fluorescence spectrometer on the RA with 120 micron/pixel resolution. Provides high-resolution mapping of the major and minor rock-forming elements and trace elements in individual grains in rock targets	Allwood et al. (2020)	PIXL scan of abrasion patch
Radar Imager for Mars' Subsurface Experiment	RIMFAX	Ground penetrating radar with operating frequency range of 150–1,200 MHz, located at the rover rear. Images subsurface structure and provides information on subsurface composition along the rover traverse	Hamran et al. (2020)	N/A
Mars Environmental Dynamics Analyzer	MEDA	Sensors located on the RSM and rover body including: wind sensor, barometer, relative humidity sensor, temperature-measuring sensors, radiation and dust sensor. Monitors atmospheric conditions daily	Rodriguez-Manfredi et al. (2021)	N/A
Mars Oxygen ISRU Experiment (MOXIE)	MOXIE	Technology demonstration within the rover body that dissociates atmospheric $\text{CO}_2$ into $\text{O}_2$ . Capable of producing at least 6 g/hr of $\text{O}_2$ with >98% purity	Hecht et al. (2021)	N/A
Ingenuity Helicopter	Ingenuity Helicopter	Travels independently of the rover and used to scout ahead of Perseverance after the technology demonstration. Has a downward-facing, black-and-white navigation camera and a front-facing color camera	Balaram et al. (2021)	N/A
Corer	Corer	Houses an abrasion or coring bit. Abrasion patches are between 2 and 16 mm deep and 45 mm in diameter, with 40 mm diameter of dust-cleared surface after the gDRT puffs. Core samples are 13 mm in diameter and may be up to 76 mm long	Moeller et al. (2020)	N/A

Note. FOV, field of view; RSM, remote sensing mast; RA, robotic arm; STOP, Sample Threshold Observation Protocol (a list of required observations accompanying each sample).

### 1.3. Mission Operations

The Mars 2020 Perseverance rover mission operations structure consists of four parallel processes (Milkovich et al., 2022, Figure 3). The broadest process is the ongoing Strategic process, which involves establishing the overarching mission objectives and priorities that the team should focus on over the duration of the mission. The Strategic process generates decisions such as how much time should be spent on the overall Jezero crater floor campaign. A second process, Campaign Planning, is the more detailed process through which an exploration strategy for a region like the crater floor is developed. The Campaign Planning process uses predominantly orbital datasets to produce a campaign plan and a baseline sol path for the rover's exploration of the campaign area that guides the subsequent Campaign Implementation (CI) and Tactical processes. The CI process is a daily process in which the activity plans for the upcoming ~week are formulated, guided by the campaign plan, and modeled as activity plans to ensure that the sol path is viable with respect to rover resources, orbiter relays, etc. The plans developed in CI are then handed to the Tactical process, which also operates daily and refines the activity plan outlined in CI, fleshing out the science and engineering activities in the plan, setting appropriate activity parameters, and uplinking a complete sequence bundle for each martian sol at the end of the planning day.

### 1.4. Prime Mission Scope

Early after landing during the Strategic planning process, the project determined that the first three Earth years (or 1.5 Mars years; the qualified lifetime of the rover) of the mission would be dedicated to investigating Jezero's interior units and depositing the first sample depot within Jezero. Approximately one Earth year would be dedicated to exploring and sampling each of Jezero's major geographic areas of interest—the crater floor, the western delta, and the “marginal carbonates” (Farley et al., 2020) (Figure 1b). During the prime mission, a sample depot containing one of each sample pair (Section 1.5) acquired until that point would then be deposited within Jezero crater. Afterwards, Perseverance would begin its extended mission and traverse outside of Jezero crater to investigate the crater rim and the Nili Planum terrains outside of Jezero. Outside of Jezero, Perseverance would collect samples from the crater rim and Nili Planum using the remainder of the sample tubes. A second and final sample cache, intended as the main cache to be retrieved by a future sample return mission, would then be deposited in Nili Planum (Farley et al., 2020).

### 1.5. Paired Sampling Strategy

As the Mars 2020 mission is the first step in a multi-mission Mars Sample Return (MSR) campaign, a flexible sampling strategy had to be employed to ensure the collection of a sample cache that captured the highest priority targets and diversity of both Jezero Crater and Nili Planum, both of which were deemed regions of investigation for the Mars 2020 mission (Farley et al., 2020). It was recognized prior to landing site selection that Perseverance, even with advanced driving capabilities, could not traverse and investigate both Jezero and Nili Planum within the timespan of the prime mission, much less collect 38 samples representative of both regions. A sampling strategy was thus formulated around the concept of assembling two sample caches. The first, smaller cache would be deposited within Jezero crater at the end of Perseverance's prime mission, containing only samples from Jezero crater. A second and final sample cache, containing samples from both Jezero and Nili Planum, would be acquired during an extended mission phase. Perseverance's qualified lifetime, though spanning only the duration of its prime mission, is a conservative estimate, and thus it was considered feasible to plan for Perseverance to complete sample acquisition during its extended mission. A follow-up MSR mission would ideally retrieve the second sample cache containing a more complete diversity of samples, but should Perseverance become unable to deliver or deposit the second sample cache, the MSR mission could always retrieve the first sample cache as a contingency (Farley et al., 2020).

A paired sampling strategy was thus developed to aid in fulfilling this double-cache concept, where each unique sample collected from the Jezero crater floor would be paired with a companion sample from the same location. Notionally, one sample of the pair would be deposited in the first cache, and the other sample of the pair would be carried with the rover out to Nili Planum as part of the second cache. This paired sampling strategy also had the benefit of helping the mission achieve the sampling rate needed to ensure that the first sample cache could be deposited by the end of the prime mission (Farley et al., 2020). This is because acquiring two samples in the

same rover workspace takes less time, from a sol path and rover engineering perspective, than acquiring just one sample per rover workspace.

To ensure an efficient and consistent approach to data collection at each sampling site, the project established a sampling sol path spanning 11 continuous sols, in which a prescribed sequence of measurements and observations would be made to document the two sample cores that would be obtained. This list of observations is referred to as the Sample Threshold Observation Protocol (STOP) List, which represents the minimum set of scientific observations that must be obtained and linked to every sampling event (Simon et al., 2023) (Table 1). In brief, Perseverance first acquires survey images to assess the most viable abrasion and coring candidate targets in the workspace. Perseverance then proceeds to abrade the surface of the rock, remove dust with the gDRT, and acquire PS and RS observations of the abraded patch to document the characteristics of the rock to be sampled. Two rock cores are then acquired in succession, from the unabraded portions of the rock. For more details, we refer the reader to Simon et al. (2023) and the Text S2 in Supporting Information S1.

### 1.6. Naming Conventions

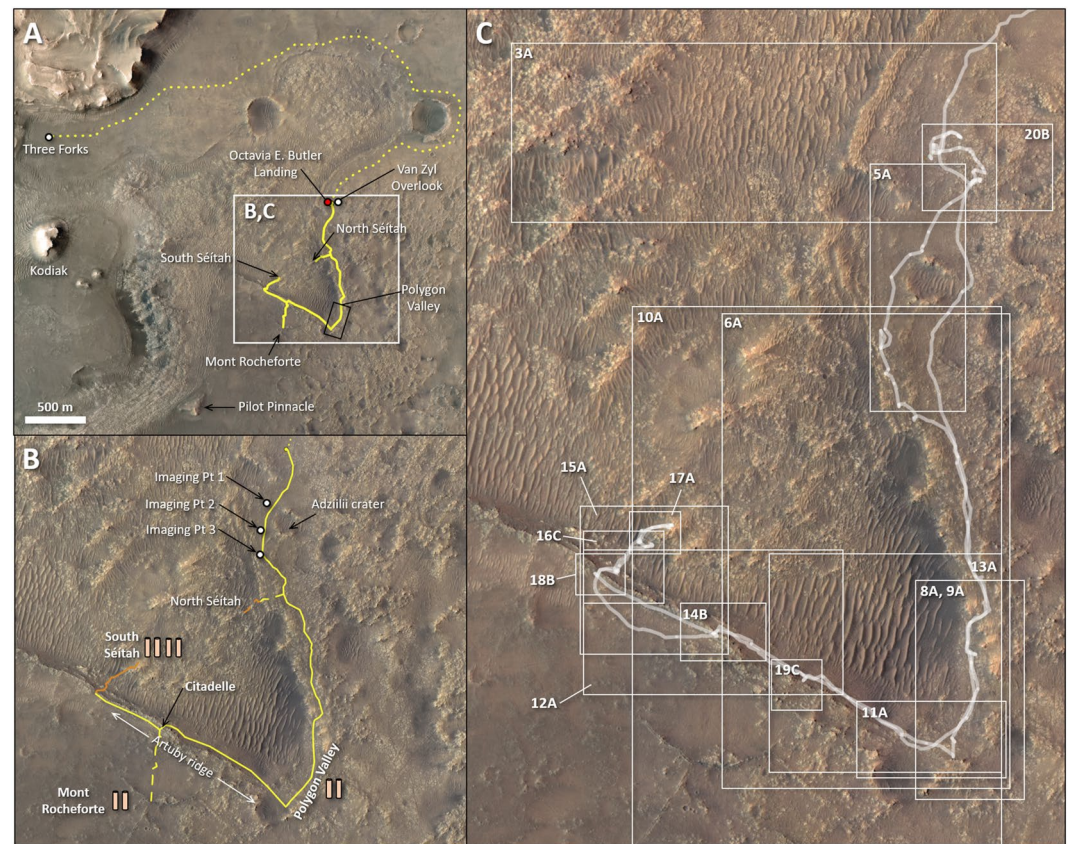
Throughout this paper, scientific targets and landforms are referred to using names assigned during operations. These names are used to provide both the rover team and Mars community with a common language for observed features, which facilitates rover operations as well as scientific discussions of results. Some names for orbital-scale features, such as those in white and black text in Figures 1a and 1b are approved by the International Astronomical Union (IAU). Targets identified and observed by Perseverance on the ground during the mission are informally named without approval by the IAU, using the convention described below.

The majority of target names follow a convention similar to that employed by the Mars Science Laboratory Curiosity mission (Vasavada et al., 2014). Before landing during the Mars 2020 science team's geologic mapping effort (described in Stack et al., 2020), the Jezero landing ellipse region was divided into 1.2 km by 1.2 km quadrangles, or “quads,” named after national parks or preserves on Earth. After landing, a list of target names was generated for each quad that the rover would traverse through, with each name being a named geographic location (e.g., town, river, trail) from the parent national park or preserve. For example, the target name “Artuby” originates from the Artuby river in France, which is located within the Verdon Natural Regional Park after which the Verdon quad in Jezero was named. During operations, these names were assigned to both landforms identified from orbit (e.g., the Pilot Pinnacle remnant mound) and rocks and outcrops observed by the rover. In some cases, target names may be elevated to the level of geologic formations and members, which are named after a representative target from that formation (fm.) or member. For example, the “Mááz formation” is named after the Mááz target observed by Perseverance on sol 12.

There are a few exceptions to the above convention. The OEB Landing site (Figure 2a) was named in honor of the science fiction author OEB. Van Zyl Overlook (Figure 2a) was named in recognition of Jakob Van Zyl, a former Director for Solar System Exploration and Associate Director for Project Formulation and Strategy at the Jet Propulsion Laboratory. Polygon Valley (Figure 2a) was named after the polygonal pattern of the terrain as viewed from orbit. Targets in the Canyon de Chelly quad, in which Perseverance landed, originate from the Navajo language as its namesake park is located on Navajo tribal lands. The Mars 2020 project collaborated with representatives from Navajo Nation to develop a list of target names consisting of Navajo translations of words that are common or relevant to the mission (Farley et al., 2022, Supplementary Materials). This paper therefore includes translations for any discussed targets with Navajo names, but does not provide translations for non-Navajo targets that are named after existing geographic locations on Earth.

### 1.7. First 100 Sols

Immediately after landing, Perseverance and its operations team underwent an approximately 100-sol period of rover and Ingenuity helicopter commissioning activities (Lange et al., 2022). The initial period of commissioning was designed to verify rover health and safety and to perform initial checkouts of the rover's various subsystems and instruments, including: transitioning from cruise flight software to surface flight software (Sol 5–8), deployment of the RSM (Sol 2), deployment of the RA (Sol 12), the first drives (beginning on Sol 14), and health checks on all of the science instruments. Perseverance then deployed the Ingenuity helicopter (Sol 36–43) and drove to Van Zyl Overlook (Figure 2). There, Perseverance oversaw the Ingenuity helicopter technology demonstration



**Figure 2.** (a) Overview of the crater floor campaign area, consisting of the main science investigation area (b), and the rapid traverse to the delta (dotted line). (b) Overview of the initial (**not** the executed) science campaign plan (Section 3.4), with campaign stops and anticipated sampling locations annotated in bold text. Sample tubes indicate how many samples were initially intended for collection at each location in the campaign plan. Orange drive paths show where slower progress was anticipated in sandy Séitah terrains, and dashed lines show paths to notional targets. Please refer to Figure 4 for the comparison to the actual campaign as executed. (c) Context figure showing the extent of the orbital views used in subsequent figures (Figures 3, 5, 6, 8–20) illustrating the main observations along each campaign leg.

(Balam et al., 2021; Sol 44–73), consisting of a series of flight tests that demonstrated the first powered, controlled flight on another planet. Thereafter, Perseverance continued checkouts of the RA, unstowed the SHA, and checked out the ACA. Several First Time Activities (FTAs)—first time, controlled executions of complex rover capabilities prior to formally releasing the capability for nominal use—were also performed (Table 2). FTAs performed in the first 100 sols included running the first MOXIE O<sub>2</sub> cycle (FTA-2), several tests to check out Visual Odometry (VO; FTAs 3–5), the first Autonomous Navigation (Autonav; FTAs 10–12) tests (Verma et al., 2022), and the first natural (i.e., no abrasion) PS observations with WATSON (FTAs 6–7). During the periods of commissioning and Ingenuity helicopter demonstrations, the Mars 2020 science team began planning for its first science campaign to explore the Jezero crater floor. Preliminary science observations made during the first 100 sols (Figure 3) were incorporated into campaign planning.

## 2. Geological Background

### 2.1. Jezero Crater Regional Context and History

Jezero crater lies within the Nili Planum cratered highlands, northwest of Isidis Planitia and south of Nili Fossae (Figure 1a), in an area historically recognized as one of the best-preserved Noachian landscapes (~3.7–4.1 Ga; Nimmo & Tanaka, 2005) hosting diverse hydrated mineral assemblages (Ehlmann et al., 2008, 2009; Mustard et al., 2009). Geomorphological and stratigraphic features such as valley networks, channels, and layered deposits throughout the Nili Planum region (Fassett & Head, 2005; Schon et al., 2012) have helped establish that abundant



**Table 2**  
*Summary of First Time Activities (FTAs) in Their Order of Execution*

FTA #	Description	Sol accomplished
1	FSW S6.4.1 Cold Patch for MEDA	14
2	MOXIE O <sub>2</sub> Cycle Checkout	59
3	Visual Odometry (VO) while Stationary	64
4	VO while Moving	65
5	First Use of VO	72
6	Natural Proximity Science—Close Observation with WATSON using the Facility Contact Sensor	78
10	Autonav—Create and Telemeter a Height Map	84
11	Autonav—Mapping while Driving	91
7	Natural Proximity Science—Close Observation with WATSON using WATSON Range Finding	96–97
12	Autonav—Guarded Drive Towards Hazard	99
13	Autonav—Guarded Drive	107
14	Autonav—Drive Along a Path without Hazard Avoidance	113
19	Bit Carousel Witness Tube Assembly Processing and Sealing	118–120
15	Autonav—Drive Around a Hazard	122
9	Natural Proximity Science—Observation with PIXL and SHERLOC	125
20	Turret Cleaning Using Percussion in Free-Space and with the Launch Abrading Bit	142–147
21	Launch Abrading Bit Dropoff to Martian Surface and New Bit Pickup from Bit Carousel	148–150
22	Abraded Proximity Science—First Abrasion and Dust Clearing with Science Observations	159–162
23	First Core Collection and End-to-End Processing	164

*Note.* FTAs accomplished during the crater floor campaign were completed after sol 100. The number of the FTA is simply a unique identifier.

liquid water once flowed at the surface and in the near subsurface of ancient Noachian Mars (Bibring et al., 2006; Carr & Clow, 1981; Pieri, 1980; Scott & Carr, 1978; Squyres & Kasting, 1994). Mineral assemblages including Fe/Mg clays, Al clays, carbonate, hydrated silica, and serpentine present throughout the Nili Planum and adjacent Nili Fossae regions bolster this interpretation of a rich and well-preserved aqueous history (Bramble et al., 2017; Ehlmann & Mustard, 2012; Ehlmann et al., 2009; Goudge et al., 2015; Mangold et al., 2007; Salvatore et al., 2018).

The Nili Planum terrains that the Jezero bolide impacted into preserve a well-documented sequence of units that extend throughout the broader northwestern Isidis basin and are exposed in key geologic features such as Nili Fossae (Bramble et al., 2017; Ehlmann & Mustard, 2012). The inferred base of this regional sequence are Early Noachian rocks and sediments associated with low-calcium pyroxene and Fe/Mg phyllosilicate signatures from orbital data (Ehlmann & Mustard, 2012; Mustard et al., 2007, 2009). The Isidis impact occurred around 3.85–4.06 Ga (Schultz & Frey, 1990; Werner, 2009) and impacted into this Early Noachian basement, likely deforming and modifying the basement into an assemblage of Early Noachian and Isidis impact products (Bramble et al., 2017; Pascuzzo et al., 2019; Saper & Mustard, 2013; Scheller & Ehlmann, 2020) and resulting in the formation of the Nili Fossae graben (Greeley & Guest, 1987).

At some point during the Middle Noachian period, the Jezero impact struck this Isidis-modified terrain (Sun & Stack, 2020). A regional olivine-rich unit, spanning the Nili Fossae to Nili Planum regions and possibly as far south as Libya Montes (Kremer et al., 2019; Mandon et al., 2020; Tornabene et al., 2008), was emplaced over this Noachian basement around 3.82 Ga (Mandon et al., 2020). Prior to Perseverance's investigations, the olivine-rich unit has been hypothesized to represent any of a variety of deposits, ranging from lava flows (Hamilton & Christensen, 2005; Tornabene et al., 2008) to ashfall or pyroclastic surge deposits (Kremer et al., 2019; Mandon et al., 2020; Ruff et al., 2022) to Isidis basin impact melt (Mustard et al., 2007, 2009). An olivine-rich unit occurring along the western and northern Jezero crater rim and on the Jezero crater floor (Section 2.2.1) has been hypothesized to be related to this regional unit (Goudge et al., 2015; Rogers et al., 2018; Sun & Stack, 2020).

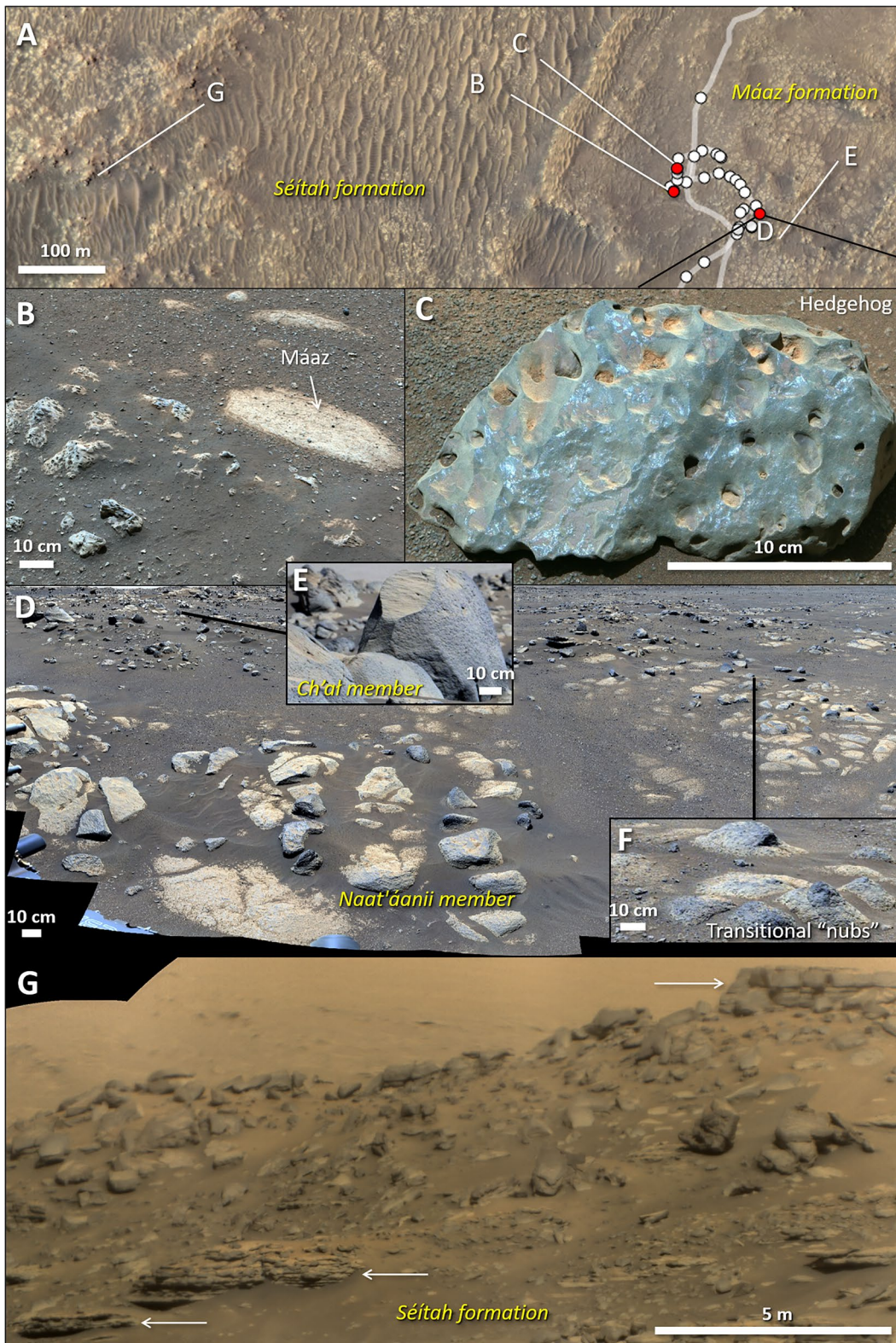


Figure 3.

A regional mafic and crater-retaining capping unit was emplaced on top of the olivine-rich unit in Nili Planum, Nili Fossae, and Libya Montes (Bramble et al., 2017; Hundal et al., 2022; Mustard et al., 2009). This capping unit has been hypothesized to be related to a similar unit found on the Jezero crater floor and on the crater rim (Sun & Stack, 2020). The specific occurrence of this mafic unit on Jezero's crater floor (Section 2.2.2) has attracted a wide range of crater count-derived ages ranging from Noachian-Hesperian (Late Noachian, Sun & Stack, 2020; 3.5 Ga, Goudge et al., 2015; >3 Ga, Quantin-Nataf et al., 2021) to Amazonian ( $2.6 \pm 0.5$  Ga, Shahrzad et al., 2019; 1.4 Ga, Schon et al., 2012), possibly due to burial of parts of the crater floor for varying durations (Quantin-Nataf et al., 2021).

During the Late Noachian to Early Hesperian, aqueous activity in the Jezero and Nili Planum region resulted in the incision of channels and fluvio-lacustrine landforms including Jezero's inlet channels (Neretva Vallis to the west, Sava Vallis to the north), outlet channels (Pliva Vallis to the east), and the western and northern delta deposits (Fassett & Head, 2005, 2008; Ivanov et al., 2012; Mangold et al., 2007, 2020; Salese et al., 2020; Sun & Stack, 2020) (Figure 1b). These aqueous events may or may not have been related to the events that altered portions of the regional olivine-rich unit to Mg-carbonate and occasional serpentine (Ehlmann et al., 2008).

## 2.2. Pre-Landing Hypotheses for the Jezero Crater Floor

From Spring 2020 to just prior to Perseverance's landing, the Mars 2020 science team engaged in a series of exercises, including literature review, geologic mapping (summarized in Stack et al., 2020), development of hypotheses and methods to test them, and discussion of the locations Perseverance may go to test hypotheses and collect a diverse suite of samples. These exercises were designed to (a) familiarize the team with the existing literature on Jezero and this region of Mars, (b) prepare the team for decisions that may need to be made during on-the-ground operations, and (c) create a scientific framework and stratigraphic model against which observations from the rover payload may be compared.

Perseverance's landing site occurs near the boundary between two major units on the Jezero crater floor (Figures 1c and 1d) the origins of which have been of substantial debate in the Mars community for more than a decade. Despite uncertainties in their origin(s), these two units have been consistently mapped in a number of studies. The olivine-rich floor unit within Jezero (Section 2.2.1) has been referred to as the LTF (light-toned floor; Goudge et al., 2015), the Cf-f-1/2 (Crater floor fractured 1 and 2; Stack et al., 2020), and the Nle (lower etched unit; Sun & Stack, 2020) units. The mafic crater-retaining floor unit (Section 2.2.2) has been mapped as the VF (volcanic floor unit; Goudge et al., 2015), the Cf-fr (Crater floor fractured rough; Stack et al., 2020), and the Njf (Jezero floor; Sun & Stack, 2020) units. Hereafter we will adopt the terminology resulting from Perseverance's investigations of the crater floor and refer to the olivine-rich floor unit as the "Séítah formation" (Séítah meaning "amidst the sand" in Navajo) and the mafic crater-retaining floor unit as the "Mááz formation" (Mááz meaning "Mars" in Navajo).

### 2.2.1. The Olivine-Rich Séítah Formation

The olivine-rich Séítah formation is the oldest unit accessible to Perseverance within Jezero's interior, as determined by analysis of stratigraphic relationships between the Séítah formation and the other units within Jezero (Goudge et al., 2015; Stack et al., 2020; Sun & Stack, 2020). The Séítah formation, located on Jezero's crater floor, has been hypothesized to be related to the regional olivine-rich unit spanning the circum-Isidis region from Nili Fossae to Libya Montes (Figure 1a) and which also drapes Jezero's northern and western crater rim and inner walls (e.g., Goudge et al., 2015; Kremer et al., 2019; Sun & Stack, 2020). Proposed origins for the olivine-rich unit have ranged from lava flows (Hamilton & Christensen, 2005) to ashfall or pyroclastic surge deposits (Kremer et al., 2019; Mandon et al., 2020; Ruff et al., 2022) to Isidis basin impact melt (Mustard et al., 2007, 2009). More recent orbital studies have favored an ashfall or pyroclastic deposit interpretation due to its draping morphology, observed banding, and spatial and elevation extent (Kremer et al., 2019; Mandon et al., 2020; Ruff et al., 2022; Sun & Stack, 2020). The occurrence of the

**Figure 3.** Examples of pre-campaign observations of the Mááz formation (b–f) and Séítah formation (g) from the first 100 sols of the mission. Please refer to Figure 4b for a description of the members. (a) Orbital context showing locations of images (b–g), and the extent of imaging shown in (d). Note the polygonal textures in the area of (d) as the orbital expressions of the Naat'áanii member. (b) Perseverance's first science target, a paver from the Naat'áanii member named Mááz (after which the Mááz formation would be named) (sol 12, zcam03100). (c) The Hedgehog target, showing vesicular textures (sol 37, zcam03108). (d) Mastcam-Z enhanced color mosaic (sol 78, zcam08039, NASA/JPL-Caltech/ASU/MSSS/Corrine Rojas) showing Naat'áanii member pavers in the foreground, (e) Ch'al member massive rocks in the background, and (f) gradations from the Naat'áanii pavers to higher-standing resistant nubs more similar to the Ch'al member. (g) Supercam RMI mosaic of Séítah (sol 69, scam01069), with layering indicated by white arrows.

olivine-rich unit across ~4 km of elevation difference within the Jezero and Nili Planum region (Kremer et al., 2019; Mandon et al., 2020; Sun & Stack, 2020) has been used to discount a singular lava flow origin (Hamilton & Christensen, 2005) as that would require the emplacement and subsequent erosion of a kilometer-thick lava flow over a large areal extent. While initial investigations suggested that the olivine-rich unit was Isidis impact melt (Mustard et al., 2007, 2009), the occurrence of the olivine-rich unit on top of the Isidis-modified basement unit, as well as its draping relationship with the Jezero rim, which impacted after Isidis, suggests that the olivine-rich unit is a later unit unrelated to the Isidis impact (Horgan et al., 2020; Kremer et al., 2019; Mandon et al., 2020). Impact melt from a different, yet-to-be-identified impact event has yet to be substantiated, and would require a large impact event to generate the large areal extent of the olivine-rich unit. It has been hypothesized that the Séítah formation shares the same origin as the regional olivine-rich unit, although it is possible that Séítah may have been modified by subsequent lacustrine processes that filled Jezero (Goudge et al., 2015; Sun & Stack, 2020), or that the Séítah formation and the olivine-rich unit formed through different but related processes, not necessarily in the same event.

Regionally and in areas within Jezero, the olivine-rich unit has been variably altered to carbonate and, more rarely, serpentine (Ehlmann et al., 2008; Goudge et al., 2015; Horgan et al., 2020; Mandon et al., 2020). The presence of carbonate in this unit is indicative of past aqueous alteration under clement conditions, and further analyses of a returned carbonate sample in a terrestrial laboratory may yield information about the ancient Mars carbon cycle and its role in regulating the atmosphere during Mars' early period of surface water (e.g., Horgan et al., 2020; Simon et al., 2023). The Séítah formation—as the oldest rock unit in the interior of Jezero crater, a carbonate-rich unit, and potentially part of a regional olivine-rich unit—was thus assessed as a high-priority region to investigate and sample in order to understand ancient martian climate and habitability and to anchor reconstruction of the history of geologic and aqueous events that occurred within Jezero (Simon et al., 2023).

### 2.2.2. The Mafic, Crater-Retaining Mááz Formation

The mafic, crater-retaining Mááz formation is a widespread unit across the floor of Jezero crater and occurs on top of the Séítah formation where both units are observed (Goudge et al., 2015; Schon et al., 2012; Sun & Stack, 2020). The Mááz formation has historically been hypothesized to represent a lava flow on the basis of its mafic composition, lobate margins, and inferred embayment relationships with delta remnants on the crater floor (Goudge et al., 2015), although a volcanic vent source has yet to be conclusively identified. The Mááz formation has also been hypothesized to be linked to a regional mafic capping unit observed in the circum-Isidis region (Nili Fossae to Libya Montes, Figure 1a; Hundal et al., 2022) which exhibits similar compositional and morphologic characteristics and also occurs along the western Jezero crater rim (Sun & Stack, 2020). If the units within and outside of Jezero are related, this capping unit would thus occur across more than 1–3 km of elevation range in the general circum-Isidis region and across more than 700 m of elevation difference between Jezero's crater rim and crater floor, and is not restricted to topographic lows (Hundal et al., 2022; Sun & Stack, 2020). These observations argued against a single lava flow event, which would have required the emplacement and erosion of a substantially thick volcanic unit (hundreds of meters to several kilometers thick) that far exceeds the unit's present-day thickness of tens of meters (Goudge et al., 2015; Kremer et al., 2019; Shahrzad et al., 2019). The pre-Perseverance consensus was that if the Mááz formation did not represent a lava flow, then its origins were likely clastic, such as a volcanic ash or aeolian deposit (Hundal et al., 2022; Sun & Stack, 2020), similar to the arguments presented for the ashfall or pyroclastic origin for the Séítah formation (Kremer et al., 2019; Mandon et al., 2020).

The age of the Mááz formation is also of significant intrigue and importance. The Mááz formation is notably crater-retaining, especially in comparison to the crater-lacking Séítah formation, which has led several workers to estimate the age of this unit based on crater count. Ages for the Mááz formation widely range from 3.5 Ga during the Noachian-Hesperian (Goudge et al., 2015; Quantin-Nataf et al., 2021; Sun & Stack, 2020) to  $2.6 \pm 0.5$  Ga (Shahrzad et al., 2019) and 1.4 Ga (Schon et al., 2012) during the Amazonian, calling into question the accuracy of its age determined by crater counting. If the Mááz formation is igneous, radioisotope analysis of datable minerals in a returned Mááz sample could derive an absolute age that can be compared to its crater count age estimates (Quantin-Nataf et al., 2021; Simon et al., 2023). The Mááz formation is also in contact with the Jezero western delta (Goudge et al., 2015; Holm-Alwmark et al., 2021; Stack et al., 2020) and therefore can help place constraints on the age of the western delta (otherwise dated to the Late Noachian or Hesperian; Fassett & Head, 2008; Mangold et al., 2020) and samples obtained from it (Farley et al., 2020; Simon et al., 2023). Additional value of returned sample science on “in place” Mááz bedrock includes paleomagnetism analyses that could

reveal information about the timing of planetary dynamo (Simon et al., 2023). Given its possible widespread occurrence, estimated age, and possible igneous origin, a sample from the Mááz formation was assessed by the Mars 2020 science team as a critical region to explore and sample in order to help calibrate Mars crater chronology models, with broader applications to crater chronology on other planetary bodies, and to provide age constraints on samples obtained elsewhere in the crater, including the western delta (Farley et al., 2020; Quantin-Nataf et al., 2021; Simon et al., 2023).

### 2.2.3. Fractures

Various fractures are prevalent across the surface of the Mááz formation (Stack et al., 2020) and raise the potential to be related to past aqueous activity that may be preserved in fracture fills and alteration minerals (similar to what has already been observed at the orbital-scale, e.g., Pascuzzo et al., 2019). Analysis of mineral fill, or even hydration or compositional differences between the fracture and the host bedrock, may yield information about secondary or diagenetic processes that affected the Mááz formation after its emplacement. Investigation or even sampling of fracture or mineral fill would be important to understand past habitability conditions in Jezero. Of the many fractures on the crater floor that were identifiable from orbital data, a network of two-sided ridges dubbed Mont Rocheforte gained interest amongst the Mars 2020 team as the intersection of three raised linear features (Figure 2), though it was ultimately not visited by Perseverance during the campaign (Sections 3.3.4 and 4.2.1).

### 2.2.4. Possible Delta Remnants

Several topographic mounds have been observed on the Jezero crater floor and interpreted as erosional remnants. These mounds have been hypothesized as representing more distal deposits of the western delta that have been preserved after significant erosion of the western and/or northern deltas to their current state (Goudge et al., 2015; Stack et al., 2020). Some mounds, such as Kodiak, exhibit similar morphology and stratigraphy as the delta (Mangold et al., 2021) and are therefore convincingly interpreted as delta remnants, whereas other mounds like Santa Cruz, Isle Royale, Mauna Kahālawai, and Pilot Pinnacle, have different morphology and therefore have less certain origins (Figure 1c; Goudge et al., 2015; Stack et al., 2020). The Mars 2020 science team therefore had a keen interest in potentially exploring these mounds with Perseverance and searching for fine-grained lacustrine sediments, which may exhibit the highest preservation potential for organics and morphological biosignatures (Farley et al., 2020; McMahan et al., 2018). However, many of these mounds lack visible stratification or extensive outcrop in orbital images, which raised concerns about sufficient outcrop being available to sample, and if sufficient context could be assessed for any acquired rock core samples. Although observations of the western delta and the Kodiak remnant were planned and obtained throughout the crater floor campaign, they are not described in this work and we instead refer the reader to Mangold et al. (2021) for a summary of results during Perseverance's first year of investigation.

## 3. Crater Floor Campaign Objectives and Notional Plan

### 3.1. Campaign Objectives

The primary objectives of the crater floor campaign were to:

1. Investigate the nature and origin of the Mááz and Séítah formations, including the depositional and emplacement mechanisms.
2. Characterize the contact between the two formations.
3. Characterize any aqueous alteration and modification of the formations, including fractures along the traverse (notably one feature dubbed Mont Rocheforte; Figure 2)
4. Document Pilot Pinnacle and other potential delta remnants.
5. Investigate the martian atmospheric and surface regolith to better understand the past and present climate on Mars, and to characterize the aeolian processes and depositional history in Jezero crater.

Sampling was of course a key objective in and of itself, with a focus on sampling the diversity of lithologies that would be encountered on the crater floor. Because of the enigmatic origin of the crater floor (Section 2.2), specific lithologies could not be designated for sampling a priori and the team therefore described the desirable traits of potential samples, with the final sampling decisions to be made as we obtained more information during campaign execution (described in more detail in Sections 3.3 and 4 campaign narrative). In total, four sample pairs (Section 1.5) were allocated for acquisition: one pair of the Mááz formation, two pairs of the Séítah formation, and one pair for Mont Rocheforte or that could be reallocated to a different target of opportunity.

The crater floor campaign was the first science campaign of the Perseverance mission and therefore experienced the unique circumstances of needing to interleave science objectives with FTAs (Section 1.7) and learning the capabilities of the rover as we used them. At the start of the campaign on sol 100, key capabilities that still needed to be checked out prior to nominal use included:

- Natural PS using PIXL and SHERLOC on a natural (i.e., un-abraded) surface.
- Autonomous navigation (Autonav), which allows the rover to autonomously determine its drive path in terrains deemed suitable by the Rover Planners, and generally allows for significantly longer distances to be traversed (upwards of 150 m/sol). Autonav capabilities were checked out in a series of FTAs right at the beginning of the crater floor campaign (Verma et al., 2022), so that we could take advantage of the ability to drive longer distances as soon as possible.
- Sampling, which needed to be released via a series of FTAs. First, Perseverance had to process its first witness tube, which had been in the BC since launch and was intended to capture any particulate contaminants from the rover's ambient environment (Section 4.1). Perseverance also had to clean its turret, attach a new abrasion bit (Section 1.2), and perform the first abrasion and dust-clearing, as well as the first core collection and sample processing. Due to other FTAs that needed to be executed prior, and to ongoing work in the testbeds at the Jet Propulsion Laboratory, these sampling FTAs were not able to be performed until beginning on sol 142.

### 3.2. Campaign Planning Parameters

In late April 2021, around sol 70 of the mission, the Campaign Planning Science Group (CPSG), led by two Campaign Science Leads (CSLs; V.Z. Sun and K.P. Hand), was assembled and tasked with leading the CPSG through decisions to assemble the campaign plan. Two Campaign Science Engineering Liaisons (SELs; S. Milkovich and R. Kronyak) acted as liaisons between the science team and the Strategic Rover Planner (SRPs; O. Toupet and T. Del Sesto), who constructed the strategic drive route between scientific locations of interest. The CPSG was tasked with constructing a campaign plan, which consisted of identifying (a) scientifically important locations to visit, (b) the strategic drive route in between the science locations, (c) an allocation of the samples that would be acquired along the campaign, (d) an allocation of time for other RS or PS to establish the geologic context of the crater floor units that would be explored and sampled, and (e) potential decision points that the team may encounter during the campaign. This campaign plan was to be delivered on 1 June 2021, after a month of biweekly CPSG meetings to progress through the science decisions that would need to be made, and just in time for CI and Tactical operations on sol 100.

Because the crater floor was the unit that Perseverance landed on and thus the first target for its Jezero investigations, the crater floor campaign only began after the initial period of commissioning and the helicopter mission. The crater floor campaign was thus initially planned to begin on sol 100 after this period, and was planned to extend until sol 365. Although the total number of sols dedicated to the campaign would be less than the one Earth year set aside for studying each of Jezero's major units (Section 1.4), this was deemed preferable to taking sols from the delta or marginal carbonates, which were considered higher-priority targets, especially for advancing the mission's objectives of searching for habitable environments and biosignatures. In planning the very first science campaign for the Perseverance rover mission, the Mars 2020 CPSG faced unique challenges in balancing a thorough scientific investigation of the crater floor with ongoing commissioning and checkout activities. As a result, the team had to remain flexible and reactive to changes in the campaign parameter space throughout the course of Campaign Planning, and even during the campaign execution as the team gained knowledge about rover performance and how to best estimate anticipated progress.

#### 3.2.1. Crater Floor Campaign Area

The initial campaign area considered by the CPSG was bounded by the OEB landing site to the north, by Pilot Pinnacle to the south and southwest, and by the accessible portion of Séítah, where Perseverance would eventually "toedip" into the Séítah unit, to the west (Figure 2a). This specific region was identified to enable, if desired and deemed feasible by the CPSG, the investigation of: Pilot Pinnacle (a potential delta remnant), the Mááz formation, the Séítah formation, and Artuby ridge (an escarpment near the inferred contact between the Mááz and Séítah formations) (Figure 2b).

The region north of OEB was not further considered due to the higher prevalence of the Cf-U<sub>s</sub> unit (Stack et al., 2020), inferred to be largely regolith-covered terrains lacking outcrop, and the lack of escarpments at the

Mááz-Séítah border with outcrop quality surpassing that of Artuby ridge. Although the exact final extent of the campaign had yet to be determined by the CPSG, it was determined early on that the crater floor campaign would consist of an out-and-back traverse, wherein the Perseverance rover would traverse south of OEB, potentially as far south as Pilot Pinnacle and/or as far west as the Séítah toedip region, and then drive back north back to OEB (Figure 2b). At that point the science campaign would be complete, and Perseverance would then continue driving counter-clockwise around the adjacent Séítah exposure to arrive at the Three Forks location at the base of the Jezero delta (Figure 2a). Even though Perseverance would have to cover more distance performing this out-and-back traverse and counterclockwise drive to the delta, this route was determined to be faster than one where Perseverance continued driving clockwise past Pilot Pinnacle to reach Three Forks. If traveling clockwise, the rover would have to cross the sandy and rough terrains of the Séítah formation to reach the delta, whereas much faster drive progress using Autonav could be made if traversing counter-clockwise over the more easily navigable Mááz formation (Verma et al., 2022).

The out-and-back traverse concept also benefited other science and engineering purposes. Traversing the same region twice allowed the science team to perform reconnaissance of geologic units during the out-trip and provided time to analyze the data so that better informed decisions could be made about sampling during the back-trip (Yingst et al., 2017). This philosophy also helped accommodate the rover's commissioning and FTA schedule, which was yet to be fully completed. For example, Autonav capabilities were not yet ready at the beginning of the campaign, and sampling capabilities were estimated then to not be ready until midway through the campaign around sol 142. Thus, it was most reasonable to make drive progress and cover more ground while waiting for Autonav and sampling capabilities to come online.

### 3.2.2. Sol Allocation

During the Campaign Planning process, the crater floor campaign was planned to begin on sol 100, and end with arrival at a location at the base of the delta named Three Forks by sol 365 (Figure 2a). It was estimated that 64 of those sols would be needed to make the drive from OEB to Three Forks, thus the science portion of the campaign was initially allocated a total of 201 sols (executing from sol 100 to no later than sol 301). This number included 23 sols for Solar Conjunction (a period where Mars and Earth cannot communicate due to being on opposite sides of the Sun), 36 constrained sols (i.e., sols that lack ground-in-the-loop from the preceding sol and are typically not as productive as a nominal, unconstrained sol), and 142 nominal sols, of which 15% or 21 sols were withheld as engineering margin sols and 5% or 8 sols were withheld as science margin sols, to be used in case of unexpected engineering or science delays to the sol path. This left 113 nominal sols for the CPSG to distribute between drives, science sols, and sampling sols. This overall sol allocation was commensurate with the assumption that this campaign would result in the collection of four paired samples, or eight total cores, in order to keep with the expected sampling rate required to deposit an initial sample depot by the end of the prime mission (Section 1.5). With the sampling sol path estimated at 11 sols per sample pair collected (Section 1.5), 44 nominal sols were allocated to sampling, with the remaining 69 sols to be split between drive sols and science sols.

Drive sols would likely take up the majority of these remaining 69 sols, depending on the distance to be driven during the campaign. Importantly, RS activities could also be obtained on drive sols at no additional cost to the sol path. Rover resource limitations dictate that the entire sol could not feasibly be spent on driving, and thus less-resource intensive RS activities could still be planned and help advance campaign objectives even as Perseverance continued to drive. Science sols were intended to represent sols when the team would plan more extensive science activities than could be typically accommodated on a drive sol, such as PS or substantial RS that would take up the majority of the rover's awake time. As campaign planning progressed and better estimates of FTA readiness and drive capabilities were determined, an additional 32 sols were given to the CPSG (16 for FTAs, 16 for science/drives), resulting in a total science campaign duration of 233 sols (Table 3).

### 3.3. Campaign Trades and Decisions

Although the crater floor campaign carried several objectives to investigate the most prominent features on the Jezero crater floor—the Mááz formation, Séítah formation, fractures, and Pilot Pinnacle (Section 2)—it would not be possible to visit and investigate all of these features within the timeframe allotted to the campaign (Section 3.2.2). Various high-level trades and decisions were made to best utilize the campaign duration and to

**Table 3**  
*Summary of Campaign Planning Nominal Sol Allocations to Different Legs of the Campaign*

Corresponding main text	Campaign leg	Nominal sols allocated
	Drive, science, sampling sols	
Section 3.4.1	Drive to North Séítah Overlook	14
	RS from North Séítah Overlook	1
Section 3.4.2	Drive to Polygon Valley	11
	RS/PS at Polygon Valley	3
	Sample Máaz—pair 1	11
Section 3.4.3	Drive to Citadelle	6
	Drive to South Séítah	9
Section 3.4.4	RS/PS at South Séítah	6
	Sample Séítah—pairs 2 and 3	22
Section 3.4.5	Drive back to Citadelle	9
	Drive to Mont Rocheforte	8
	RS/PS at Mont Rocheforte (or Target of Opportunity)	3
	Sample Mont Rocheforte (or Target of Opportunity)—pair 4	11
	Drive back to OEB	15
	Subtotal	129
	Other sols	
	FTA	16
	Science Margin	7
	Engineering Margin	22
	Solar Conjunction	23
	Constrained	36
	Total sols	233

Note. RS, Remote Sensing; PS, Proximity Science. Green cells represent drives, yellow cells represent RS or PS, and orange cells represent sampling.

maximize science return, and are described below. The resulting campaign plan is described in Section 3.4, and the summary of the executed campaign and decisions made are in Section 4.

### 3.3.1. Pilot Pinnacle

Of the remnant mounds on the Jezero crater floor, Pilot Pinnacle was the only remnant within the prescribed campaign area (Figure 2a; Section 3.2.1). The CPSG discussed the merits of including Pilot Pinnacle in the baseline campaign plan, but it became apparent that the drive to and from this possible delta remnant would consume too much time. Committing to driving to Pilot Pinnacle would effectively mean that the campaign plan would consist only of driving and sampling, with no sols remaining for exploratory science if, for example, the team desired to perform PS to better understand rocks outside of the sampling sol path, or to allow for discovery-driven exploration of targets that we could not anticipate at this point in campaign planning. Furthermore, the team was not convinced that Pilot Pinnacle, or any of the other remnant mounds (Section 2.2.4), contained sufficient outcrop exposure for meaningful investigation or sampling. A drive to Pilot Pinnacle was therefore not included in the baseline campaign plan, although the CPSG would insert various points in the plan where reconnaissance imaging of Pilot Pinnacle could be acquired, and the decision to divert to Pilot Pinnacle could be made if there was compelling evidence that there existed sufficient outcrop for sampling and geologic contextualization. During the execution of the campaign, such outcrop quality was not observed and Pilot Pinnacle was eventually discarded from the campaign plan (Section 4.1.2).



### 3.3.2. Séítah Formation

There were two main challenges in planning the exploration of the Séítah unit. (a) Whereas Perseverance had landed on the Mááz formation and thus the science team was able to obtain some observations of the Mááz formation during the first 100 sols of commissioning (Figures 3b–3f), the science team had very few observations of Séítah while the CPSG was planning the campaign. The only observations of Séítah prior to the crater floor campaign were made on sols 69, 92, 94, and 99, which had shown spectral evidence of olivine and layering in the Séítah outcrops (Figure 3g; e.g., Wiens et al., 2022). However, in situ compositional data of Séítah remained unavailable and the sedimentary or igneous origin of Séítah remained in debate. (b) Large portions of the Séítah region are notably covered in sandy dunes (Day & Dorn, 2019; Stack et al., 2020), which considerably limited traverse options as sand traps could immobilize the rover or slow drive progress to the point of breaking the campaign schedule.

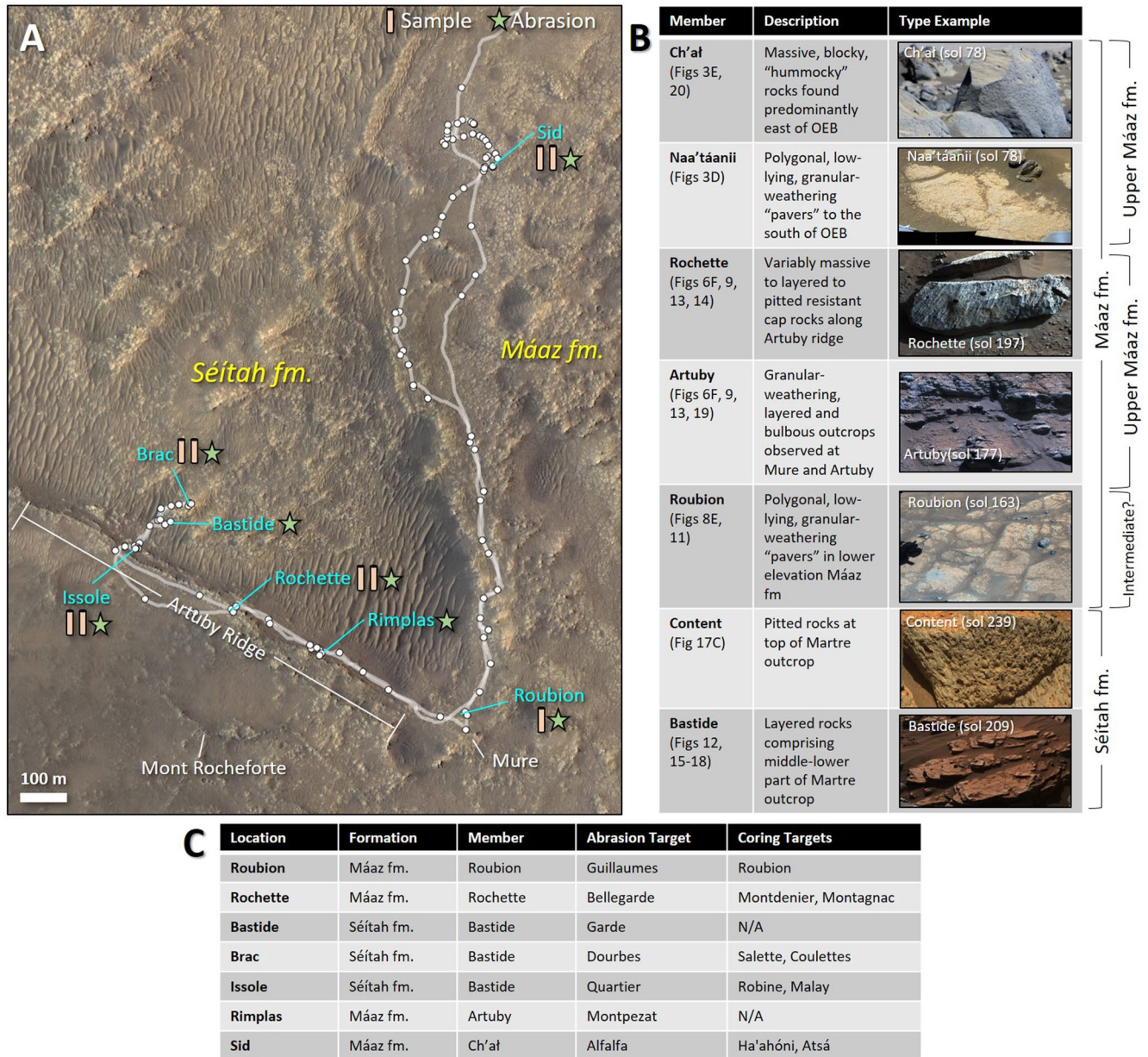
The possibility of driving through a large region of Séítah was eliminated due to the traversability and efficiency concerns generated by the sand cover and uneven terrain. Instead, a “toedip” strategy was considered to explore Séítah, where Perseverance would drive into Séítah for a short distance, performing RS, PS, and sampling, and then drive back along the same path to return to the Mááz formation. Two locations within the campaign area surfaced as candidate toedip options, named North Séítah and South Séítah (Figure 2b). Both locations appeared less covered by sand and offered the possibility of traversing into Séítah for 100–200 m of distance. The South Séítah toedip option was favored due to it likely having more bedrock exposures accessible to the rover, as well as the opportunity to observe the vertical stratigraphy exposed on Artuby ridge, located near the inferred Mááz–Séítah contact. However, as the trek to South Séítah would be a substantial traverse commitment, the North Séítah location was kept as a back-up option. A deviation to the North Séítah overlook, a local topographic high at the edge of the Mááz formation adjacent to the North Séítah toedip traverse path (Figure 2b), was planned to acquire reconnaissance of North and South Séítah and traverse paths. After acquiring reconnaissance data at North Séítah, the team would then decide whether to continue towards South Séítah as initially planned, or if an investigation at North Séítah would be sufficient (Sections 3.4.1 and 4.1.1).

### 3.3.3. Mááz Formation

During the first 100 sols of commissioning, Perseverance had opportunities to make initial science observations of the Mááz formation. These first observations revealed the presence of at least two different surface expressions of the Mááz formation: a low-lying “paver” morphology that was expressed as polygonal outcrops in the orbital view (later named the Naa'táanii member in the vicinity of OEB, meaning “leader” in Navajo; Figures 3d and 4), and a higher-standing morphology that appears as rockier, more rubbly textures in the orbital data (later named the Ch'a'al member, meaning “frog” in Navajo; Figures 3e and 4) (J. Bell et al., 2022; Wiens et al., 2022). The traverse path through the campaign area would pass through similar polygonal and rocky terrains, especially in the Polygon Valley region, thus there was no reason to believe that the morphologies observed in the landing area would not be present elsewhere in the campaign area. Regions to the east of Polygon Valley in Figure 2b were discussed as possible stops along the campaign, but these diversions would come at a substantial sol cost and there was insufficient confidence that these eastern regions would be substantially different than the Mááz formation that would be encountered along the traverse. Thus, the CPSG planned to study and sample the Mááz formation at locations close to the most expedient traverse route to lower the sol impact.

### 3.3.4. Mont Rocheforte

Mont Rocheforte was included as part of the campaign baseline plan but with the understanding that the features of interest—mineral or fracture fill—might not be present (Section 2.2.2). Though Perseverance had already passed by some fractures in its first 100 sols, these fractures were always filled with regolith and the team observed no mineralogic or physical evidence for fracture fill (Section 2.2.3). Thus, there was doubt if we would encounter fill in the fractures elsewhere in the Mááz formation. However, Mont Rocheforte was near the traverse to South Séítah, and could be investigated at the cost of <10 sols deviation. The CPSG therefore recommended that Mont Rocheforte could be investigated on the drive back to OEB, which would also give the team opportunities to perform reconnaissance of Mont Rocheforte along the drive to South Séítah and assess whether there existed mineral or fracture fill. If Mont Rocheforte was later deprioritized for investigation due to the absence of fracture fill, its associated sol and sample allocation could be reassigned to another target of opportunity. The



**Figure 4.** Summary of Perseverance's exploration of the Jezero crater floor. (a) Map view of Perseverance's traverse in white (white circles indicate individual end-of-drive locations) and abrasion or sampling locations annotated in cyan. Other locations referenced in the text are annotated in white, in addition to the features annotated in Figure 2. The extent of this image is the same as Figures 2b and 2c. For the mapping of the formation members over this traverse path, we refer the reader to Figure 1C in Farley et al. (2022). (b) Table describing the members of the Mááz and Séítah formations with images of type examples: Ch'at (zcam08039), Naa'taanii (zcam08039), Rochette (zcam08214), Artuby (zcam08190), Roubion (zcam08172), Content (zcam08262), Bastide (zcam08243), in approximate stratigraphic order with the stratigraphically highest unit at the top, following Farley et al. (2022). "Upper Mááz" and "lower Mááz" designations follow Horgan et al. (2022). Roubion may be intermediate between upper Mááz and lower Mááz (Horgan et al., 2022) or the lowermost Mááz member (Crumpler et al., 2023). Further potential subdivisions of the Séítah formation are described in Crumpler et al. (2023). The Content member of the Séítah formation may be equivalent to the upper Mááz members (Udry et al., 2023). (c) This table summarizes the locations where Perseverance performed abrasion or sampling.

latter scenario did indeed come to fruition when the team decided not to visit Mont Rocheforte as more observations were obtained during the campaign (Section 4.2.1).

### 3.4. Campaign Plan

The final campaign plan delivered from the CPSG on 1 June 2022 is summarized in Table 3 and Figure 2b. Overall, the campaign plan emphasized making expedient drive progress except for specific designated stops where dedicated science or sampling sols would be spent. Extended stays at rover workspaces due to unexpected discoveries would be subject to a high level of scrutiny (e.g., only if compelling evidence of biosignatures was discovered). However, the out-and-back strategy (Section 3.2.1) allowed for the opportunity to revisit interesting locations on the trip back to OEB Landing. The CPSG also identified possible decision points, described below, throughout the campaign to insert opportunities to discuss modification to the campaign plan as new observations were obtained during campaign execution. Section 4 describes the actual campaign outcomes and decisions made during the campaign.

#### 3.4.1. Reconnaissance From North Séítah Overlook

From OEB Landing, Perseverance would drive south to the North Séítah overlook location, stopping at several imaging stops along the way, referred to as Imaging points 1, 2, and 3 (Figure 2b). During this portion of the campaign, the team would also prioritize execution of Autonav FTAs as early as possible so as to enable faster drive progress that could be used for the remainder of the mission. The North Séítah overlook would be a site with a higher vantage point where the team would stop and dedicate an entire sol to reconnaissance RS of the Séítah formation. Objectives at the North Séítah overlook were to image the Séítah outcrops there to obtain a better understanding of Séítah's lithology and possible origins. The team would also attempt to image South Séítah where the intended toedip traverse would be, if visible. If time allowed, reconnaissance imaging of Pilot Pinnacle would also be collected to assess if there were compelling outcrop exposures that would warrant a possible in situ investigation at the remnant mound. Imaging points 1, 2, and 3 were inserted along the way to North Séítah as additional opportunities to accomplish this imaging prior to arriving at North Séítah; stopping at these imaging points was opportunistic and not to come at any cost to the sol path.

After this reconnaissance imaging was accomplished, the team would come to a decision point to affirm that a toedip at South Séítah was still preferred over North Séítah. If the outcrops at North Séítah looked more enticing than at South Séítah, then the team would toe-dip at North Séítah and forgo the lengthier trip out to South Séítah. This decision would be based on technical Rover Planner assessment of traversability at both North Séítah and South Séítah, and scientific assessments of the quality of Séítah outcrop and any visible contact between Mááz and Séítah, prioritizing clear contacts unobscured by sand or talus and outcrops that could be traced and related to one another. Sampling feasibility would also be considered, such as engineering assessments if there were rocks of sufficient size for sampling and placing the drill stabilizers, and science assessments of the apparent diversity of composition, sedimentary structures, and inferred grain size.

#### 3.4.2. Sampling at Polygon Valley (One Sample Pair)

From North Séítah, the rover would then drive to Polygon Valley at the southernmost region of the campaign traverse to acquire the first abrasion and samples of the Mááz formation (Figure 2b). At the time of campaign development, a sample pair from the Mááz formation was desired to provide absolute ages to compare with Mars crater chronology models (Section 2.2.2), and Polygon Valley was considered representative of the Mááz formation at the time (Section 3.3.3). Polygon Valley was chosen in part because Perseverance's expected arrival there would coincide with the anticipated time frame (sol 142) that the team would be ready to execute sampling FTAs (Table 2), and also because of the presence of both the low-lying (e.g., Roubion member; Figure 4) and high-standing (e.g., Ch'ał member) Mááz morphologies (Figures 3d–3f). In this region, Perseverance would spend a few sols performing natural PS on the Mááz formation (prior to the abrasion FTA), obtaining a sample pair of the Mááz formation, and performing more context imaging of South Séítah and Pilot Pinnacle, as well as scoping out Mont Rocheforte at this closer location. If observations of Pilot Pinnacle were sufficiently compelling (Section 3.3.1) and if the mission was ahead of the campaign schedule, then the team could decide to divert to Pilot Pinnacle in lieu of South Séítah, in which case it would then toedip at North Séítah on the drive back.

### 3.4.3. Driving to South Séítah via Artuby Ridge

Barring changes to the campaign plan, however, the plan after sampling the Máaz formation was to drive towards South Séítah to execute the toedip. Along the drive to South Séítah, the team would pass by and investigate the Máaz-Séítah contact near Artuby ridge. The most expedient traverse would first take the rover along the base of Artuby ridge to an ascent point (later named Citadelle; Figure 2b), where the rover would then climb back on top of the Máaz formation to continue towards the South Séítah toedip entry point. In the first portion of the traverse to Citadelle, the team would prioritize imaging of Artuby ridge to the port side of the rover and attempt to identify the exact contact between the Máaz and Séítah formations. As part of this effort at Citadelle, the team planned to document any compositional or morphologic differences between the base of Artuby ridge and top of the ridge on the Máaz formation. During the second portion of the northwestwardly traverse, which would be back on topographically higher Máaz terrain, Perseverance would also perform additional reconnaissance of Mont Rocheforte to look for evidence for mineral or fracture fill that would warrant an in situ investigation at Mont Rocheforte. Perseverance would cross the inferred Máaz-Séítah contact again at the beginning of the South Séítah toedip.

### 3.4.4. Sampling at South Séítah (Two Sample Pairs)

Once in the Séítah unit, the team anticipated slower drive progress through the sandy and duned terrain. This would allow for more frequent RS observations of the Séítah rocks, which the team anticipated investigating in situ for the first time in the South Séítah region. Science observations would be made and analyzed quickly to establish the database of Séítah formation compositions and facies and to determine which Séítah outcrops to sample. Early images of Séítah showed apparent layering (Figure 3g), which raised the possibility that Séítah could potentially be a sedimentary deposit with fine-grained rocks that would be of high sampling interest (Section 3.3.2; Farley et al., 2020; Simon et al., 2023). If a sedimentary fine-grained Séítah rock could not be found or sampled, the team would instead sample a representative rock from Séítah that is olivine-rich and potentially carbonate-bearing, as this could be correlated to the major olivine-bearing unit inside and potentially outside Jezero and would likely be the best indication of past water activity and thus habitability so far observed (Section 2.2.1).

Six science sols were allocated for dedicated RS and PS outside of the nominal sampling sol path, which would help characterize the Séítah formation lithologies and select specific lithologies to sample. After acquiring two sample pairs (taking 22 sols), Perseverance would exit Séítah via the same drive path and retrace its steps back into the Máaz formation. The exact extent of the toedip into Séítah was not determined during campaign planning as it would be highly dependent on actual terrain conditions. However, nine sols of driving were allocated for the drive to the South Séítah sampling locations from Citadelle (Figure 2).

### 3.4.5. Sampling at a Target of Opportunity (One Sample Pair) and Returning to OEB

After collecting the Séítah samples, Perseverance would begin to drive back towards OEB Landing. Along the traverse back, Perseverance would either drive to Mont Rocheforte to acquire the fourth sample pair of the campaign, or if reconnaissance of Mont Rocheforte did not reveal fracture or mineral fill to sample, the team would consider sampling another target of opportunity depending on what was observed during the campaign until that point (e.g., a second sample pair of the Máaz formation if different lithologies were observed). The rover would then drive expeditiously back to OEB, where the science portion of the crater floor campaign would end, and Perseverance would then embark on a rapid traverse towards Three Forks at the base of the Jezero delta (Figure 2a).

### 3.4.6. Routine Geologic Observation Plan

Routine science activities (Section 1.2) were identified during the campaign planning process to maintain systematic observations at the above locations and during the traverse.

During drives, standard RIMFAX observations would be performed to document subsurface structures and potentially connect and extrapolate observed surface structures across larger spatial scales (e.g., Hamran et al., 2022). After every drive, post-drive imaging in the form of Navcam, Hazcam, and occasionally Mastcam-Z (when duration and data volume allowed) would be obtained to enable driving and science targeting the next day.

Reconnaissance imaging, for example, planned at the North Séítah overlook, would consist largely of Mastcam-Z landscape imaging at the highest Z110 resolution, as well as SuperCam RMI imaging for even higher resolution

surveying of sedimentary structures. For targets with anticipated compositional significance, such as Mont Rocheforte with possible hydrated mineral fill or the Séítah formation with its olivine-rich composition, Mastcam-Z multispectral (440–1,020 nm; J. F. Bell et al., 2021) and SuperCam VISIR observations (0.4–0.85 and 1.3–2.6  $\mu\text{m}$ ; Fouchet et al., 2022) would be obtained to look for mineralogic characteristics from a distance.

Perseverance would be able to perform RS of its local workspace prior to driving later in the sol. Standard RS activities in the workspace would consist of Mastcam-Z imaging and multispectral observations at the highest Z110 resolution to document fine-scale textures and structures in the local rocks and image outcrops in the mid-to far-field. SuperCam LIBS, VISIR, and RMI observations would yield information on the elemental and mineralogic composition of individual points on rock targets. Performing these Mastcam-Z and SuperCam observations systematically along the rover traverse would be important for building up a database of observations from which broader compositional and textural trends could be assessed. Navcam panorama mosaics, acquired at each rover workspace, would fill in the spatial gaps and provide more complete context for the other RS observations. PS with PIXL, SHERLOC, and WATSON would occur more rarely, either as part of the sampling sol path or as designated science sols used to follow-up on the most interesting rock targets at the highest resolution possible from the Perseverance payload.

### 3.4.7. Atmospheric Campaign Plan

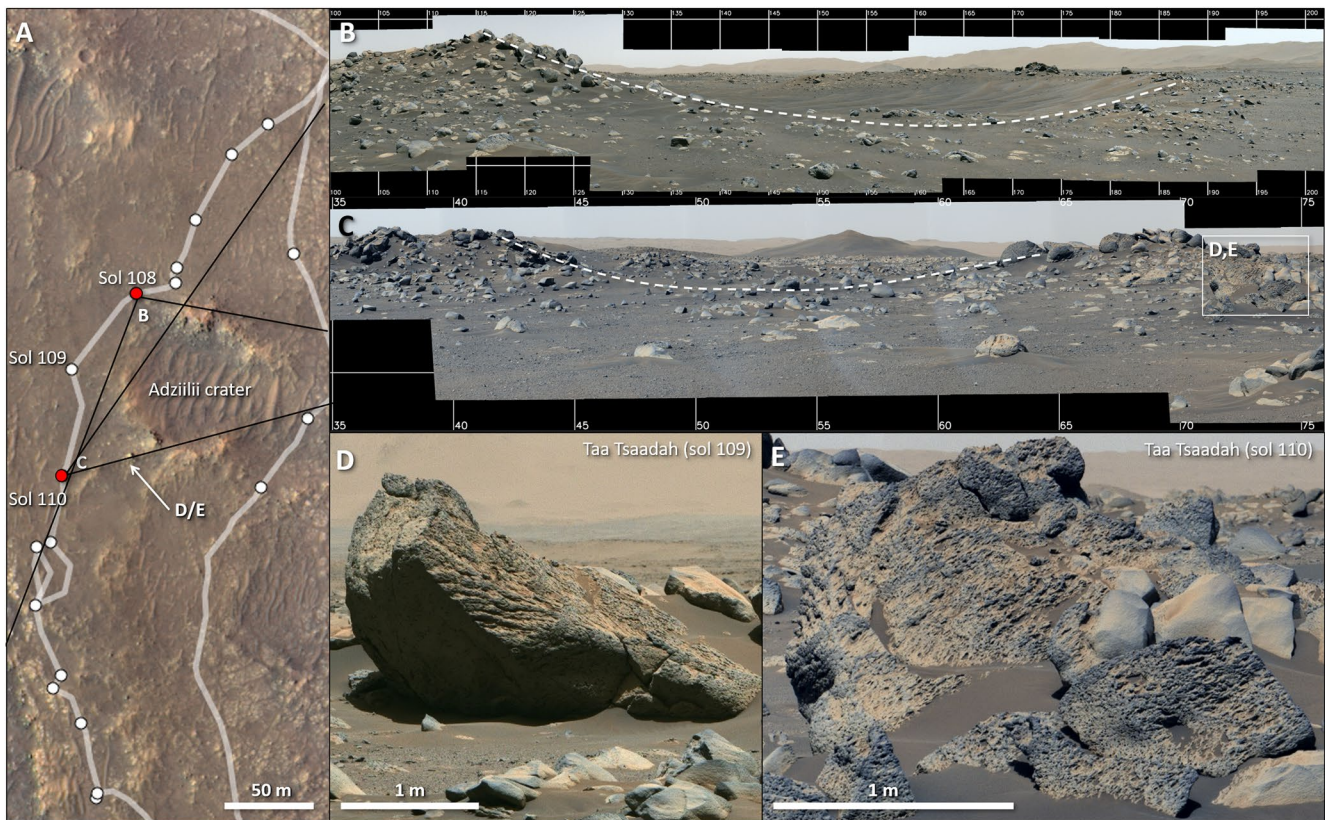
Throughout the entirety of the crater floor campaign, Perseverance would also make observations of the local atmospheric environment, including aeolian (wind-driven) activity such as sand motion and dust lifting, as called out by several Mars 2020 objectives (Farley et al., 2020) to characterize atmospheric dust and to make surface weather measurements to validate atmospheric models. Prior to landing, a set of atmospheric science goals were established, including determining what controls the circulation, weather, and climate, the dust and water cycles, and trace gas abundances, as well as determining aeolian processes and rates, and characterizing the atmospheric alteration of the surface. All of these goals would be addressed by the nominal atmospheric science campaign, which involves repeated observations of the atmosphere and surface environment over multiple Mars years, to measure the diurnal, seasonal, and year-to-year variation of atmospheric forcing and response. Atmospheric observations also provide input for planning Ingenuity flights and MOXIE  $\text{O}_2$  generation, and characterize the local environment during sampling. The primary measurements are made by the MEDA, Mastcam-Z, and the SuperCam instrument suite, as well as the rover's Navcams (Table 1; Text S1.1 in Supporting Information S1). The typical cadence of atmospheric science activities during nominal and dust storm campaigns, as well as observations associated with sampling, are summarized in Figure S1 in Supporting Information S1.

## 4. Crater Floor Campaign Narrative

This section describes the execution of the campaign plan described in Section 3.4. Rover observations referenced in this section will be discussed according to the mission's current geologic formation and member designations, as described and illustrated in Figure 4, following Farley et al. (2022). We refer the reader to Crumpler et al. (2023) and Horgan et al. (2022) for more discussion of the various Mááz and Séítah formation members and different stratigraphic models under consideration. Scientific findings from the campaign are summarized in Section 5; this section focuses on the campaign narrative and only mentions scientific findings as it pertained to future campaign plans. The following subsections are accompanied by Figures 5–20, which provide the orbital context for each campaign segment and examples of the main observations and activities from each location.

### 4.1. Initial Observations From Imaging Point 3 and the North Séítah Overlook

The crater floor campaign began execution on sol 101. From sols 101–118, we drove to Imaging Point 3 (Figure 2b) and acquired initial reconnaissance imaging of Séítah from there and along the traverse. During this segment of the campaign, drive progress towards the North Séítah overlook was interleaved with several Autonav FTAs that progressively unlocked the rover's autonomous navigation capabilities (Table 2) but occasionally, by design, limited drive progress towards campaign locations on certain sols. Imaging Points 1 and 2 were removed from the campaign plan, partly to recover sols in the sol path and because the intended reconnaissance imaging could be recovered at future locations, like Imaging Point 3 and the North Séítah overlook. The traverse to Imaging Point 3 passed along the perimeter of Adziilii (meaning “power” in Navajo) crater, allowing for observations from multiple angles of upturned Mááz formation rocks, some of which appeared vesicular with flow-like features



**Figure 5.** Ropey and pitted textures observed around Adziilii crater. (a) Orbital context showing locations of Mastcam-Z images in (b–e). Viewsheds in this work are generated from the Campaign Mapping and Planning tool (Calef et al., 2020). (b) Mastcam-Z enhanced color view of Adziilii crater, corresponding to the yellow viewshed in (a) (sol 108, zcam08080; NASA/JPL-Caltech/ASU/MSSS/K. Crawford). The dashed white line in (b) and (c) indicates the Adziilii crater rim in the foreground. Vertical and horizontal white lines in (b) and (c) indicate the azimuth and elevation, respectively, relative to the location where the image was taken from. (c) Mastcam-Z enhanced color view of Adziilii crater, corresponding to the red viewshed in (a) (sol 112, zcam08088; NASA/JPL-Caltech/ASU/MSSS/K. Powell). (d) Mastcam-Z enhanced color image of the Taa Tsaadah target (sol 109, zcam03159), a possible ejecta block from Adziilii crater. (e) The Taa Tsaadah target from the angle of the sol 110 rover location, from the same mosaic as (c).

and were interpreted as possible ejecta blocks excavated by the Adziilii impact (Figure 5; Crumpler et al., 2023). Otherwise, few rock outcrops were observed along this traverse, consistent with the orbital interpretation of these smooth terrains as being predominantly covered by regolith (Stack et al., 2020).

Perseverance stayed at Imaging Point 3 from sols 118–122. The team began to survey the North Séítah area (Figure 6) and remained stationary to accomplish a sampling FTA and prepare for the last Autonav FTA. Perseverance had carried in its BC a witness tube that had been activated and exposed to the ambient environment ever since it was installed on the rover, so that it could capture any contaminants the rover would encounter from its launch through landing on Mars. On sol 120, this witness tube was sealed, which marked the first successful processing of a sample tube (FTA-19; Table 2). The last Autonav FTA-15 was completed right after departing Imaging Point 3 on sol 122.

Between the execution of these FTAs, the science team obtained closer observations of Séítah for the first time as Perseverance was now positioned closer to the Máaz-Séítah contact. Results of these RS observations of Séítah again confirmed earlier detections of olivine (e.g., J. Bell et al., 2022; Wiens et al., 2022), as well as layering in Séítah formation outcrops. Between sols 122–126, Perseverance drove towards the North Séítah overlook, but first diverted to a nearby outcrop suitable for performing the first natural PS observations using PIXL, on the target Naltsos (meaning “paper” in Navajo) on sol 125 (FTA-9; Figure 2). As this was a natural surface observation, initial PIXL-derived compositions were primarily consistent with the Mars global dust composition, although compositional variability may have been due to bedrock components (Schmidt et al., 2021). Rocks that

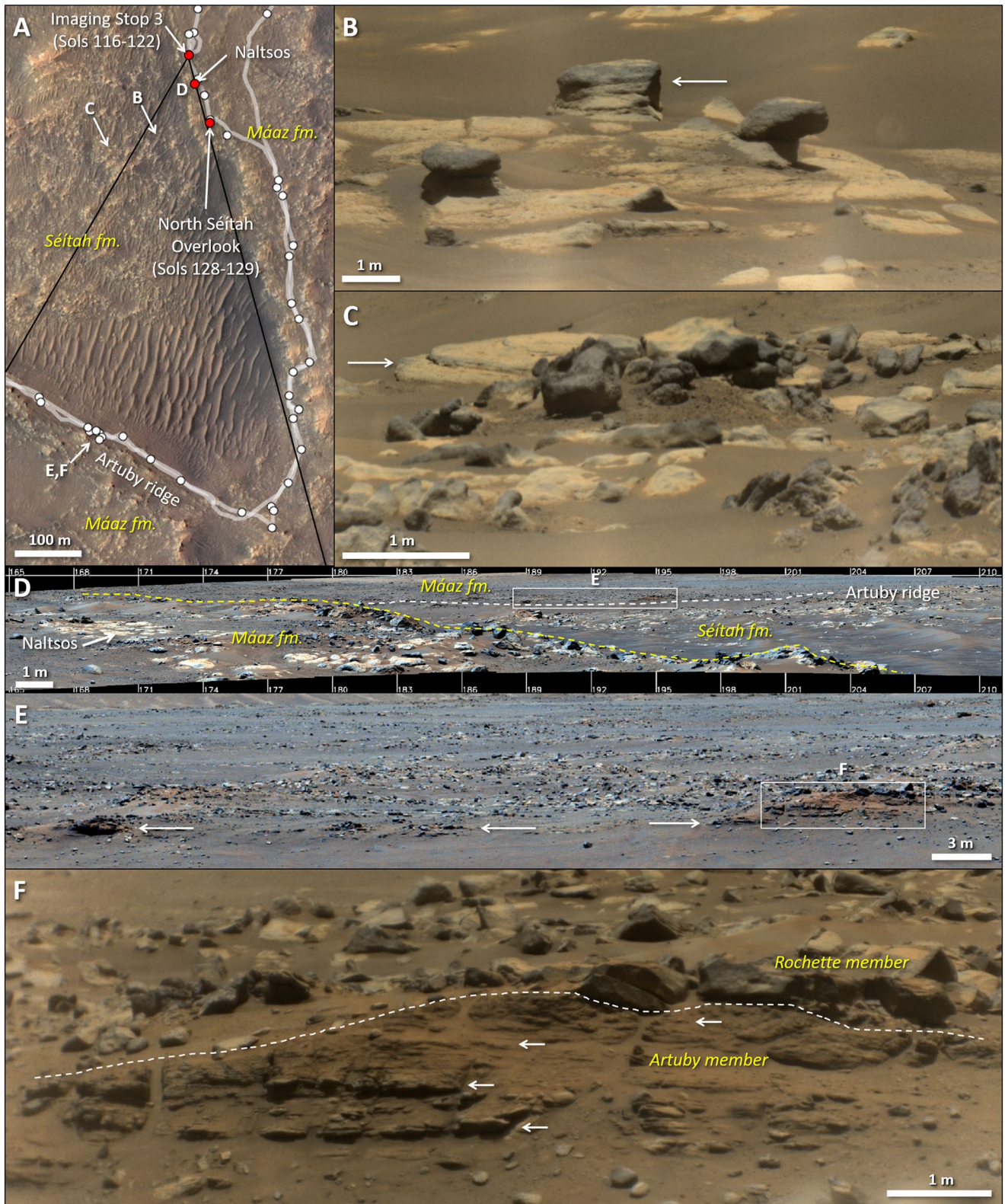
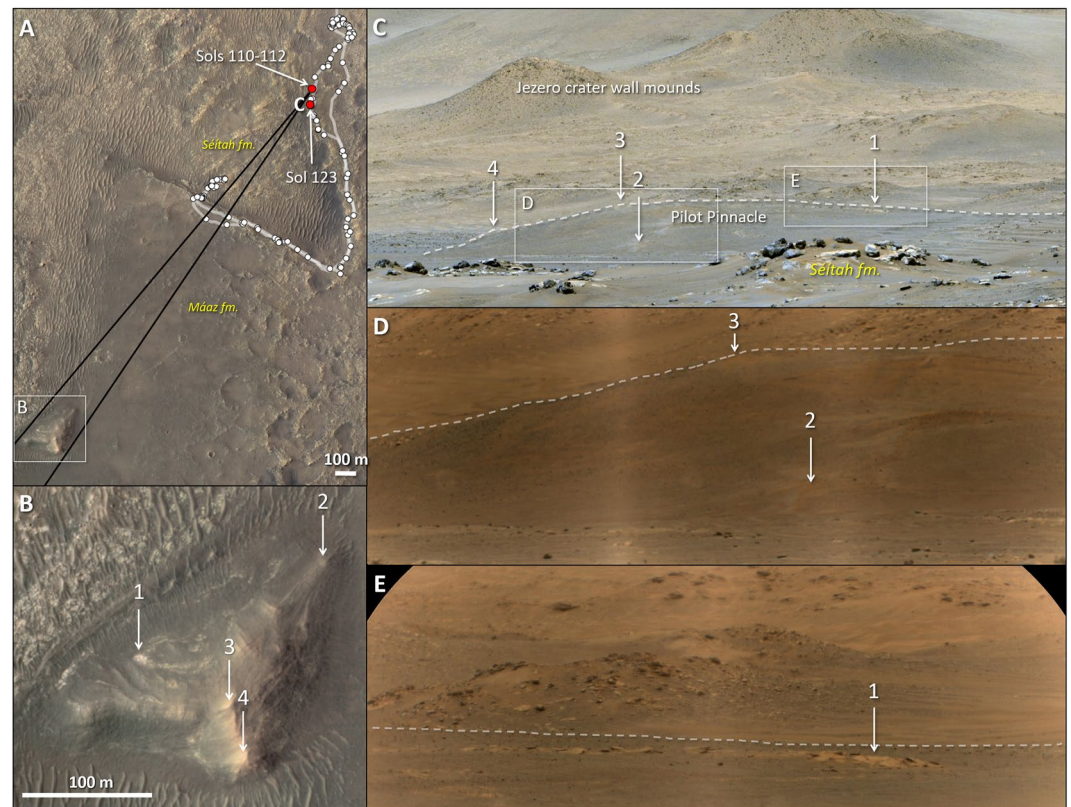


Figure 6.



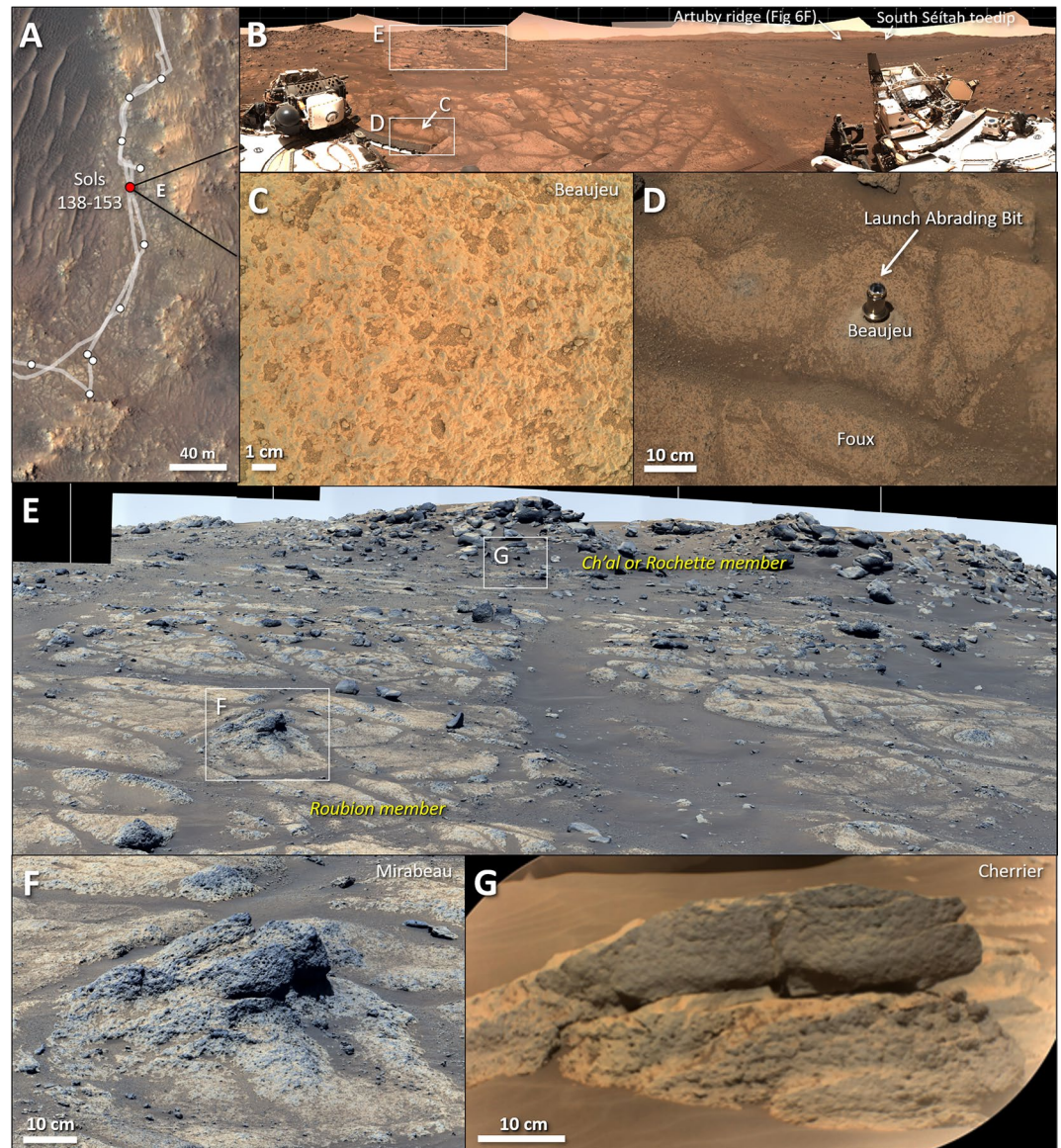
**Figure 7.** Imaging of Pilot Pinnacle from Imaging Point 3 (sols 110–112) and the North Séitah Overlook area (sol 123). (a) Orbital context showing locations of (b–e) and extent of imaging shown in (c). (b) Close up of Pilot Pinnacle from orbital data, with features 1–4 correlated to those observed by Perseverance in (c–e). (c) Mastcam-Z enhanced color view of Pilot Pinnacle, corresponding to the viewshed in (a) (sol 111, zcam08084; NASA/JPL-Caltech/ASU/MSS/J. Bell). The dashed white line in (c–e) outlines the top of Pilot Pinnacle. Note the Séitah formation in the foreground and mounds from the Jezero crater wall in the background. (d) Supercam RMI of the LD\_Pilot\_Pinnacle\_113 target (sol 113, scam05113). Arrows indicate features correlatable to the orbital view in (b), but note the lack of obvious outcrop or bedrock. (e) Supercam RMI of the LD\_Pilot\_Pinnacle\_123 target (sol 123, scam01123). The arrow indicates a light-toned feature that may correspond to the only exposed outcrop visible in these views of Pilot Pinnacle.

were encountered along the edge of the Máaz formation in this region, such as Naltsos, were later classified as part of the Rochette member (Figure 4; Crumpler et al., 2023; Horgan et al., 2022).

Perseverance arrived at the North Séitah overlook and acquired several reconnaissance observations on sols 128 and 129 (Figure 6). The team observed the local Séitah outcrops nearby, and although the rover was still not close enough for in situ compositional measurements of Séitah, it did acquire more SuperCam VISIR and Mastcam-Z multispectral observations. These observations revealed more paver-like surfaces within Séitah as well as layered protrusions inferred to be more erosively resistant than the pavers (Figures 6b and 6c). Perseverance also imaged the potential North Séitah toedip traverse path to aid in engineering analyses of a potential toedip (Figure 6a) and imaged in the direction of the South Séitah toedip area, although none of the intended South Séitah traverse path was visible from the North Séitah vantage point.

**Figure 6.** Observations of Séitah (b–d) and Artuby ridge (e, f) from Imaging Point 3 and the North Séitah Overlook. (a) Orbital context showing locations of (b, c), and extent of imaging shown in (d). The actual rover drive path is shown in white. (b) Supercam RMI of the LD\_Seitah\_129a target showing layered protrusions (sol 129, scam04129). Arrows indicate layering. (c) Supercam RMI of the LD\_Seitah\_129b target showing layered bedrock (sol 129, scam05129). Arrows indicate layering. (d) Mastcam-Z enhanced color view of Séitah, corresponding to the yellow viewshed in (a) (sol 122, zcam08115; NASA/JPL-Caltech/ASU/MSS/J. Bell). (e) Closeup of (b) with focus on the portions of Artuby ridge that were imaged from Imaging Point 3 and North Séitah. Arrows indicate parts of Artuby ridge where layering was observed in Supercam RMI observations obtained on sols 116 and 118. (f) Supercam RMI of the LD\_Artuby\_116 target showing layering (white arrows) at Artuby ridge (sol 116, scam02116). The dashed line shows the apparent delineation between the Artuby member and Rochette member along Artuby ridge.

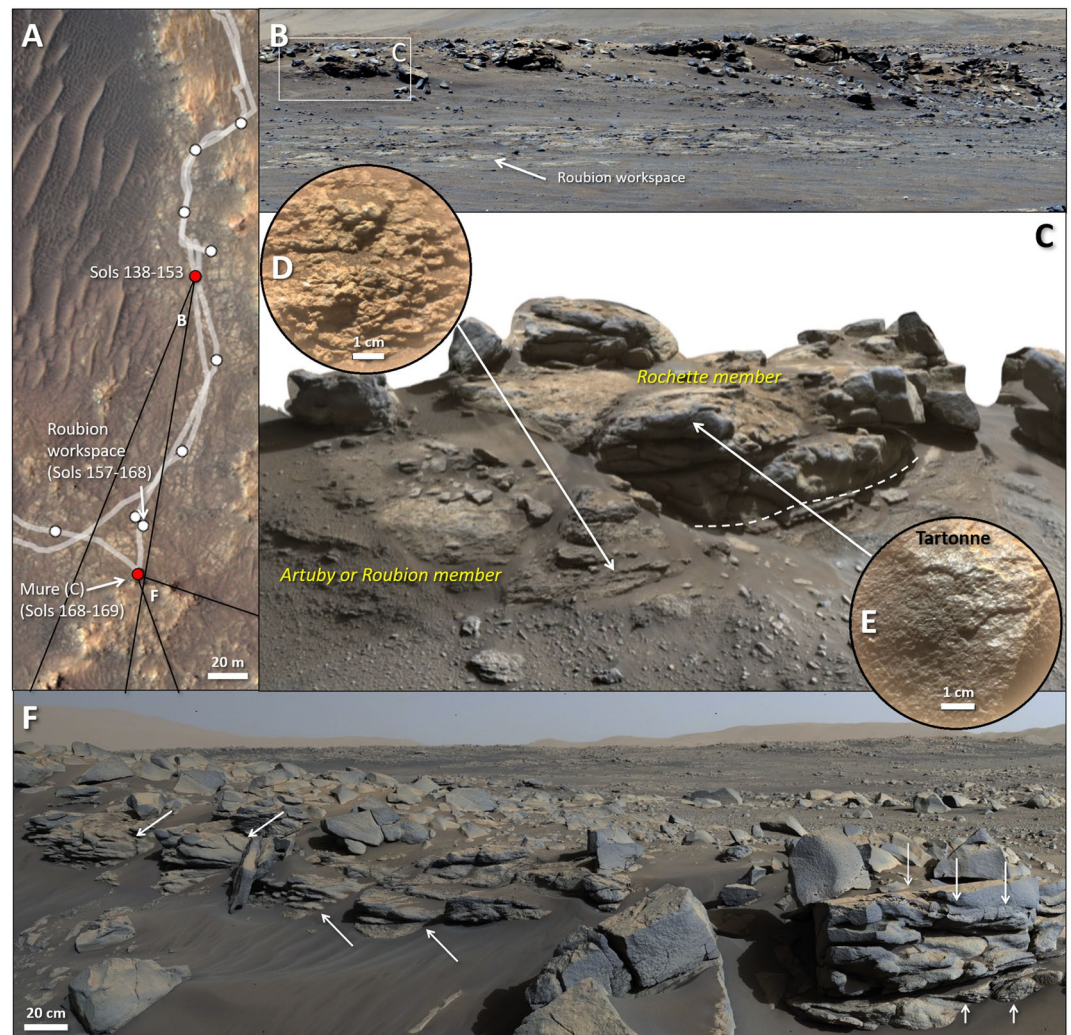




**Figure 8.** Observations from Polygon Valley and the workspace where we completed natural proximity science observations of Foux and Beaujeu, and completed FTA-20 and FTA-21. (a) Orbital context showing Perseverance's location between sols 138–153 and extent of the image shown in (e). (b) Navcam 360° mosaic from sol 137, showing the immediate workspace (d), the transition from pavers to higher-standing rocks (e), and Artuby ridge and the South Séítah toedip area in the distance. (c) WATSON image of the Beaujeu target from 25 cm standoff on sol 138, before the launch abrading bit was deposited. (d) Navcam image after depositing the launch abrading bit on sol 148, with targets Beaujeu and Foux (Figure 5) annotated. (e) Mastcam-Z enhanced color view of the paver-to-high-standing transition (sol 138–139, zcam08147-zcam08148; NASA/JPL-Caltech/ASU/MSSS/A. Bailey). (f) Close up of area within (e) showing the Mirabeau target, which is a transition from low-lying pavers to a higher-standing nub. (g) Supercam RMI of the Cherrier target showing potential layering or fracturing in the higher-standing rocks (sol 140, scam02140).

#### 4.1.1. First Observations of Artuby Ridge

Imaging along the 4–6 m tall escarpment (now named Artuby ridge) near the inferred Mááz-Séítah contact (Figures 6a and 6d) returned surprising results, as the team observed distinct layering along the ridge (Figures 6e and 6f). Overall, these early observations of layering in both Séítah and Artuby ridge again revived debate over the origin of the Mááz and Séítah formations and whether they were igneous or sedimentary rocks (Section 3.3.2). The observed fine-scale layering was initially hypothesized to represent aqueously deposited sediments that

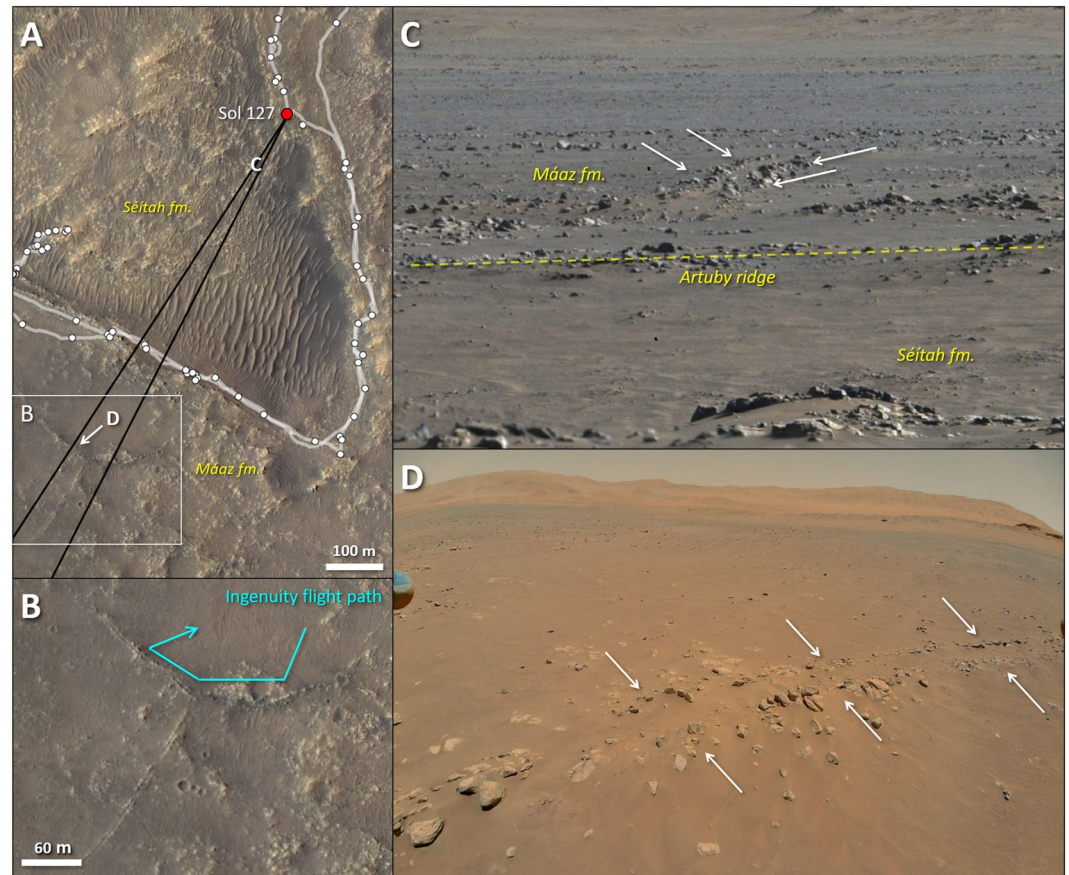


**Figure 9.** Observations of Mure and adjacent outcrops extending from Artuby ridge. (a) Orbital context showing the context and extent of imaging shown in (b–f). (b) Mastcam-Z enhanced color view of the Artuby ridge, specifically the Mure outcrop (c), and the context for the future Roubion sampling location (sol 143, zcam08151; NASA/JPL-Caltech/ASU/MSSS/C. Rojas). (c) 3D model of the Mure outcrop using Mastcam-Z data (sol 168, NASA/JPL/MSSS/ASU/Cornell/C. Tate), with a white dashed line delineating the Rochette member on top of the Artuby or Roubion member. (d) Supercam RMI of the Baume target, representative of the Artuby member (sol 169, scam04169). (e) Supercam RMI of the Tartonne target, representative of the Rochette member (sol 169, scam05169). (f) Mastcam-Z enhanced color view of the outcrops to the east of Mure (a), with arrows indicating examples of layering and vesicular textures (sols 168–169, zcam08180 and zcam 08181; NASA/JPL-Caltech/ASU/MSSS/K. Powell).

might be expected in the Jezero lacustrine system. Inconclusive results from the RS data, and even the natural PS data, in hand increased motivation to abrade the surfaces of these rocks and acquire abraded PS data to elucidate their origins. The observations of layering at Artuby ridge also cemented the decision to continue driving south towards South Séítah, which would take the rover by Artuby ridge and allow the team an opportunity to investigate the origins of these layers in situ.

#### 4.1.2. Removal of Pilot Pinnacle From the Campaign Plan

During these initial legs of the crater floor campaign, the Pilot Pinnacle remnant mound (Figure 7b) was also imaged on sols 113 and 123. However, the highest resolution images of Pilot Pinnacle did not reveal compelling outcrop exposures or evidence for traceable layered rocks. The mound appeared mostly smooth-textured, indicative of surficial regolith or other unconsolidated material. The most likely exposure of bedrock is indicated by feature 1 in Figure 7, though the in-place nature of this exposure or suitability for sampling could not be



**Figure 10.** Reconnaissance imaging of Mont Rocheforte by Perseverance and the Ingenuity helicopter. (a) Orbital context showing the extent of the image shown in (c) looking towards Mont Rocheforte from the sol 127 location. (b) Close up of Mont Rocheforte in orbital data, with the Ingenuity helicopter's Flight 10 flight path from sol 152 annotated in cyan. (c) Mastcam-Z enhanced color view of Mont Rocheforte, corresponding to the viewshed in (a) (sol 126–127, zcam08126, zcam08127; NASA/JPL-Caltech/ASU/MSSS/K. Crawford). White arrows indicate the perimeter of Mont Rocheforte. (d) Helicopter Return to Earth image of Mont Rochefore during its Flight 10 on sol 152. White arrows indicate the perimeter of Mont Rocheforte.

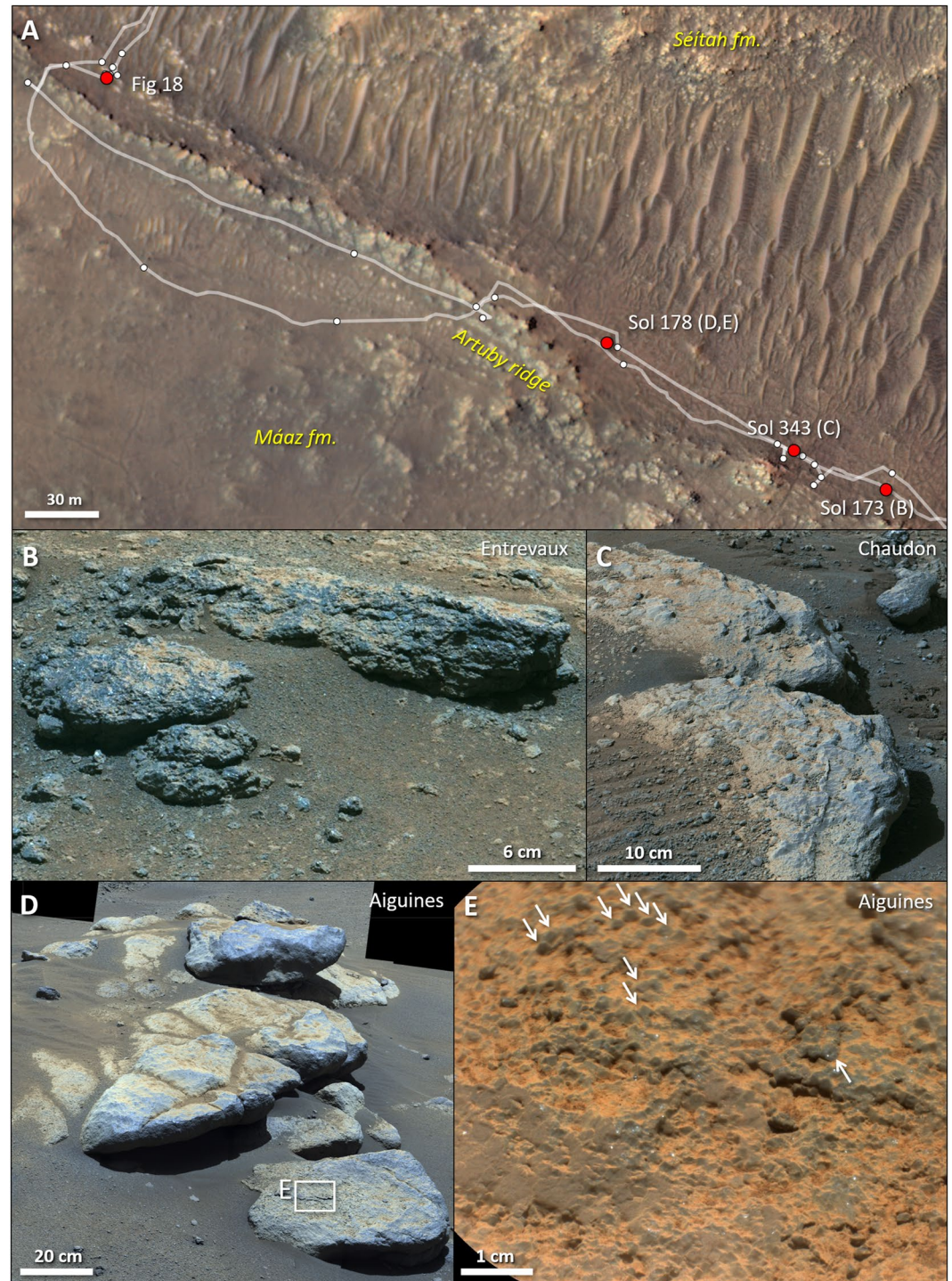
ascertained. The team remained concerned that any in situ investigation or sampling at Pilot Pinnacle would be hampered by lack of geological context, and Pilot Pinnacle was thus formally removed from the campaign plan.

#### 4.2. Observations From Polygon Valley

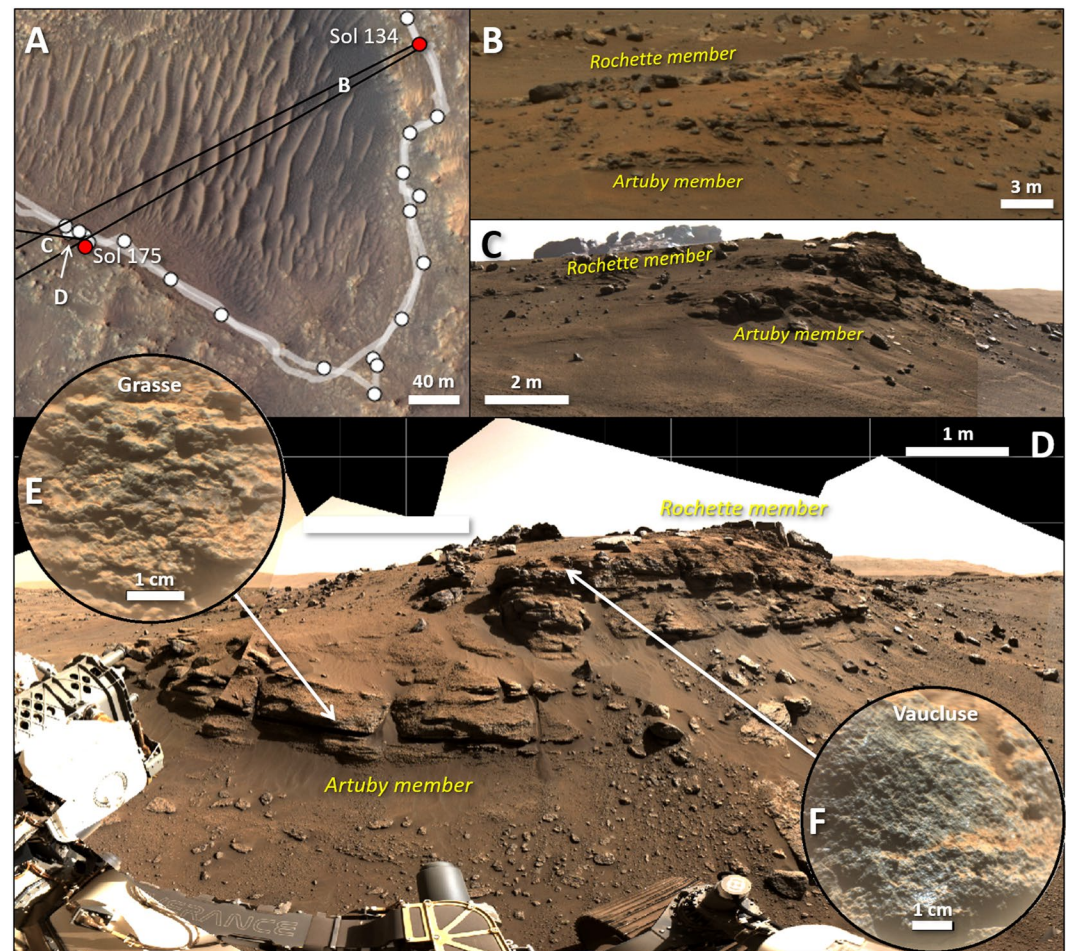
Beginning on sol 129, Perseverance began driving towards the southern Polygon Valley region (Figure 2b) where the team would aim to acquire their first sample of the mission, from the Máaz formation. At this time, Autonav capabilities had been fully released and so the team was able to make rapid progress towards Polygon Valley, covering more than 440 m in only four drive sols, whereas earlier drives had been less than 30–50 m/sol. During the drive south, Perseverance acquired several landscape mosaics of the Artuby ridge to the southwest, which would be helpful for contextualizing future observations when Perseverance traversed the ridge. On sol 136, Perseverance entered Polygon Valley and began searching for locations in which to perform the remaining sampling FTAs, including acquiring the first sample. Prior to launch, Perseverance's corer was installed with a “launch abrading bit” that provided a seal to the corer mechanism to protect against contamination (Moeller et al., 2020). To prepare for the first sample acquisition event, Perseverance had to perform turret cleaning (FTA-20), in which the turret would percuss (i.e., vibrate) in free-space (i.e., not in contact with a rock target) to shake off any potential terrestrial contaminants from the coring mechanisms. This would be followed up by FTA-21, which would deposit the launch abrading bit on the surface of Mars and pick up a new, uncontaminated abrading bit from the BC, to be used for abrasions during the remainder of the mission.



**Figure 11.** First abrasion at Guillaumes and first sampling attempt (FTAs 22–23) at Roubion from sols 157–168. (a) Orbital context showing the extent of the image shown in (b) at the Roubion sampling location. (b) Mastcam-Z enhanced color view of the Roubion workspace in the foreground, acquired after the Guillaumes abrasion, with Mure (Figure 9) in the background (sol 163, zcam08172; NASA/JPL-Caltech/ASU/MSSS/UH/F. Cary). (c) Mastcam-Z enhanced color view of the Roubion workspace after the Guillaumes abrasion (d) and the Roubion target had been cored, producing a pile of drill tailings (sol 166, zcam05075; NASA/JPL-Caltech/ASU/MSSS/K. Powell). The shadow cast in both (b, c) is due to the rover's extended arm. (d) WATSON image of the Guillaumes abrasion patch from 7 cm standoff, acquired on sol 160. White arrows point to irregularly shaped pits lined with dark material, and purple arrows point to a purple coating on the natural surface of the rock, exposed after dust removal by the gDRT. (e) Cachecam image of the Roubion sample tube prior to sealing, showing a mostly empty tube (diameter of 13 mm) except for several particles of martian dust (black arrows, sol 164).



**Figure 12.** Examples of olivine-rich rocks along the base of Artuby ridge, indicating the closest extent of the Séítah formation to Artuby ridge and the Mááz formation. (a) Orbital context showing the locations of the rocks in (b–e) and Figure 18, with sol numbers annotated. (b) Mastcam-Z enhanced color image of the Entrevaux target, showing a crumbly texture (sol 173, zcam03203). (c) Mastcam-Z enhanced color image of the Chaudon target (sol 343, zcam03311). (d) Mastcam-Z enhanced color image of the Aiguines target (sol 178, zcam08193; NASA/JPL-Caltech/ASU/MSSS/K. Powell). (e) Supercam RMI of the Aiguines target, with individual crystals, inferred to be olivine crystals (compare with Figure 16e), indicated by white arrows (sol 178, scam01178).



**Figure 13.** Various perspectives of the main outcrop of interest along Artuby ridge (first imaged on sol 116; see Figure 6f) showing the Artuby member and the Rochette member. (a) Orbital context showing the extent of images shown in (b, c) and the location of (e). Sol numbers are annotated. (b) Mastcam-Z enhanced color view of Artuby ridge showing the layered Artuby member along the face of the ridge and the Rochette member at the top of the ridge (sol 134, zcam08138; NASA/JPL-Caltech/ASU/MSS), corresponding to the viewshed in (a). (c) Navcam mosaic of the same outcrop on sol 175, corresponding to the viewshed in A the sols before Perseverance approached the front of the outcrop. The Rochette member at the top of the ridge is more apparent from this perspective. (d) Navcam mosaic of the same outcrop on sol 177 when Perseverance approached the front of the outcrop. (e) Supercam RMI of the Grasse target, representative of the Artuby member (sol 177, scam01177). (f) Supercam RMI of the Vaucluse target, representative of the Rochette member (sol 177, scam03177).

While the team waited for this pair of FTAs to be ready for execution, the team identified and arrived at a suitable parking location on sol 138 which provided a workspace with sufficiently large rocks on which to perform the FTAs (Figures 8a and 8b). This workspace was also scientifically interesting as the science team could make PS observations of the pavers in the workspace (targets Foux and Beaujeu), as well as observe how the low-lying pavers, later named the Roubion member (Figure 4b), grade into the higher-standing rockier outcrops of the Ch'al or Rochette member (Figure 4b; Crumpler et al., 2023; Horgan et al., 2022) along the eastern edge of this region (Figure 8e). Though the Roubion member shares many morphologic characteristics as the pavers of the Naa'taanii member, it was distinguished as a separate member due to its distinctly lower elevation as well as possibly compositional differences (Section 5.1.1; Crumpler et al., 2023; Horgan et al., 2022; Udry et al., 2023).

In some areas of this workspace, the Roubion pavers transition into higher-standing nubs (Figure 8f) in a manner similar to what was observed near OEB Landing (Figure 3f). Natural surface observations of the Foux and Beaujeu targets (Figure 8c) again showed dust-covered surfaces on these pavers and fluorescence from SHER-LOC data (Section 5.3). From sols 147–150, both the turret cleaning and launch Abrade Bit dropoff FTAs were

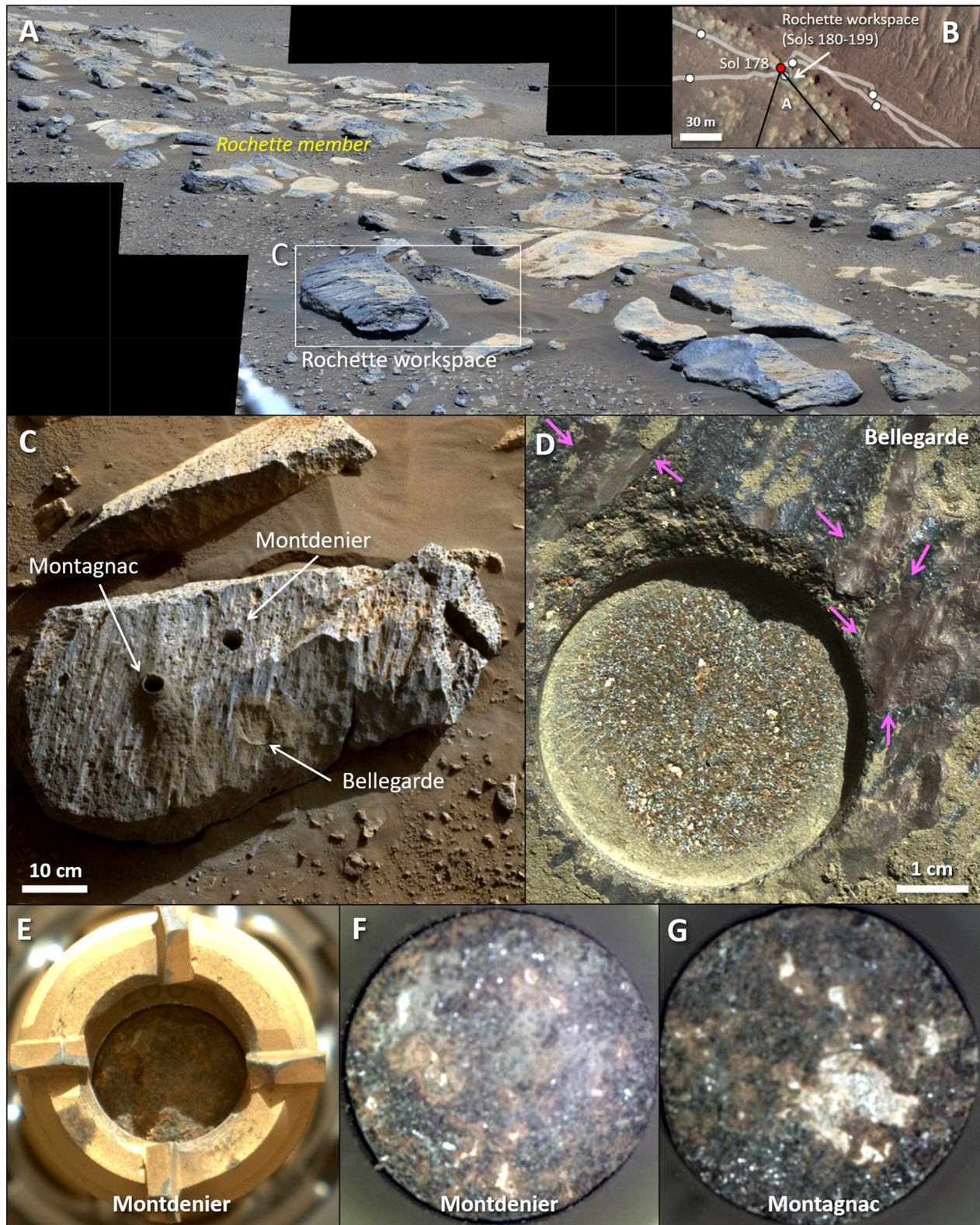
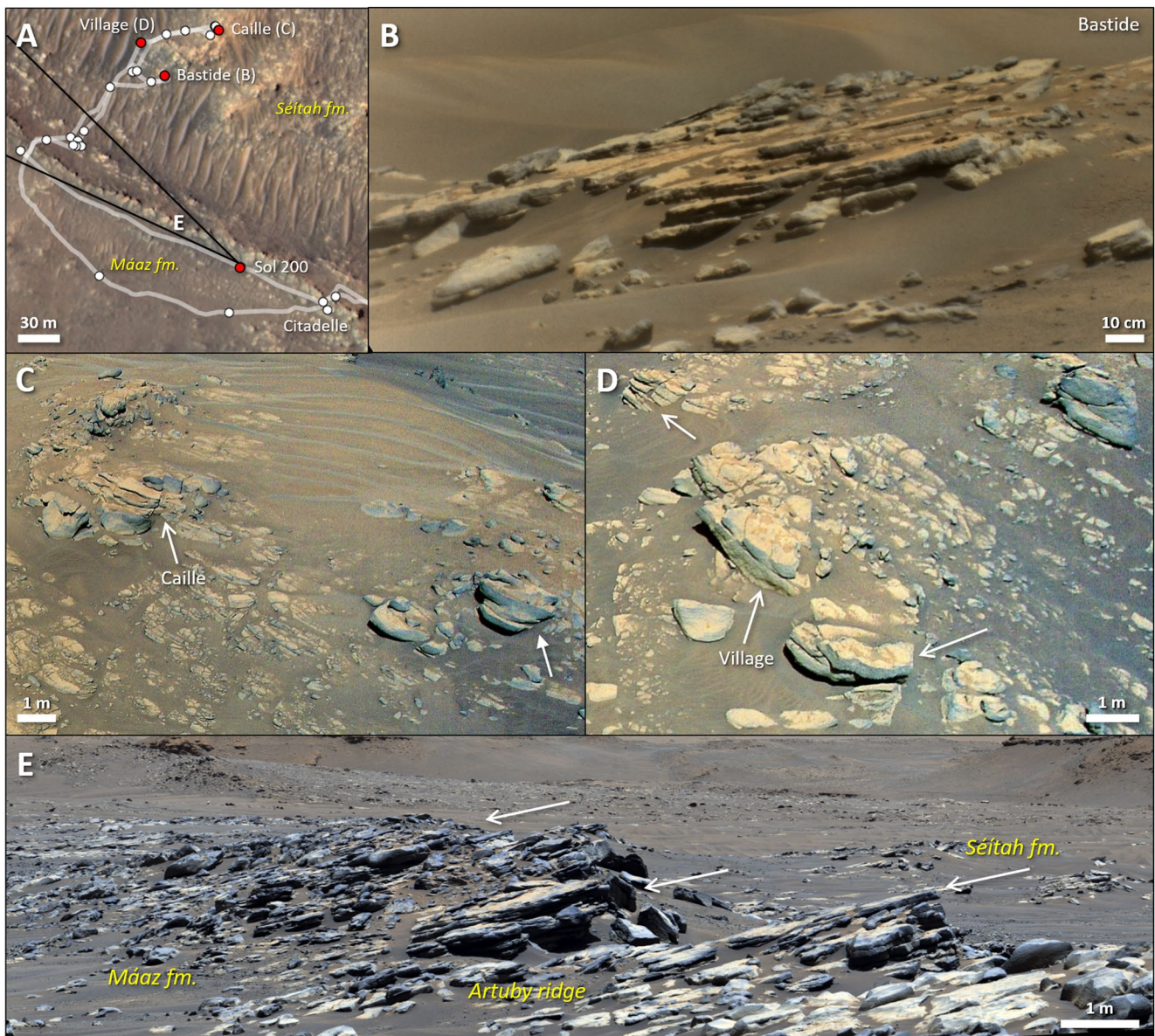


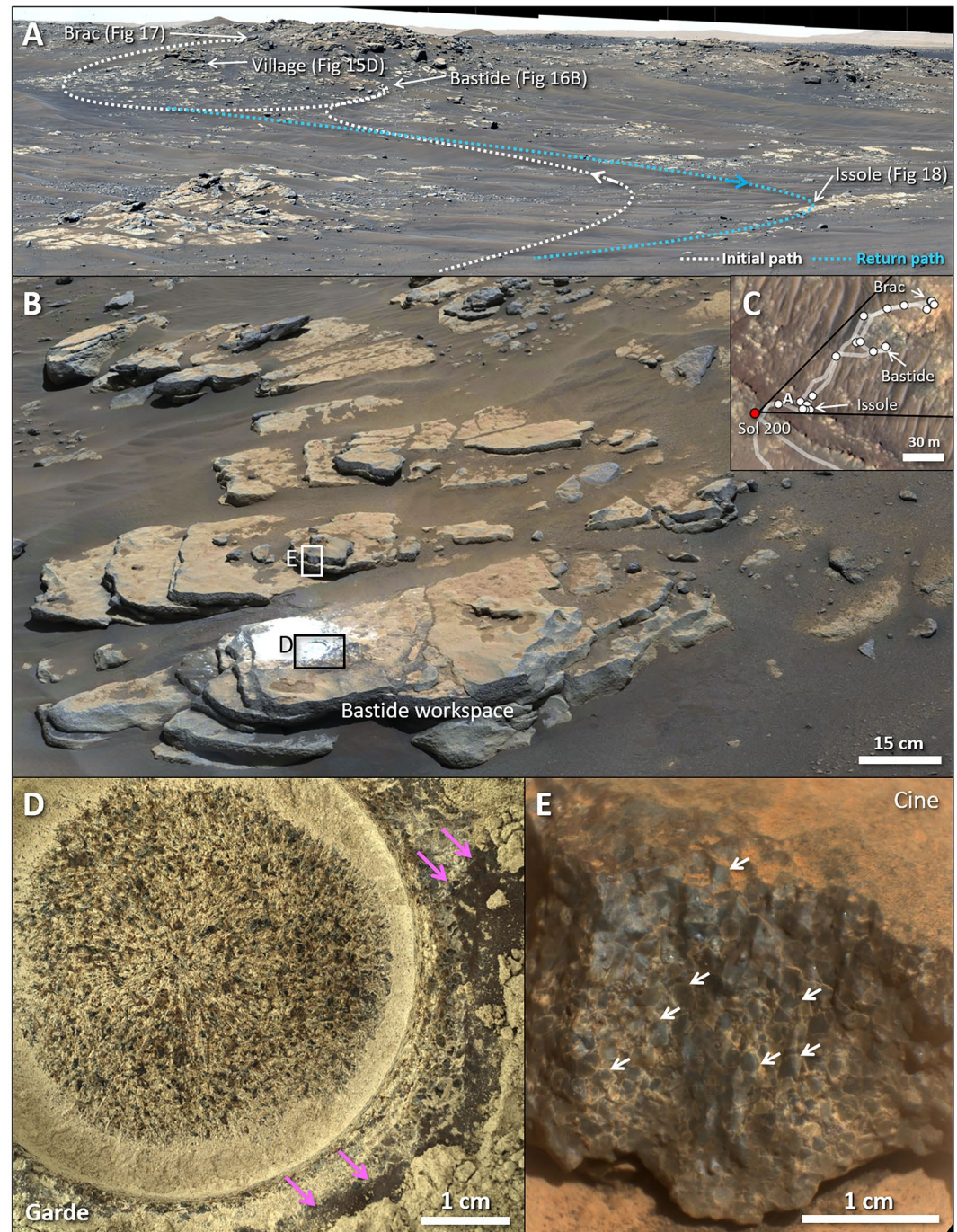
Figure 14.



**Figure 15.** Reconnaissance imaging of South Séítah and observations along Artuby ridge during the drive to the South Séítah toedip area. (a) Orbital context showing the extent of imaging shown in E and the locations of the Séítah outcrops observed during reconnaissance prior to starting the South Séítah toedip. Sol numbers are annotated. (b) Supercam RMI image of the Bastide target (Figure 16), showing layering on the order of several centimeters. VISIR observations of this target also revealed the presence of olivine in this outcrop (sol 194, scam01194). (c) Helicopter Flight 12 images of the Caille outcrop (Figure 17), showing potential layering, as well as neighboring outcrops with more thickly layered or massive textures (white arrows). (d) Helicopter Flight 12 images of the Village outcrop, showing more thickly layered or massive outcrops (white arrows). (e) Mastcam-Z enhanced color mosaic of the tilted layered rocks (Rochette member) along the top of Artuby ridge (sol 200, zcam08217, NASA/JPL-Caltech/ASU/MSSS/K. Crawford). These rocks at the surface appear to be tilted and dipping towards the southwest.

**Figure 14.** Context for the first rock samples acquired, from the Máaz formation Rochette member, on the Rochette block. (a) Mastcam-Z enhanced color view of the Rochette block and other Rochette member blocks at the top of Artuby ridge at the Citadelle location (sol 180, zcam08195, NASA/JPL-Caltech/AS/MSSS/L. Mehall). (b) Orbital context showing the viewshed for A (during the approach to Rochette) and the location of the Rochette workspace from sols 180–199. Sol numbers are annotated. (c) Navcam image of the Rochette rock on sol 196 after abrading the Bellegarde target and collecting the Montdenier and Montagnac sample cores. (d) WATSON image of the Bellegarde abrasion from 25 cm standoff on sol 188. Purple arrows indicate where a purple-toned coating is present on the natural surface of the rock after surficial dust has been removed by the gDRT. (e) Mastcam-Z imaging of the coring bit containing the Montdenier core after the first sampling attempt after Roubion. This was taken on sol 190 shortly after coring in order to confirm the presence of a rock core in the bit (sol 190, zcam05076) (f) Cachecam image of the Montdenier sample core on sol 194. The cores are 13 mm in diameter. (g) Cachecam image of the Montagnac sample core on sol 196.





**Figure 16.** Context for the South Séítah toedip traverse and the Garde abrasion at the Bastide workspace. (a) Mastcam-Z enhanced color mosaic looking into Séítah from the South Séítah toedip entrance (sol 201, zcam08221, NASA/JPL-Caltech/ASU/MSS/L. Mehall), with key outcrops and abrasion/sampling locations annotated. (b) Mastcam-Z enhanced color mosaic of the Bastide outcrop with context for the Garde abrasion (d) and the Cine target (e) (sol 207, zcam08235, NASA/JPL-Caltech/ASU/MSS/K. Powell). (c) Orbital context showing the viewshed for A and the locations of outcrops identified in (a). (d) WATSON image of the Garde abrasion patch from 25 cm standoff on sol 206. Purple arrows indicate purple-toned coatings on the natural surface of the rock. (e) Supercam RMI of the Cine target, with white arrows indicating distinct gray-colored crystals, later confirmed to be olivine crystals through VISIR and LIBS data (sol 206, scam01206) and corroborated by results from the abrasion patch (d).

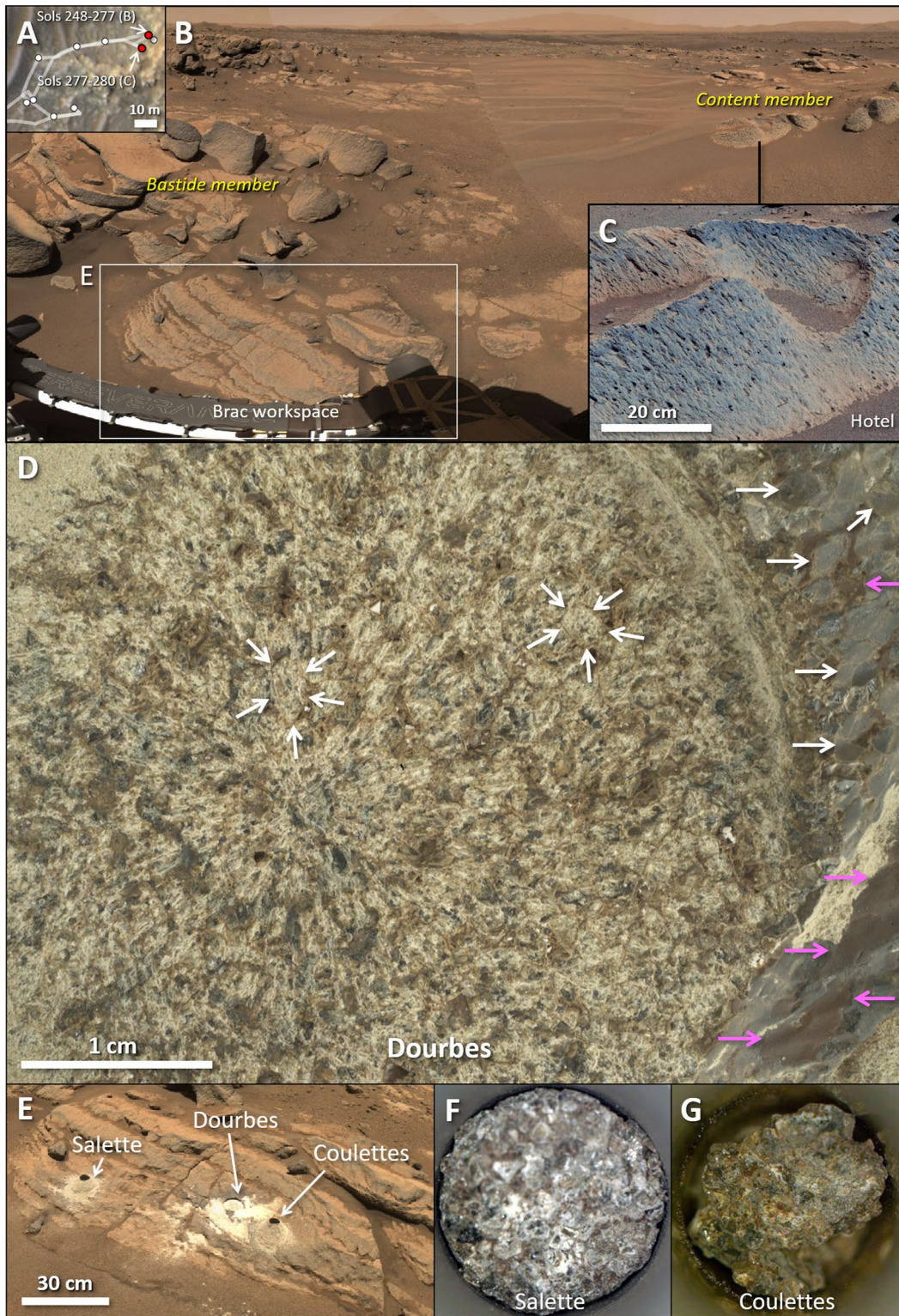
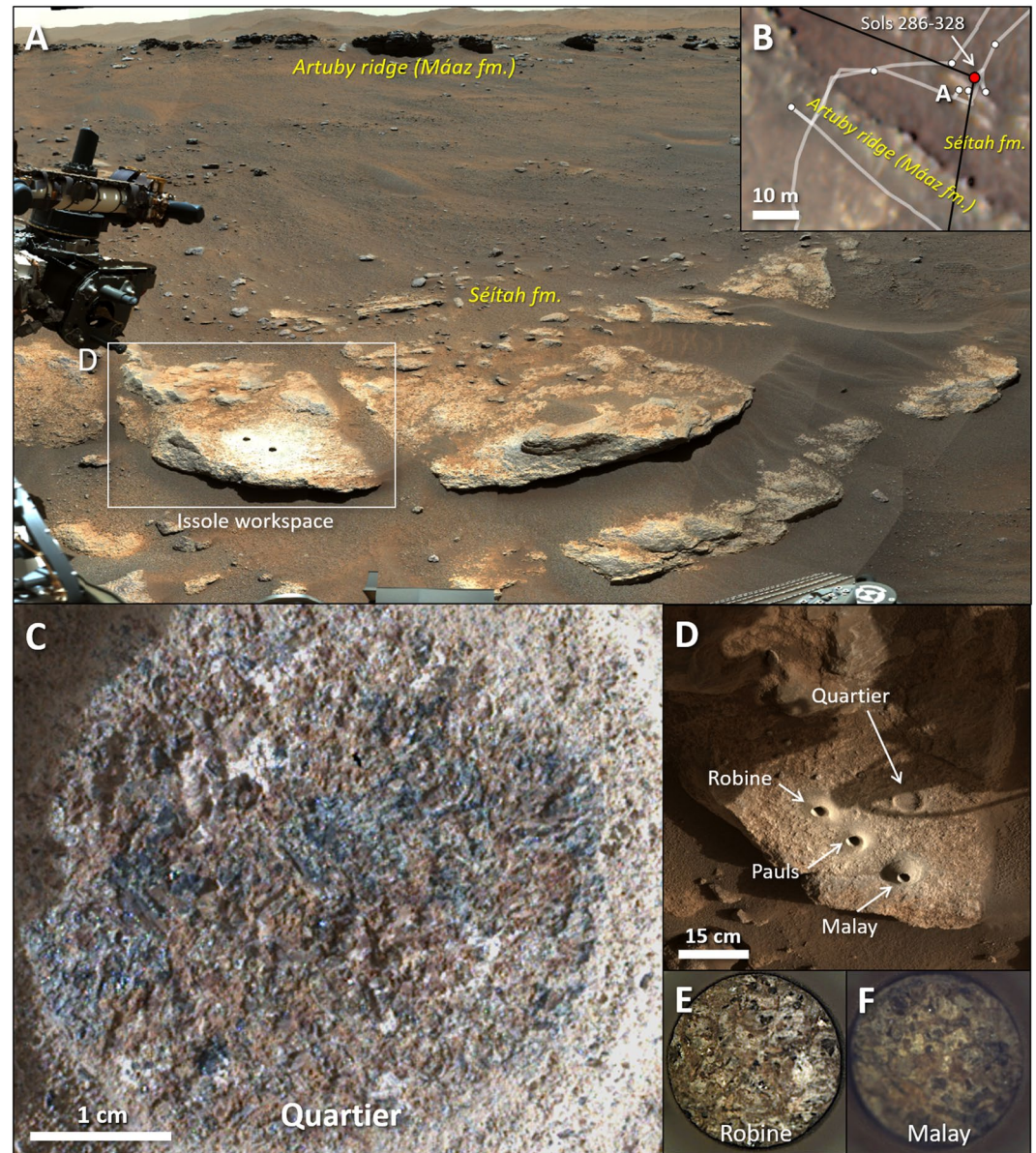
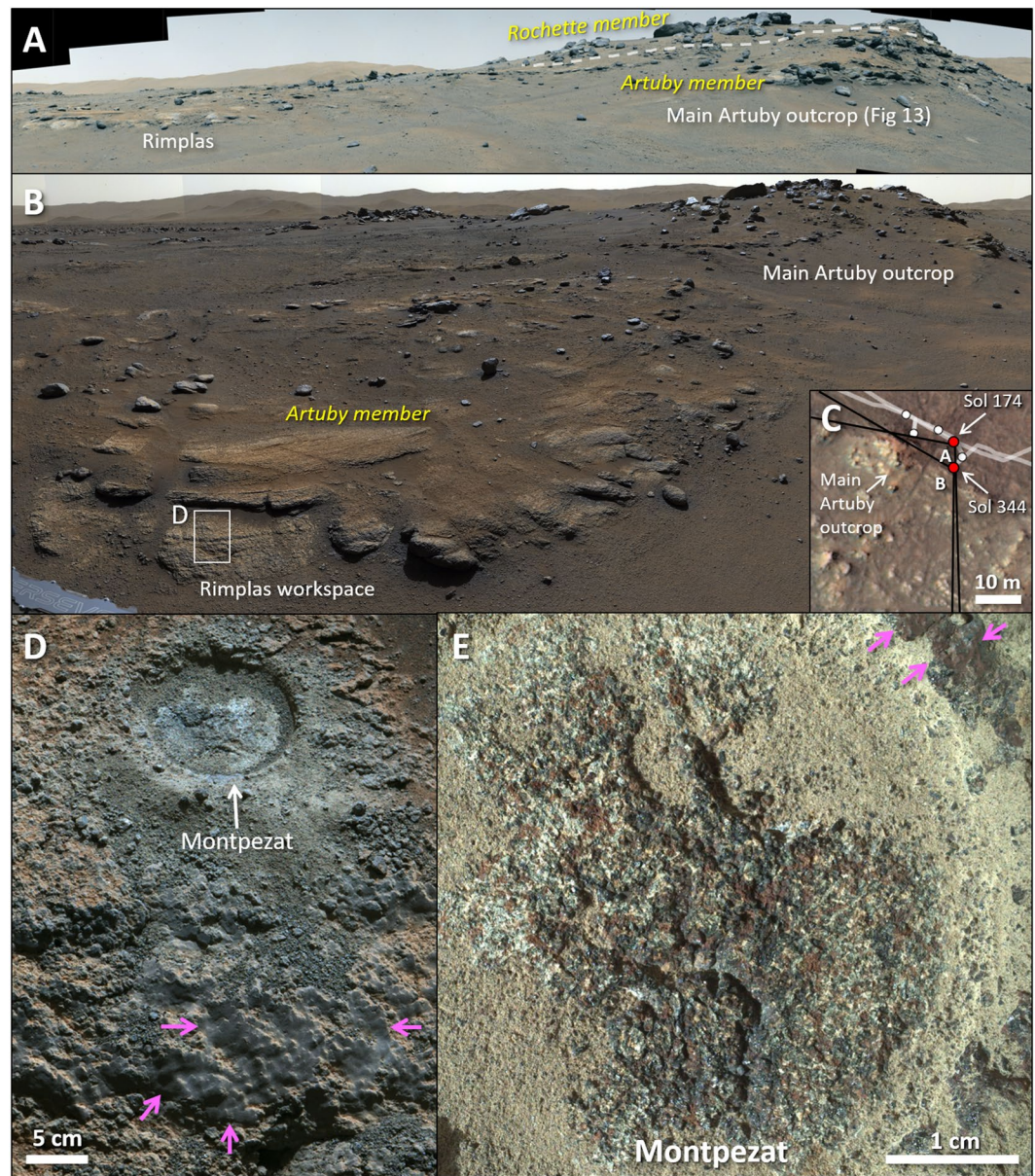


Figure 17.



**Figure 18.** Context for the second Séítah sample pair, acquired at the Issole workspace. (a) Mastcam-Z enhanced color view of the Issole workspace, after the Quartier abrasion and the Robine and Pauls sampling attempts (sol 320, zcam08341, NASA/JPL-Caltech/AS/MSSS/C. Rojas). Note the expansive regolith cover obscuring the contact between the Séítah formation (Issole workspace) and the Máaz formation (Artuby ridge). (b) Orbital context showing the extent of imaging shown in (a). Note the four different rover positions around the Issole workspace, needed to reposition the rover to recover from the pebble anomaly and re-acquire the second core, this time of the Malay target. (c) WATSON image of the Quartier abrasion patch from 7 cm standoff on sol 292. (d) Navcam image of the Issole workspace on sol 337 after acquiring the Malay core. (e) Cachecam image of the Robine sample core on sol 298. The cores are 13 mm in diameter. (f) Cachecam image of the Malay sample core on sol 337.

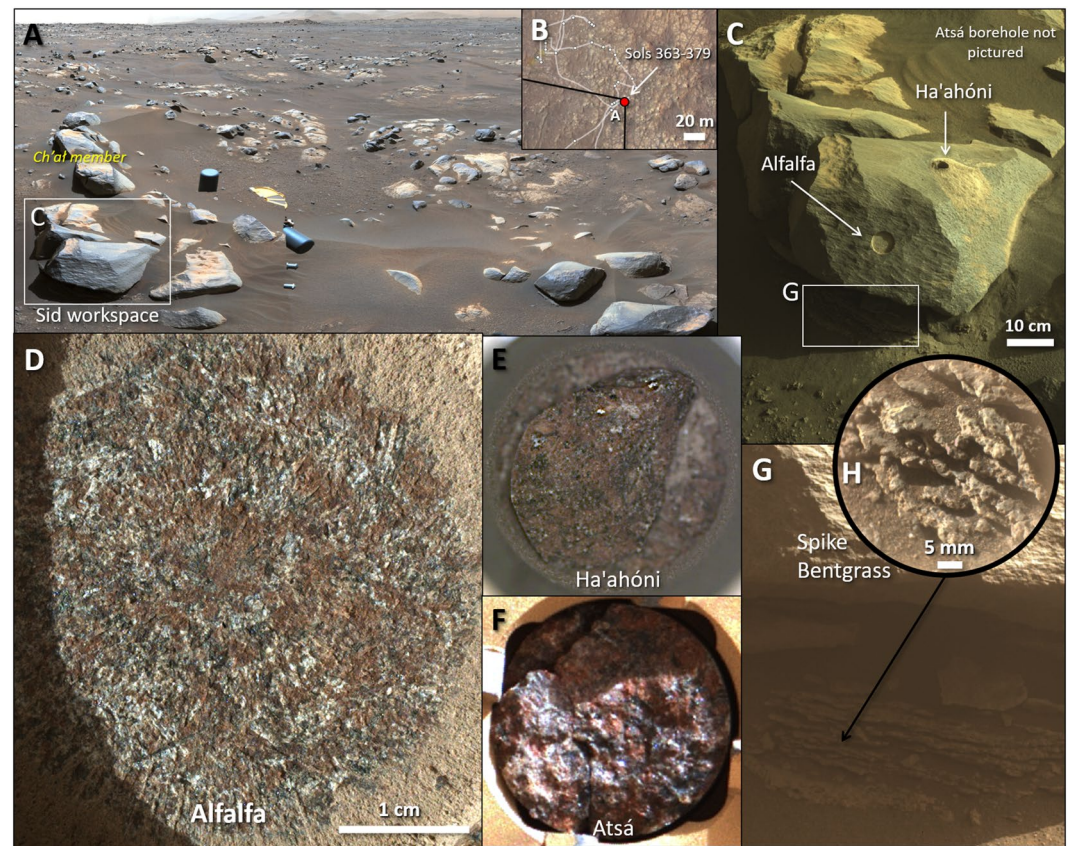
**Figure 17.** Context for the first Séítah sample pair, acquired at the Brac workspace. (a) Orbital context showing the locations of (b, c). (b) Navcam mosaic from sol 248 showing the local distribution of the layered olivine-bearing Bastide member and the pitted, non-olivine-bearing Content member. (c) Mastcam-Z enhanced color image of the Hôtel target to show the pitted texture of the Content member (sol 256, zcam03254). (d) WATSON image of the Dourbes abrasion patch from 7 cm standoff on sol 253. Purple arrows indicate where a purple-toned coating is present on the natural surface of the rock, and white arrows indicate gray olivine crystals on the natural surface, which appear as tan-colored olivine crystals, sometimes rimmed with brownish material, in the abraded patch. (e) Front Hazcam image of the Brac workspace on sol 275 after abrading Dourbes and collecting the Salette and Coulettes sample cores. (f) Cachecam image of the Salette sample core on sol 262. The cores are 13 mm in diameter. (g) Cachecam image of the Coulettes sample core on sol 271.



**Figure 19.** Context for the Montpezat abrasion at the Rimplas workspace, to the east of the main Artuby outcrop. (a) Mastcam-Z enhanced color view of the Rimplas and main Artuby outcrop (Figure 13) from the sol 174 location, showing possible lateral equivalency with the lower Artuby member (zcam08187, NASA/JPL-Caltech/AS/MSSS/L. Mehall). (b) Mastcam-Z enhanced color view of the Rimplas workspace with the main Artuby outcrop in the background, from the sol 344 location (zcam08371, NASA/JPL-Caltech/AS/MSSS/C. Rojas). (c) Orbital context showing the extent of images shown in A and (b). (d) Mastcam-Z enhanced color image of the Montpezat abrasion patch (sol 350, zcam03318). Purple arrows point to a smooth coating on the natural surface of the rock. (e) WATSON image of the Montpezat abrasion patch from 7 cm standoff on sol 346. Purple arrows point to a purple-toned coating on the natural surface of the rock.

completed, resulting in the launch abrading bit being deposited onto the surface of Mars (coincidentally where the Beaujeu observation occurred; Figure 8d).

While at this workspace, the team also deliberated where to drive next in order to perform the remaining two sampling FTAs: first abrasion and dust clearing, and first core collection and sample processing (Table 2). The pavers at the southernmost tip of Polygon Valley were favored for these important events, as preliminary imaging in that direction indicated that there would likely be sufficient workspace on those pavers on which to abrade and sample. This location would also take Perseverance closer to Artuby ridge, which extended into this southern



**Figure 20.** Context for the second Mááz sample pair (of the Ch'al member), acquired at the Sid rock. (a) Mastcam-Z enhanced color view of the Sid workspace and surrounding area (sol 363, 364, 369; zcam08394, zcam08396, zcam8401; NASA/JPL-Caltech/AS/MSSS/L. Mehall). There are some artifacts showing portions of the rover, resulting from stitching different mosaics together. (b) Orbital context showing the viewshed of (a). Note Perseverance's location on the polygonal paver terrain and how this terrain is continuous at the larger orbital scale. (c) Navcam image of the Sid block on sol 371, after the Alfalfa abrasion and Ha'ahóni coring. (d) WATSON image of the Alfalfa abrasion patch from 7 cm standoff on sol 367. The left side of the image is shadowed by the wall of the abrasion patch. (e) Cachecam image of the Ha'ahóni sample core on sol 371. The cores are 13 mm in diameter. (f) Mastcam-Z imaging of the coring bit containing the Atsá core (sol 377, zcam05068). Note that Cachecam images of Atsá were not acquired due to an engineering issue while the imaging was occurring during a communications pass. (g) Front Hazcam image showing likely Naa'tánii member layering under the Sid block on sol 362. The image has been stretched to illuminate the layers in the shadows. (h) Supercam RMI image of the Spike Bentgrass target, showing the rubbly nature of these potential layers (sol 365, scam01365).

area and also exhibited layering (e.g., in the Mure outcrop, Figures 2b and 9) that could be studied by the team while parked at the abrasion and sampling location. Perseverance departed the FTA-20/21 location on sol 153 and proceeded to drive to the Roubion sampling location.

#### 4.2.1. Removal of Mont Rocheforte From the Campaign Plan

Perseverance and Ingenuity acquired several observations of the ridges of Mont Rocheforte in order to assess whether an in situ investigation was warranted (Section 3.3.4). Mastcam-Z imaging (Figure 10c) and multispectral observations of Mont Rocheforte did not reveal any physical indications of fill material between the ridges or compositional variations among the Mont Rocheforte rocks that could suggest a fracture fill of different composition than the host Mááz formation rocks. The Ingenuity helicopter, which had been flying and keeping pace with Perseverance, was now being used to perform reconnaissance in support of the science campaign. Ingenuity's tenth flight on sol 152 approached and imaged Mont Rocheforte from a much closer position than Perseverance, and the returned images also showed that the space between the ridges was regolith-covered with no obvious evidence for fracture fill (Figures 10b and 10d). With this information from both Mastcam-Z and Ingenuity datasets, the science team eventually decided to forgo an in situ investigation of Mont Rocheforte and to allocate those sols to a different, to be determined, target of opportunity.

### 4.3. First Sampling Attempt at Roubion

On sol 157 Perseverance made its precision approach to the workspace where it would attempt to perform the first abrasion and sampling FTAs (FTA-22, 23). This particular workspace, representative of the Roubion member (Figures 11a and 11b), was chosen on the basis of having sufficient paver surface area on which to perform the abrasion and sampling, including space to place the drill stabilizers, as well as the ability to place the rover at an appropriate tilt for abrading and drilling. From sols 157–163, the sampling sol path proceeded largely as designed (Section 1.5). The first abrasion produced an abrasion patch of ~8 mm depth at the Guillaumes (Figure 11d) target, on which SHERLOC, WATSON, and PIXL observations were acquired after dust clearing by the gDRT (Simon et al., 2023).

The Guillaumes abrasion revealed a pitted and heterogeneous texture dissimilar to the dust-covered, granular surface of the rock. The interior of the rock was composed of light-toned, dark-toned, and brown patches and grains/crystals approximately 0.5 mm in diameter. The overall texture was initially remarked to resemble that of a fine-grained gabbro or holocrystalline basalt (Simon et al., 2023). Several irregular pits, approximately ~5 mm in diameter and a few mm deep, were also observed and appeared to be lined with the dark-toned material (white arrows in Figure 11d). Plagioclase and pyroxene (notably no olivine) were associated with the dark-toned grains, Ca-sulfate, halite, perchlorate, and phosphate with the white patches, and Fe-oxides in the brown-toned patches. On the natural, unabraded surface of the rock, the removal of dust by the gDRT now exposed occurrences of purple-toned coatings (purple arrows in Figure 11d; Garczynski et al., 2022). The diversity of alteration phases suggested for the first time in the campaign that multiple aqueous episodes may have affected the crater floor rocks (e.g., Farley et al., 2022; Tice et al., 2022; Wiens et al., 2022).

The first sampling event was planned for sol 164 on the Roubion target, after which the Roubion member in the Mááz formation was later named (Figure 4b). From the initial automated engineering data returned, no abnormalities were detected, and it appeared that sample collection and tube processing was fully successful, resulting in a sealed sample tube. However, it soon became apparent that no rock core was collected in the Roubion sample tube, as the tube appeared empty in Cachecam images and was confirmed by the volume probe (Figure 11e). From sols 165–168, the team investigated reasons for the “missing” core and took extensive imaging around the rover and in the workspace to see if the core may have fallen out of the tube. No missing core was found, and eventually it was determined that the most likely scenario was that the Roubion target was too low strength and disintegrated during the act of coring (Farley et al., 2022; Simon et al., 2023).

### 4.4. Investigations at Mure and Artuby Ridge

#### 4.4.1. Observations at the Mure Outcrop

On sol 168, Perseverance drove away from the Roubion sampling location after obtaining comprehensive imaging of the workspace and rover surroundings. Although the cause of the Roubion missing core had not yet been ascertained at that time, the team decided that the most expedient path forward was to proceed with the campaign while the engineering investigation into the missing core continued in parallel. Perseverance then drove ~30 m south to an outcrop called Mure, which from orbital data appeared to be an extension of the main Artuby ridge (Figures 4a and 9a) and in closer imaging contained layering similar to that observed in the initial observations of Artuby ridge (Figures 6 and 9b). As escarpments at the edge of the Mááz formation, both Mure and Artuby ridge were considered to contain, at least in part, Mááz formation rocks. The location of the Mááz-Séítah contact was still to be identified, and the motivation for studying the Mure outcrop was to see if there was any evidence for Séítah formation rocks in its vertical exposure.

Observations at the Mure outcrop revealed at least two distinct lithologies exposed along the face of the outcrop (Figures 9c–9e), in contrast to the low-lying pavers of the Roubion member that Perseverance just attempted to sample. However, the relationship of the Mure outcrop to the rest of the Maaz formation is unclear (Crumpler et al., 2023; Horgan et al., 2022). In some locations, the base of the Mure outcrop exhibits crude layering and a granular texture, which may be an outcrop view of the Roubion member but is also similar to outcrops encountered later along the base of Artuby ridge and named the Artuby member (Figures 4 and 9d). This lithology is overlain by a more competent and thickly layered to massive member possibly analogous to Artuby ridge cap rocks later named the Rochette member (Figures 4 and 9e). Despite the difference in textures, there was no

significant difference in bulk composition as measured by SuperCam (e.g., Wiens et al., 2022). Importantly, neither lithology contained the olivine signatures characteristic of the Séítah formation, thus the Artuby and Rochette members were considered part of the Mááz formation. Observations of the rocks adjacent to this main outcrop showed the presence of apparent layers, some of which appear pinched or wavy, as well vesicular textures following the planes of some layers (right side of Figure 9f).

#### 4.4.2. First In Situ Detections of Olivine in Rocks Along Artuby Ridge

From sol 169–176, Perseverance drove along the base of Artuby ridge, acquiring RS of the Artuby ridge rocks to the port side of the rover as well as imaging towards Séítah to the rover's starboard side. The team also searched for rocks along the drive to perform compositional analyses with SuperCam LIBS and VISIR to see if there was an identifiable contact in the form of a transition from olivine-bearing Séítah formation rocks to olivine-poor Mááz formation rocks. Up until this point in the mission, olivine had never been detected in rocks, only in soils in the Mááz formation (e.g., Vaughan et al., 2023; Wiens et al., 2022). However, two observations along the base of Artuby ridge, on rock targets Entrevaux (sol 173) and Aiguines (sol 178) (Figure 12) were significant because olivine was identified in the SuperCam LIBS (via a ratio of Fe + Mg/Si converging towards 2) and VISIR data (via olivine's one micron reflectance feature). This indicated that Perseverance had encountered Séítah rocks in situ for the first time on the mission (e.g., Wiens et al., 2022).

These Séítah rocks appeared texturally different from previously encountered Mááz formation rocks as well, appearing more crumbly in nature (Figure 12b). Closer inspection with Supercam RMI imaging also revealed the presence of individual grains or crystals (Figure 12e), which were later identified as olivine crystals when correlated to the textural and compositional results from later targets such as Cine from the Bastide workspace at South Séítah (Section 4.6.2). Future observations along the base of Artuby ridge would bolster these results: targets at the Issole workspace on sol 202 at the South Séítah toedip entrance and the Chaudon target on sol 343 (Figure 12c) during the return trip to OEB also were determined to be olivine-bearing rocks of the Séítah formation. Despite these detections of olivine-bearing Séítah rocks in close proximity to Artuby ridge and the Mááz formation, the precise contact between the Mááz and Séítah formations remained hidden, as much of the terrain was obscured by regolith and sand.

#### 4.4.3. Observations at Artuby Ridge

On sol 177, Perseverance also stopped in front of the original Artuby ridge outcrop that was first imaged on sol 116 (Figures 6f and 13) in order to perform in situ observations of the rocks that make up this ridge. Similar to what was observed at Mure (Section 4.4.1), the team observed two Mááz formation lithologies making up Artuby ridge: a rubbly lithology forming coarse layering (Artuby member, Figures 4b and 13e) and a more competent caprock unit overlying the rubbly lithology (Rochette member, Figures 4b and 13f). The stratigraphic position of the Rochette caprock member above the Artuby member was especially visible from Perseverance's position on sol 175 prior to approaching the front of the Artuby outcrop (Figure 13c). There was again no significant difference in composition between the two members, similar to what was observed at Mure (Wiens et al., 2022). The team was especially interested in the nature of the layered Artuby member and whether its origins were sedimentary or igneous (Alwmark et al., 2023). Conversations about future investigation of the Artuby member would continue throughout the campaign and result in the investigation of the adjacent Rimplas outcrop (Section 4.9) during the return trip back to OEB.

#### 4.5. First Mááz Sample Pair at Rochette

Between sols 178–180, after Perseverance's investigations at Artuby ridge, it traversed back up to the Mááz formation at the Citadelle crossing point (Figure 2). During the Artuby ridge traverse, the team decided to reattempt sampling activities again at the top of Citadelle. This decision was made for both science and engineering reasons. Because it was hypothesized that Roubion was too low-strength to be collected as a rock core, the sampling reattempt was desired to be on more competent rock, in part to increase the chance of successful rock core collection and to prove that Perseverance's sampling capabilities were working as expected despite the attempt at Roubion. Based on observations at the Mure and Artuby ridge outcrops (Section 4.4), the Rochette caprock at Citadelle was inferred to be more competent (Figure 13) and therefore favored for the sampling reattempt from an engineering perspective. Sampling the Rochette member was also favored from a science perspective as the cumulative

observations from the campaign led the team to interpret these rocks as a Mááz formation lithology that was different from those previously encountered.

Sampling at the Rochette outcrop therefore commenced on sol 180 with a precision approach to place the rover in position for abrasion and sampling (Figure 14). On sol 185, the Bellegarde abrasion patch (10 mm abrasion depth) was created and subsequent PIXL, SHERLOC, and WATSON observations were made on the abrasion. In contrast to the jagged edges of the Guillaumes abrasion patch (Figure 11d), which demonstrated the crumbly and disintegrative nature of the Roubion coring target, the edges of the Bellegarde abrasion patch were immediately recognized as being sharper (Figure 14d), a promising indication that these Rochette member rocks were more competent than the Roubion member rocks. Similar to the Guillaumes abrasion, the team observed that the rock interior was composed of light-toned, dark-toned, and brown grains/crystals and patches which measured 0.2–0.5 mm in diameter. Light-toned patches appeared in a variety of shapes, suggesting that they were void-filling alteration products like Ca sulfates and Ca phosphates (Figure 14d). One such light-toned patch was even captured at the bottom of the Montagnac core (Figure 14g). Dark-toned crystals were identified as pyroxene, plagioclase, and FeTi oxides, and brown-toned areas were associated with Fe oxides. Overall, the bulk composition of the Bellegarde abrasion patch was consistent with an aqueously altered basalt, though less altered than the Guillaumes abrasion patch (e.g., Tice et al., 2022). The unabraded surface near Rochette also contained purple-toned coatings as well, similar to what was observed outside the Guillaumes abrasion patch (Garczynski et al., 2022; Figure 11d).

In this sampling reattempt, the sampling activities, originally planned to occur on one sol (Text S2 in Supporting Information S1), were split up over the course of three sols in order to ensure over ground-in-the-loop cycles that there was rock core present in the tube before the irreversible sample tube sealing process. On sol 189, Perseverance inserted a sampling tube into the coring bit and exchanged the bit previously used for abrasion. On sol 190, the Montdenier core was collected, and the sampling sol path was updated to include additional activities to image the sample tube before and after the sample was ingested (Figure 14e). On sol 192, after confirmation that a rock core was successfully acquired in the tube, the Montdenier sample tube was processed and sealed. With successful acquisition of the Montdenier core, its paired sample Montagnac was planned and also successfully acquired on sol 196, this time with all sampling activities occurring on a single sol since the Montdenier sampling events had gone smoothly. Sampling activities at Rochette fully completed by sol 199 (Simon et al., 2023).

#### 4.6. South Séítah Toedip

With the successful acquisition of the first rock cores from the Mááz formation, Perseverance then continued on the campaign drive path on sol 199 to enter the Séítah formation at South Séítah. Earlier, as Perseverance was still traversing Artuby ridge, the Ingenuity helicopter had been used to perform reconnaissance of the South Séítah toedip region during its twelfth flight on sol 174. The data returned by Ingenuity were used to inform both engineering and science teams about the exact toedip route (Figure 15). Rover Planners used the helicopter data in conjunction with orbital and rover images to plan the most efficient route between the science locations of interest. The science team used the helicopter images to identify outcrops that had layering and could be traced across larger spatial scales, which could be viable abrasion and sampling locations.

Ingenuity images and Mastcam-Z and Supercam observations showed a variety of outcrops in Séítah with varying degrees of apparent layering. Some outcrops such as Bastide and Caille appeared to have thinner layers (usually on the order of several cm thick, Figures 15b and 15c) whereas others such as Village appeared to have thicker layers (greater than 10 cm thick) or a massive texture (Figure 15d), causing the team to debate whether these differences in layering reflected differences in grain size. A fine-grained sample was desired from an astrobiological perspective, but in the absence of a fine-grained rock, the team wanted to collect at least one sample pair from an olivine-bearing and ideally carbonate-bearing rock (Section 3.4.4). One of the best candidates for sampling of thin layers, inferred to potentially be fine-grained, in Séítah were identified in the Bastide target, which was also assessed to be olivine-bearing based on remote Supercam VISIR data (Figure 15b). Bastide was therefore determined to be the first stop in the South Séítah toedip traverse. Acknowledging that more of Séítah may need to be explored in order to document the full geologic diversity of this unit, the team also planned a possible longer traverse extending out towards Caille (Figure 15a). The team decided to not traverse further into



Séítah past Caille, due to the time it would take to navigate the sandy terrain and the relative lack of nearby outcrop beyond Caille.

#### 4.6.1. Tilted Rocks in Artuby Ridge and Séítah

Surface and subsurface observations extending from Citadelle to the South Séítah toedip region, and then to Bastide, revealed that the Máaz and Séítah rocks near Artuby ridge are tilted. Mastcam-Z images parallel to Artuby ridge showed that the Rochette and Artuby member rocks at the top of the ridge dip about  $10^{\circ}$ – $15^{\circ}$  to the southwest (white arrows in Figure 15e; Farley et al., 2022). These surface observations were corroborated by subsurface RIMFAX observations that showed a similar southwest dip (Hamran et al., 2022), including in the adjacent Séítah rocks by the Issole outcrop (Figures 16a and 16c). The consistent southwest dips between both the Máaz and Séítah formations, as well as the observation of Séítah exposures being topographically higher than the Máaz formation, confirmed that the Máaz formation overlaid the Séítah formation, resolving a key stratigraphic objective of the campaign even if the Máaz–Séítah contact could not be directly observed. These results also initiated discussions of the processes that could have resulted in such a dip to the southwest; these rocks were likely not emplaced in this manner, thus there was likely a post-emplacement deformation process for one or both of the Máaz or Séítah formations that created this dip (Section 5.2.3; Farley et al., 2022).

#### 4.6.2. Abrasion at Bastide

Perseverance entered the Séítah formation at the South Séítah toedip entry point on sol 200 and began collecting more RS data of Séítah as it drove further into Séítah (Figure 16). On sol 204, Perseverance parked at the Bastide outcrop as planned. There, Perseverance abraded the Garde target (11 mm abrasion depth; Figure 16d) and acquired SHERLOC and WATSON on the abrasion patch, forgoing PIXL due to the higher relief of the Bastide block complicating PIXL placement. These observations revealed a much different lithology from the previous Guillaumes and Bellegarde abrasions and showed that the Garde abrasion patch was dominated by coarse olivine crystals, with pyroxene and feldspar crystals interspersed between the olivine crystals. Amorphous silicates, carbonate, and organics were also identified as likely secondary products (e.g., Clavé et al., 2023; Mandon et al., 2023; Tice et al., 2022). The identification of olivine grains in the Garde abrasion patch corroborated recent observations on the natural surface of these rocks as well. High-resolution Supercam RMI images of the Cine target revealed the presence of dark gray grains set in a lighter-toned and/or recessed matrix (Figure 16e); subsequent LIBS and VISIR measurements showed that the dark gray grains were associated with olivine signatures (e.g., Wiens et al., 2022). The observations at Cine shed light on similar textures observed earlier in the mission (e.g., Aiguines in Figure 12e) that had not been recognized as being indicative of olivine grains until this point in the campaign.

Thus, for the first time, Perseverance acquired in situ confirmation from its highest-resolution PS instruments that Séítah is an olivine-rich unit, as well as visual identification of olivine crystals on natural surfaces. In addition to these observations, a purple-toned coating was once again identified on Bastide's natural surface (Figure 16d), similar to what was observed on the natural surfaces of the Guillaumes and Bellegarde abrasions (Garczynski et al., 2022). Although the Bastide rock itself appears to be layered, the Garde abrasion was on top of the rock and therefore may not have crossed any layers; in any case no evidence of layering was apparent within the abrasion patch.

Though Bastide had been discussed as a potential sampling location, the PIXL placement difficulties precluded collection of the requisite STOP list data (Section 1.5) and therefore dissuaded the team from sampling as the collected cores would have incomplete abraded science documentation. The layered rocks in the Séítah formation would eventually be referred to as the Bastide member (Figure 4b), named after this outcrop.

#### 4.6.3. Conjunction and FSWX

After Bastide, Perseverance headed towards an outcrop named Caille, driving further towards the interior of the Séítah formation. This destination would mark the end of the South Séítah toedip and was chosen to maximize the chance of Perseverance encountering more layered and potentially fine-grained outcrops along the traverse (Figure 15). On sol 211, the rover arrived at the Village outcrop (Figure 16a), partway to Caille, and prepared to

park for approximately a month over Solar Conjunction when Perseverance would not be able to communicate with Earth due to the Sun being between Mars and Earth. Between sols 211 and 237, Perseverance remained parked at Village and performed a prescribed schedule of atmospheric and change detection activities as these did not require ground-in-the-loop over Conjunction. On sol 237, Perseverance came out of Conjunction and the operations team began preparing for Flight Software Transition (FSWX), during which the rover would once again have to remain parked for six sols while the rover flight software was updated. Prior to beginning FSWX on sol 243, Perseverance was able to drive to and park at the Caille location, and acquired a few RS observations before FSWX began.

#### 4.7. First Séítah Sample Pair at Brac

Once Perseverance exited FSWX on sol 248, it began the sampling sol path at the Brac rock, representative of the Bastide member (Figure 17). Preliminary observations of Brac showed it to have similar qualities as Bastide, including apparent layering and the presence of olivine from RS observations, which satisfied the desire to sample an olivine-rich rock from Séítah (Section 3.4.4). Brac had an additional advantage over Bastide in that the orientation of the rock allowed for placement of all PS instruments on the rock surface, including PIXL, which was not achievable at Bastide.

On sol 253, the Dourbes abrasion patch was created (abrasion depth of 7 mm) and subsequent abraded science observations were acquired on the patch. This data bolstered the results from Bastide (Section 4.6.2; Figure 16e) and showed clearly that the gray olivine crystals on the natural surface (white arrows to the right of Figure 17d) corresponded to the tan-colored olivine crystals in the abrasion patch, which sometimes appeared rimmed by brownish material (two such examples are indicated by white arrows in the center of Figure 17d). The olivine grains were relatively coarse-grained, measuring 1.2–1.8 mm in size. The darker grains between the olivine crystals were identified as pyroxene and plagioclase. Like in the Guillaumes and Bellegarde abrasion patches, the brown-toned materials in the Dourbes abrasion patch were associated with Fe-rich phases. Other alteration phases identified were sulfate, carbonate, and amorphous silicate, in addition to organics that did not have any apparent correlation with texture (Corpolongo et al., 2023; Sharma et al., 2022). The texture, mineralogy, and bulk chemistry of Dourbes was consistent with Brac and the Bastide member representing a cumulate igneous rock formed as olivine crystals settle in a slowly cooling lava body, with subsequent crystallization of pyroxene and plagioclase in the interstitial regions (e.g., Farley et al., 2022; Liu et al., 2022). Purple coatings (purple arrows in Figure 17d) were once again observed on the natural surface of the rock, and even though the Brac rock appears layered, no evidence of layering was observed in the Dourbes abrasion patch. The first Séítah sample, Salette, was then collected on sol 262 and its sample pair, Coulettes, was acquired on sol 271 (Simon et al., 2023).

##### 4.7.1. Non-Olivine-Bearing Rocks of the Content Member

After acquiring the Salette and Coulettes cores between sols 248 and 277, the science team decided to take a brief detour to investigate a target named Hôtel, which was a pitted rock outcrop near the Brac sampling location (Figure 17c). While parked for sampling at Brac, the science team acquired RS of the rover's surroundings and noticed several pitted rocks that did not contain olivine signatures (Wiens et al., 2022), which was anomalous in the context of the Séítah formation, which had been consistently olivine-rich from both orbital and rover observations to date. To better understand this second Séítah formation lithology, Perseverance drove to the Hôtel rock on sol 278 and prepared to abrade. However, a series of events precluded this detailed investigation at Hôtel, including the Deep Space Network going offline during the sol 274 uplink and subsequent complications that delayed Perseverance's arrival at Hôtel, less than 5 m from Brac. Once at Hôtel, Perseverance experienced an arm fault that precluded the abrasion activity. Given these challenges and the delays incurred thus far to the campaign sol path, the team decided that it was best to forgo abraded science at Hôtel and move on to obtain the second set of Séítah samples to get back onto the campaign schedule.

#### 4.8. Second Séítah Sample Pair at Issole

Perseverance then began retracing its steps to exit Séítah, with the plan to acquire a second Séítah sample pair on the way out of Séítah (Figure 18). While sampling at the Brac outcrop, the team decided on where to perform the next abrasion and sampling. With the highly desired fine-grained rocks still remaining elusive (Section 3.4.4), the team

decided to acquire a second sample pair from the Séítah formation, given the importance of the olivine-bearing lithology and the implications of carbonate for the mission's astrobiological objectives. It was required that this sample pair should complement the first sample pair from Brac. Data from RIMFAX and surface images had suggested that Artuby ridge and nearby Séítah rocks were dipping southwest at a tilt of  $10^{\circ}$ – $15^{\circ}$ , which suggested that the Séítah rocks closer to Artuby ridge would actually be stratigraphically overlying the Brac outcrop that had just been sampled (Section 4.6.1, Hamran et al., 2022). The science team also sought to sample a different stratigraphic interval of Séítah as well as in a location closer to the Máaz–Séítah contact at Artuby ridge in the event that the geologic events forming the contact caused alteration of the nearby Séítah rocks. Additionally, the Séítah outcrops closer to Artuby ridge also appeared more recessive than those at Bastide or Brac, raising the possibility that these rocks might have a finer grain size, potentially even the fine-grained rocks that the mission had been seeking to sample. During sols 280–286, Perseverance therefore drove to Issole, where the team had acquired RS observations on sol 202 on the way into Séítah (Figure 16a).

Perseverance arrived at the Issole workspace (of the Bastide member) on sol 286 and began executing the sampling sol path. Abrasion was first attempted on the Soberro target on sol 288, but faulted, potentially due to topography on the rock surface that caused the abrader bit to slip and triggered the fault. Abrasion was reattempted on the Quartier target on sol 292, which was successful (abrasion depth 7 mm; Figure 18c). SHERLOC, WATSON, and PIXL activities were performed on sol 293 with additional SHERLOC activities on sol 303. Compared with the Dourbes abrasion, the Quartier abrasion contained a more heterogeneous distribution of the light-toned, dark-toned, and brown materials that make up both patches (Figure 18c). Like Dourbes, the primary mineralogy of Quartier was olivine, present as tan to greenish-gray crystals in the abrasion patch and often rimmed by brown-toned materials associated with Fe-rich alteration. Lighter-toned patches again corresponded to secondary phases such as Mg and Ca sulfate, carbonate, and other hydrated phases. Organics were detected, some in association with sulfate phases (Corpolongo et al., 2023; Sharma et al., 2022). Purple-toned coatings, observed at all previous sampling workspaces, were also observed on the natural surfaces of the rocks at Issole. Compared to the Brac outcrop, Issole appeared to have experienced a greater degree of aqueous alteration.

The first sample core at Issole, on the Robine target, was acquired over sols 295–298 following the more conservative engineering approach where sampling was split across several sols to ensure that there was sample in the tube prior to sealing, similar to what was done for the first rock core, Montdenier (Section 4.5). This procedure was used as the more recessive nature of Issole compared to Brac raised concern that a rock core may not be acquired, as was the case at Roubion. However, a core was successfully acquired at the Robine target and the second coring attempt was made on the Pauls target on sol 306 (Figure 18d). The Pauls rock core was successfully acquired, but the subsequent sample processing steps autonomously stopped when the coring bit containing the sample tube was to be dropped off to the BC. The cause for this anomaly was not immediately understood, but diagnostic activities eventually revealed the presence of two pebbles, likely fallen from the sample tube, in the bit holder; these prevented the coring bit from seating correctly in the bit holder.

While the engineering teams worked to recover from this anomaly, the science team continued using RS instruments to make observations of the Issole workspace and Artuby ridge in the background (Figure 18a). A specific objective was to document where olivine signatures were observed in order to delineate the possible transition from the Séítah formation to the Máaz formation. While the exact contact between the two formations remained unidentified, the RS results indicated that the rocks near the Issole workspace were decidedly olivine-bearing and part of the Séítah formation, whereas the rocks of Artuby ridge continued to lack olivine signatures, consistent with the Máaz formation.

After considering several mechanisms to resolve this anomaly, the best solution was ultimately to dump the Pauls sample, still in the coring bit, to proceed with recovering nominal BC movement. By this point, the Pauls core had been held in the coring bit, unsealed, for more than 2 weeks, and from a science perspective the Pauls sample was deemed not as desirable as a new core would be as volatiles could have been lost to the environment. After dumping the Pauls sample on sol 322, Perseverance continued with recovery activities to restore range of movement in the BC, which were complete by sol 332. Thereafter, Perseverance performed a short drive to reposition itself in preparation for re-acquiring the second sample at Issole. The second sample was acquired on the Malay target on sol 337 (Figure 18d). In total, sampling activities and fault diagnostics at Issole spanned sols 286–340 (Simon et al., 2023).

#### 4.9. Investigation at Rimplas

On sol 340, Perseverance left the Issole workspace and resumed its drive back to OEB Landing, along which there was time to perform abraded PS on an additional target to build up the geologic context of the crater floor units, as well as acquire its fourth and last sample pair, which had not yet been assigned since Mont Rocheforte was removed from the campaign plan (Section 4.2.1). While at Issole, the science team assessed various options for an opportunistic abrasion and PS opportunity, to be spent anywhere along the traverse back to OEB. The team eventually decided to conduct further investigation of the Artuby member, as the rubbly layered rocks in this member still had an enigmatic origin. The team specifically wanted to understand how the layers at the base of the Mure outcrop (Figure 9) related to those at the main Artuby outcrop (Figure 13), and determine if there was evidence of a change in lithology or an unconformity between the Máaz formation members that could help disambiguate between evolving stratigraphic models (Crumpler et al., 2023; Horgan et al., 2022).

Abrading at the main Artuby outcrop was of primary interest, but the rover tilt in front of that outcrop was assessed to be challenging. Instead, a lower-lying outcrop named Rimplas, approximately 18 m southeast of the main Artuby outcrop (Figures 4a and 19), was deemed more feasible and became the site for this next abrasion opportunity. Once Perseverance exited Séítah, it took a slightly different traverse more to the southwest of its original drive (Figure 4a) in order to obtain RIMFAX data several meters offset from the original tracks. After crossing Citadelle on sol 341, the rover then arrived at the Rimplas location on sol 343 and abraded the Montpezat target on sol 346 (abrasion depth 8 mm, Figure 19e). The Montpezat abrasion revealed a generally darker-toned surface with lighter-toned or brown areas showing interlocking igneous crystals. Secondary minerals were consistent with carbonate and possible phosphate and perchlorate. Purple-toned coatings were again observed on the natural surface adjacent to the abrasion patch and even appeared as more extensive patches below the abrasion patch (purple arrows in Figures 19d and 19e). Despite the appearance of layering in the Rimplas rock and the Artuby member, no obvious layering was observed within the Montpezat abrasion patch.

#### 4.10. Second Máaz Sample Pair at Sid

With the removal of the Mont Rocheforte ridges from the campaign plan (Section 4.2.1), the target of the fourth and final sample pair of the crater floor campaign was debated as the team wrapped up sampling in Séítah. In assessing the sample suite that had been collected so far, the team determined that suite still lacked a Máaz formation sample that could be related to the broader crater-retaining unit, which could yield absolutely ages that could help calibrate Mars crater chronology models and provide age constraints for future delta samples (Section 2.2.2). The team determined that this sample would come from the Ch'ał member, given its resistant nature and its occurrence east of the OEB landing site, where more craters are observed in orbital data (Figure 2a). Thus, the decision was made to drive back to OEB to where we initially observed Ch'ał member rocks to sample (Figure 3e).

Perseverance departed Rimplas on sol 350 and reached the vicinity of OEB by sol 360, taking full advantage of the rover's Autonav capabilities. For comparison, the traverse from Adziilii crater to Issole took more than 22 drive sols, but the reverse trip took only 9 drive sols. On sol 362, Perseverance then approached the Sid outcrop (Figure 20), which is in the vicinity of the Ch'ał target, originally observed on sol 78 at the very beginning of the mission (Figure 3e). Perseverance proceeded to abrade the Alfalfa target (abrasion depth 9 mm) on sol 367 and acquire PS observations on sols 369–370. The Alfalfa abrasion patch revealed white feldspar laths and pyroxene grains with possible olivine and quartz (Figure 20d). Evidence for aqueous alteration was less abundant than in previous abrasion patches but included detection of Fe oxides, carbonate, and possibly phyllosilicates, chlorite, phosphate, and perchlorate, as well as low concentrations of organic matter (Corpolongo et al., 2023; Sharma et al., 2022). Overall, Alfalfa was compositionally consistent with a basaltic andesite composition (Udry et al., 2023; Wiens et al., 2022) and, while strongly oxidized (Horgan et al., 2022), is otherwise the least aqueously altered abrasion from the campaign. Drill parameters during abrasion show that Sid is the hardest rock abraded by Perseverance on the crater floor. The first sample, Ha'ahóni (meaning “perseverance” in Navajo), was subsequently acquired on sol 371 and its pair, Atsá (meaning “eagle” in Navajo), was acquired on sol 377 (Simon et al., 2023). All sampling activities concluded by sol 379, thus marking the end of the science campaign on the crater floor.

#### 4.11. Rapid Traverse to the Western Delta

After concluding the crater floor science campaign, Perseverance then drove northward from OEB, then westward towards the Three Forks location at the base of the western delta. The focus of this Rapid Traverse campaign was to maximize drive progress, so science observations were limited in order to conserve rover resources. This traverse began on sol 379 and Perseverance arrived at Three Forks on sol 410, marking 31 sols for the Rapid Traverse campaign across the crater floor.

### 5. Key Findings From the Jezero Crater Floor

#### 5.1. Geologic Members and Stratigraphy

Perseverance's investigations of the Máaz and Séítah formations resulted in the delineation of several members in each formation, based on textural, morphologic, compositional, and stratigraphic characteristics (Figure 4b; e.g., Farley et al., 2022; Crumpler et al., 2023; Horgan et al., 2022; Udry et al., 2023).

##### 5.1.1. Máaz Formation Members

The Máaz formation has been divided into five members (Crumpler et al., 2023; Farley et al., 2022) that may potentially be grouped into “upper Máaz” or “lower Máaz” based on composition (Horgan et al., 2022; Rice et al., 2023; Udry et al., 2023; Wiens et al., 2022).

The upper Máaz members consist of the Naa'táanii and Ch'ał members. The Naa'táanii member is located in the vicinity of OEB Landing and is the member on which Perseverance landed. This member consists of flat, low-lying pavers that appear as polygonal blocks in orbital images (Figures 3a and 3d) and have granular weathering patterns. The Naa'táanii member transitions (Figures 3d and 3f) into the higher-standing, gray-toned, massive, blocky meter-scale boulders of the Ch'ał member, which form hummocky landscapes and is the hardest and least altered member from the crater floor (Figure 20). Due to its comparatively more resistant nature, the Ch'ał member is thought to be related to the crater-retaining unit on which crater count ages have been derived (Farley et al., 2022; Goudge et al., 2015; Quantin-Nataf et al., 2021; Schon et al., 2012; Shahrzad et al., 2019). The distinction between the Naa'táanii and Ch'ał members is based largely on outcrop morphology not composition (Wiens et al., 2022). The bulk chemistry of these two members is more evolved and enriched in SiO<sub>2</sub>, resembling a basalt to basaltic andesite composition (Udry et al., 2023; Wiens et al., 2022).

The lower Máaz members, the Artuby and Rochette members, are best expressed along Artuby ridge near the southern contact between the Séítah formation and the Máaz formation and are also likely exposed at the Mure outcrop (Figures 9 and 13). The lower Artuby member appears coarsely layered, with granular textures in the recessive subcentimeter-scale layers (Figures 9d and 13e) and more indurated, bulbous textures in the decimeter-scale layers (Figures 9e and 13f). Above the Artuby member is the Rochette member, which is a resistant caprock unit that is variably massive to layered (on the centimeter to decimeter scale) to pitted (Figure 14). The Rochette member extends to the eastern margin of the Máaz-Séítah contact as well, bordering the Naa'táanii member (Crumpler et al., 2023; Farley et al., 2022, Figure 1c), and may also border portions of the Roubion member in Polygon Valley as well (Figure 8e). Compositionally, the Artuby and Rochette members are very similar and are characterized by less evolved compositions (i.e., lower SiO<sub>2</sub> and alkalis) and more pyroxene enrichment compared to the upper Máaz members (e.g., Horgan et al., 2022; Udry et al., 2023; Wiens et al., 2022).

The fifth Máaz member, Roubion, shares characteristics with both the upper and lower Máaz members and its stratigraphic position is still under consideration. The Roubion member closely resembles the Naa'táanii member in morphology, appearing as low-lying pavers that form polygonal patterns in orbital datasets (Figure 11), but was distinguished as a separate member on the basis of its lower elevation (Farley et al., 2022, Figure 1c). Its morphologic and geographic similarity to the Naa'táanii member has led to the idea that the Roubion member could be related to the upper Máaz members Naa'táanii and Ch'ał (Horgan et al., 2022). However, the Roubion member also appears to grade upwards into the Artuby and Rochette members in the Mure outcrop (Figure 11b), which led to the interpretation that the Roubion is the stratigraphically lowest member of the Máaz formation (Crumpler et al., 2023; Farley et al., 2022). In the Polygon Valley region, the Roubion member also appears to grade directly into either the Ch'ał or Rochette members (Figure 8e). The association of the Roubion member with the lower Máaz members was further bolstered by its compositional similarity to Artuby and Rochette (Udry et al., 2023).

### 5.1.2. Séítah Formation Members

Based on orbital (Section 2.2.1) and rover observations, the Séítah formation and its members stratigraphically underlie, and are thus probably older than, the Mááz formation (Farley et al., 2022; Hamran et al., 2022). The Séítah formation is composed of the Bastide and Content members, although further subdivisions of the Séítah formation (excluding the Content member) are possible (Crumpler et al., 2023).

The Bastide member is the more prevalent member, and is characterized by rocks that often appear layered (at various scales from the centimeter scale up to the decimeter scale; Figures 15 and 16), and are rich in olivine, some of which has been altered to carbonate (Clavé et al., 2023; Liu et al., 2022; Scheller et al., 2022). Despite the prevalence of layering in many Séítah outcrops, this layering was difficult to trace consistently across different outcrops.

The Content member contains millimeter-to-centimeter size pits, seemingly lacks layering (Figure 17c), and does not contain olivine (Udry et al., 2023; Wiens et al., 2022), despite the Séítah formation generally being associated with an olivine-rich composition from previous orbital and rover observations (Section 2.2.1). The composition of the Content member is relatively high in SiO<sub>2</sub> and alkalis, similar to that of the upper Mááz formation, and is in fact among the most evolved compositions encountered by Perseverance (Udry et al., 2023; Wiens et al., 2022). Coupled with the Content member's occurrence on top of the Bastide member, this suggests the Content member may indeed have some correlation with the members of the Mááz formation, particularly the Ch'a'l member (Udry et al., 2023; Wiens et al., 2022), which in some regions exhibits similar pitted morphologies as the Content member (compare Figure 5e and Figure 17c). Due to limited exposures of the Content member, which was observed over distances of only several meters, the nature of its contact with the Bastide member is unknown.

## 5.2. Geologic History of the Jezero Crater Floor

### 5.2.1. Igneous Origin

The in situ observations by Perseverance's payload were critical to answering questions about the enigmatic origins of the Mááz and Séítah formations (Section 2.2). PS observations on the abraded patches in particular showed that the Mááz and Séítah formations are both igneous in origin (e.g., Farley et al., 2022; Liu et al., 2022; Tice et al., 2022; Udry et al., 2023; Wiens et al., 2022). While sedimentary origins were considered, grain sorting, grain rounding, cements, and sedimentary structures such as fine-scale laminations were not observed, and visible grains appeared to be interlocking rather than sorted as would be expected in a sedimentary environment.

The Bastide member of the Séítah formation represents an olivine-rich cumulate that formed from differentiation of an intrusive body or thick lava flow or impact melt. The Séítah abrasion patches (Garde, Dourbes, Quartier; Figures 16d, 17d, and 18c) showed a large concentration of 2–3 mm olivine crystals with uniform chemistry and face-to-face contacts with each other, a poikilitic texture with pyroxene growing around and cogenetically with the olivine grains, and crystalline pyroxene and primary Fe/Ti/Cr oxides that crystallized from residual melt (Farley et al., 2022; Liu et al., 2022; Wiens et al., 2022). These observations are consistent with Séítah representing the olivine crystals settling cumulate from a slowly cooling and differentiated body of lava or magma (Wiens et al., 2022, Figure 8). Séítah's layering (Figures 15 and 16), which is observed to thicken upward in some areas (Farley et al., 2022, Figure S2C), may be attributed to magmatic layering, although the thinness and consistent composition and grain size of its layers is unusual compared to terrestrial cumulate analogs (Wiens et al., 2022).

By contrast, the presently favored hypothesis for the plagioclase- and pyroxene-rich Mááz formation is that it most likely represents a sequence of extrusive basaltic lava flows emplaced on top of the Séítah formation during a separate event. An alternate scenario is that the Mááz formation is older than the Séítah formation if Séítah was placed intrusively beneath Mááz (Farley et al., 2022; Udry et al., 2023; see also Section 5.2.3). The Mááz abrasion patches show interlocking 0.5–1.0 mm grains of pyroxene and plagioclase, with no olivine present as was found in the Séítah abrasions (Figures 11d, 14d, and 20d) (Alwmark et al., 2023; Farley et al., 2022; Horgan et al., 2022; Udry et al., 2023; Wiens et al., 2022). Rocks of the Mááz formation also exhibit flow-like morphologies (Figure 5d), vesicular textures (Figures 5e, 9f, and 11d), and layering, particularly within the Artuby member (Figures 9f and 13d). A minor contribution from pyroclastic or aeolian materials, intercalated with lava flows, is possible for the Artuby member, as observations of thin, recessive layers framing more bulbous portions (e.g., Figure 9c) are difficult to attribute to effusive processes (Alwmark et al., 2023). Though initially considered part

of the Séítah formation due to its geographic occurrence, the Content member may instead represent lava flows as well, based on its similar composition to upper Máaz (Section 5.1.2) and its pitted texture (Figure 17c), which is difficult to reconcile with a cumulate origin (Wiens et al., 2022).

Textural and geographic studies may indicate that different events created the upper Máaz and lower Máaz members. The broader geographic extent and thinner layering observed in the lower Máaz (Artuby and Rochette) members could indicate low-viscosity flows (Alwmark et al., 2023), whereas the upper Máaz members have a more limited geographic distribution and less layering, potentially indicating a smaller volume of lava with higher viscosity (Horgan et al., 2022). RIMFAX subsurface profiles and observations of extended erosion and tectonic modification of and lower Máaz may also indicate that an extended period of time passed before upper Máaz was emplaced on top of lower Máaz (Horgan et al., 2022).

An initial, alternative explanation for the Máaz formation is that it may represent the plagioclase- and pyroxene-rich fractionation complement to Séítah, that is, the uppermost part of the differentiated melt body (Farley et al., 2022; Wiens et al., 2022). However, more recent analyses using magma differentiation models contradict this and demonstrate that the parent magma that created the Máaz formation is unlikely to be consistent with the composition expected for a melt evolved from a Séítah-forming magma (Udry et al., 2023). While thermodynamic modeling shows that the upper and lower Máaz members converge in their liquid lines of descent, indicating that they may derive from the same parental melt, the liquid lines of descent for Máaz and Séítah (Bastide member) do not converge and indicate that Máaz and Séítah are not petrogenetically linked (Udry et al., 2023).

### 5.2.2. Subsequent Aqueous and Chemical Alteration

All of the abrasion patches examined, as well as RS observations of natural targets, also exhibit evidence for multiple and distinct episodes of aqueous alteration, which produced minerals such as carbonate, Fe/Mg phyllosilicate, amorphous silicates, sulfates, perchlorate, and Fe-silicates (Clavé et al., 2023; Corpolongo et al., 2023; Mandon et al., 2023; Scheller et al., 2022; Tice et al., 2022).

In the Séítah formation, the first alteration event was likely carbonation of olivine, in which CO<sub>2</sub>-bearing fluids interact with olivine to produce carbonate. This formation scenario is supported by the similar Fe/Mg ratios between the olivine and carbonate chemical compositions, the rimming of the olivine grains by carbonate (brown rims in Figure 17d), and amorphous silicate in cracks and voids, suggesting that these minerals formed at the expense of pre-existing olivine (Farley et al., 2022; Tice et al., 2022). Carbonates are more rarely detected in the Máaz formation, which more commonly contains Fe/Mg phyllosilicates. The carbonates in the Máaz formation are Fe-rich rather than Mg-rich as in Séítah, suggesting that the different carbonate compositions may have resulted from alteration in different solutions (Clavé et al., 2023).

A subsequent series of alteration events produced salts such as sulfate, halite, and perchlorate which filled in pore spaces, voids, and cracks in the Máaz and Séítah rocks after initial carbonate or phyllosilicate formation. These salts usually appear as white patches in the abrasions. Different proportions of S/Cl and Ca/Mg/Fe in salt compositions suggest that there were likely multiple different fluids that altered these rocks at different times (Farley et al., 2022; Tice et al., 2022). The perchlorates likely represent the youngest, and perhaps final, episodes of aqueous alteration, as perchlorate's high solubility and preserved presence suggests that the crater floor rocks have not interacted with fluids since perchlorate formation (Farley et al., 2022; Scheller et al., 2022). Similar to hypotheses for perchlorate formation at other sites on Mars, the perchlorates in Jezero's crater floor could result from brief and possibly recent (i.e., Amazonian) wetting events that result in percolation and evaporation of fluids (Farley et al., 2022). Areas affected by this latest episode of salt emplacement also exhibit elevated Fe/Mg ratios relative to neighboring, unaltered areas, suggesting that this episode of alteration also resulted in minor iron oxidation (Tice et al., 2022).

The prevalence of carbonate or Fe/Mg phyllosilicate, salts, and amorphous silicates in many rocks along Perseverance's traverse through the Máaz and Séítah formations altogether suggest that aqueous alteration was widespread in the Jezero crater floor. However, these alteration events likely occurred at low temperatures, low water-to-rock ratios, and likely not in an extensive open system (Farley et al., 2022). The carbonates and Fe/Mg phyllosilicates detected in the Séítah and Máaz formations, respectively, were all detected at low proportions (a few weight percent; Mandon et al., 2023), and occurred with amorphous or poorly crystalline phases (Clavé et al., 2023; Scheller et al., 2022; Tice et al., 2022). Much of the original igneous minerals remain intact in both the Máaz and Séítah abrasions, and no Al-phyllosilicates were detected, whose presence would have indicated that alteration

**Table 4**  
*Summary of Results From Abrasion Patches*

Sol	Target	Abraded depth (mm)	Formation	Member	Natural surface coatings?
161	Guillaumes	8	Máaz	Roubion	Yes
186	Bellegarde	10	Máaz	Rochette	Yes
207	Garde	11	Séítah	Bastide	Yes
257	Dourbes	7	Séítah	Bastide	Yes
293	Quartier	7	Séítah	Bastide	Yes, elsewhere in same workspace
349	Montepezat	8	Máaz	Artuby	Yes
370	Alfalfa	9	Máaz	Ch'al	Unknown

*Note.* For more information on the primary and secondary mineralogy associated with each abrasion patch, please see references in Sections 5.2.1 and 5.2.2.

occurred in an open system where soluble species like Ca, Na, K would be removed, leaving the rocks enriched in Al (Farley et al., 2022).

Other alteration is visible on the natural rock surfaces of rocks in both the Máaz and Séítah formations in the form of purple coatings (Figures 11, 14, 16, and 17; Table 4). These coatings are observed in almost all of the dust-cleared natural surfaces adjacent to abrasion patches, and have been observed in RS data throughout the campaign (J. Bell et al., 2022; Garczynski et al., 2022; Rice et al., 2023). Compositional analysis of these coatings suggest that they are similar to the typical dust composition and are hydrated, which could indicate that these coatings formed from induration of dust particles by fluids (Garczynski et al., 2022; Mandon et al., 2023).

### 5.2.3. Post-Emplacement Physical Modification

At some point after, or potentially during, the emplacement of the Máaz and Séítah formations, but at an unknown time relative to aqueous and chemical alteration, these rocks were physically modified, tilted, and eroded. All along the Artuby ridge, and in nearby parts of Séítah (Figure 15e), rocks dip about 10° to the southwest, observed both from surface images and from subsurface RIMFAX data (Hamran et al., 2022). However, the mechanism responsible for tilting these units is still under study. One possibility is that Séítah, if it was emplaced as a sill or diapir, could have tilted the lower Máaz members in contact with the Séítah magmatic body. However, Perseverance observed no evidence for contact metamorphism in the lower Máaz formation or Séítah formation rocks, which was confounded by regolith obscuring the Máaz-Séítah contact (Udry et al., 2023). The dips in the Máaz and Séítah formations are similar in magnitude to those measured for the regional olivine-bearing and mafic cap units (Kremer et al., 2019), although it is not yet understood if or how the Máaz and Séítah formations are related to the regional units and if the cause of the dips are the same (Section 6.2).

Significant erosion also produced the present day topography and features observed in the crater floor rocks. Outcrops in the Séítah are observed to exhibit ridged patterns trending in a northeast-southwest orientation, presumably carved by winds (Day & Dorn, 2019; Sun & Stack, 2020), and Perseverance encountered many wind-fluted rock surfaces with patterns consistent with observed wind directions (Herkenhoff et al., 2023). In the favored scenario where Máaz is a lava flow unrelated to the Séítah cumulate, there also would need to be erosion of the mafic olivine-depleted complement to Séítah prior to the Máaz formation being emplaced. Erosion would have also removed substantial amounts of material from the Máaz formation in order to explain the present-day variance in topography and surface textures that may have resulted in the delineation of up to five distinct members. Erosion of the Séítah formation to liberate olivine grains (Figure 16e) and subsequent transport of these grains likely explains the prevalent occurrence of olivine grains found in Máaz formation regolith (Vaughan et al., 2023; Wiens et al., 2022).

### 5.3. Discovery of Potential Organic Materials

The search for biosignatures is a primary goal of the Perseverance mission, and within that context, the search for organic materials is of critical importance (Farley et al., 2020). The SHERLOC instrument utilizes complementary deep UV Raman and fluorescence spectroscopy to detect minerals and organic matter at a close distance from the rock surface. Fluorescence is a more sensitive, though less diagnostic, technique and can be used to



optically detect aromatic organic molecules at low concentrations (ppb), though it cannot identify the specific molecules present. By contrast, Raman spectroscopy capitalizes on a weak scattering phenomenon that can reveal information about vibrational bonds within an organic molecule, thereby providing specific information useful for molecular assignment, but requiring a significantly larger amount of organic matter. In the crater floor targets observed by SHERLOC, significant Raman signatures were rare; however, fluorescence measurements revealed strong indications for aromatic compounds. Abraded targets within the Máaz formation revealed the strongest fluorescence signal, while natural surface Máaz and abraded Séítah targets were comparable in signal strength (Sharma et al., 2022). Below we summarize the fluorescence observations for the Máaz and Séítah formations; please see Text S3 in Supporting Information S1 for an overview of the results from each target.

Two natural surface (i.e., no abrasion or substantial dust clearing of the rock surface) targets were analyzed by SHERLOC: Naa'táanii and Foux (Figure 8d), representing the Naa'táanii member and Roubion member of the Máaz formation, respectively. Both targets showed fluorescence signals near  $\sim 338\text{--}350$  nm, indicating either the presence of two-ring aromatic molecules or mineral luminescence due to the presence of rare earth elements (REEs), and near  $\sim 270\text{--}288$  nm, which may be due to the presence of single ring aromatic molecules or mineral defects. The fluorescence signals were not associated with any textural patterns. These observations may indicate either low to no concentration of organics, or they were limited by (a) the low power (pulses per point) used on scans, (b) dust on target surface, and (c) significant topography, especially on the Naa'táanii surface, which would cause attenuated signal for points that were out of focus.

SHERLOC observations of the four Máaz formation abrasion patches also showed similar types of fluorescence features as in the natural surface observations. A  $\sim 275$  and  $\sim 340$  nm fluorescence feature was observed in Guillaumes (Roubion member), Bellegarde (Rochette member), Montpezat (Artuby member), and Alfalfa (Ch'af member). Again, these features may be attributed to one and two ring organic molecules, or mineral defects or REE luminescence. No correlation with texture was observed in most cases, except for an association with dust in the Guillaumes and Bellegarde target, and along crystal boundaries in the Bellegarde target.

Interestingly, features at  $\sim 303$  and  $325$  nm were observed in the Bellegarde target and found to be strongly correlated with an area of high sulfate concentration. This two-band feature was observed in multiple large grains, and unlike the previous fluorescence was found within the grains, not along their boundaries. Although these bands could be consistent with organics such as aromatic heterocycles, this is not confirmed with Raman. A single point in the Montpezat target exhibited a Raman signal that may be consistent with an organic G band that closely aligns with the known G band on the SaU008 meteorite SHERLOC calibration target (Fries et al., 2022; Sharma et al., 2022); the 340 nm fluorescence was co-located with this Raman detection.

SHERLOC observations of the three Séítah formation (Bastide member) abrasion targets—Dourbes, Garde, Quartier—again showed similar fluorescence features as in the Máaz observations. Fluorescence features at  $\sim 338\text{--}350$  nm were observed in all three targets, and a feature at  $\sim 270\text{--}288$  nm was observed in the Dourbes and Garde targets. The fluorescence measurements were associated with dust and were located along crystal boundaries for Dourbes and Garde. Interestingly, when Dourbes was analyzed with a second scan (sol 269) after 13 sols of exposure to the environment (Section 4.7), the fluorescence bands associated with organics were still detected. SHERLOC detected a doublet at  $\sim 303$  and  $325$  nm in the Quartier target, similar to what was observed in the Máaz formation Bellegarde target, which may be due to the presence of one or two-ringed aromatic molecules. The doublet fluorescence feature was frequently spatially correlated to the sulfate mineral detections, which also showed a Raman signal consistent with hydration at many points. Finally, multiple points within Quartier exhibited Raman peaks at  $\sim 1,330\text{--}1,410$  and  $\sim 1,650$   $\text{cm}^{-1}$  that may or may not be due to an organic molecule vibrational mode.

#### 5.4. Atmospheric Results

Major atmospheric science results have also been obtained by combining imaging from Navcam and Mastcam-Z, sounds from the SuperCam microphone, and MEDA time series. This includes the observation of several huge “gust lifting” events in Navcam images, which could potentially raise as much background dust as dust devils in Jezero, and one of which coincided with strong wind gusts measured by both MEDA and the SuperCam microphone (Newman et al., 2022). Furthermore, MEDA pressure and RDS data, in combination, suggest that

while vortices are only slightly more common in Jezero crater than at InSight's landing site, dusty vortices are far more prevalent in Jezero (Hueso et al., 2023; Newman et al., 2022; Vicente-Retortillo et al., 2023). Perseverance further observed a major increase in local dust lifting during onset of a late spring regional dust storm, prior to local opacities increasing significantly. These observations, summarized in Lemmon et al. (2023), are the first comprehensive atmospheric and aeolian observations to be made in the heart of a dust storm's source region. Furthermore, Jezero crater holds numerous aeolian features, from dunes and ripples to ventifacts, which show evidence of modern and past wind patterns, and include migrating megaripples (Herkenhoff et al., 2023; Sullivan et al., 2022). Overall, these results show Jezero crater to be one of the most active aeolian sites ever visited on Mars.

## 6. Campaign Summary and Debrief

Perseverance traversed a total of more than 5 km of distance within the main crater floor campaign area and almost 5 km during the Rapid Traverse campaign, created and analyzed seven abrasion patches, and filled nine sample tubes and a witness tube (Figure 4; Simon et al., 2023). Overall, Perseverance successfully accomplished its campaign objectives, as defined in Section 3.1, to the best of its ability:

1. Perseverance investigated the nature and origin of the Máaz and Séítah formations, and determined their depositional and emplacement mechanisms. This resulted in the definition of five Máaz members, including their division into upper and lower Máaz, and at least two Séítah formations (Section 5.1). Observations determined that the Séítah formation underlies the Máaz formation and represents an olivine cumulate, whereas the Máaz formation represents a separate series of lava flows.
2. Perseverance was not able to clearly observe the contact between the Máaz and Séítah formations due to regolith cover at the base of Artuby ridge where the contact was inferred to exist, despite performing a thorough traverse along most of the base of Artuby ridge. However, Perseverance did make observations of upper Séítah rocks (Figure 12) and lower Máaz (Figures 13 and 14) that represent the exposed outcrops closest to the Máaz-Séítah contact, and RIMFAX traverses perpendicular to Artuby ridge (at Citadelle and the entrance to South Séítah; Figure 2b) showed subsurface structures, though a contact was not apparent (Hamran et al., 2022).
3. Observations from Perseverance's instruments successfully characterized the extent of aqueous alteration and modification of the Máaz and Séítah formations, demonstrating that multiple and distinct fluid episodes produced carbonate, Fe/Mg phyllosilicate, sulfates, perchlorates, silicates, and surficial purple-toned coatings (Section 5.2.2). Physical modification and tilting of the crater floor rocks also occurred (Section 5.2.3). Though fractures, especially Mont Rocheforte, were a feature of interest during campaign planning, observations from Perseverance and the Ingenuity helicopter revealed no obvious physical or mineralogic evidence for fracture fill in any of the large fractures observed from orbit (Section 4.2.1).
4. Perseverance also executed the planned observations of Pilot Pinnacle (Section 3.3.1), collecting images that showed a lack of outcrop exposures (Figure 7) and provided documentation for remnant mounds on the crater floor that could be contrasted to observations of the Kodiak remnant, which is located closer to the delta (Mangold et al., 2021).
5. Perseverance also completed a successful investigation of the martian atmosphere and surface regolith, documenting dunes, ripples, ventifacts, regolith, and atmospheric opacity through a regional dust storm (Section 5.4).

Perseverance also fulfilled its plan to collect samples characterizing the diversity of lithologies on the crater floor. Two sample pairs were acquired from the Máaz formation, representing the lower Rochette caprock from lower Máaz and the crater-retaining Ch'ał member from upper Máaz. Two sample pairs were also acquired from the Séítah formation, representing different stratigraphic intervals of the layered, olivine-rich Bastide member.

### 6.1. Comparison of Notional Campaign Plan Versus Actual

Completion of the crater floor campaign took approximately 44 sols longer than planned (Section 3.2.2), ending on sol 409 instead of sol 365 (Table 5). Several factors contributed to this discrepancy that were converted to lessons learned for Perseverance's second science campaign at the delta front. During the crater floor campaign,

**Table 5**  
*Summary of Actual Sols and How They Were Spent During the Campaign*

Corresponding main text	Campaign leg	Start sol	End sol	# Sols
Section 4.1	Drive to Imaging Point 3	101	118	17
	Imaging Point 3 activities	118	122	4
	Drive to Séítah-N Overlook	122	128	6
	Séítah-N Overlook activities	128	129	1
Section 4.2	Drive to FTA-20/21 Location (Foux, Beaujeu)	129	138	9
	PS (Foux, Beaujeu) and FTA-20/21	138	153	15
Section 4.3	Drive to Roubion	153	157	4
	Sampling at Roubion	157	168	11
Section 4.4	Drive and Remote Science at Mure	168	169	1
	Drive to main Artuby outcrop	169	177	8
	Remote Science at main Artuby outcrop	177	178	1
Section 4.5	Drive to Citadelle	178	180	2
	Sampling at Rochette	180	199	19
Section 4.6	Drive to Bastide	199	204	5
	Abrasion at Bastide	204	210	6
	Drive to Village for Conjunction and Prep	210	211	1
	Conjunction Preparation	211	217	6
	Conjunction	217	236	19
	Post-Conjunction activities	236	237	1
	Drive to Caille	237	240	3
	Prep for FSW update	240	243	3
	FSW Update	243	246	3
	Post-FSW activities	246	248	2
Section 4.7	Sampling at Brac	248	277	29
	Abrasion Attempt at Hotel	277	280	3
Section 4.8	Drive to Issole	280	286	6
	Sampling at Issole	286	340	54
Section 4.9	Drive to Rimplas	340	343	3
	Abrasion at Rimplas	343	350	7
Section 4.10	Drive to Ch'af	350	362	12
	Sampling at Ch'af	362	379	17
Section 4.11	Rapid Traverse Drive to Delta	379	410	31
Total Sols				309

*Note.* Note that the sols in this table include both nominal and constrained sols, whereas Table 3 contains only nominal sols. Constrained sols are sols in which the planning team does not have data from the preceding plan, and are therefore unable to proceed along the campaign sol path. Green cells represent drives, yellow cells represent remote sensing or proximity science, orange cells represent sampling, and gray cells represent engineering-only activities.

the team encountered unexpected difficulties during FTAs and sampling events that exceeded the assumption of a 15% engineering margin. Thus, the engineering margin assumption was increased to 25% of nominal sols for the Delta Campaign. The amount of science margin (5% of nominal sols) was kept the same, as the crater floor campaign did not use up all of its science margin sols due to the mission being overall behind on schedule at the time. Several anticipated new capabilities and operational improvements would also aid the efficiency of the Delta Front Campaign, including the ability to perform multi-sol drives in multi-sol plans, execute both PS and drives in the same plan, and requiring less ground-in-the-loop intervention during the sampling sol path. Some

of these improvements also benefited the crater floor campaign towards its end. For example, time was recovered during the Rapid Traverse portion of Perseverance's traverse on the crater floor, wherein it took only 31 sols to reach Three Forks from OEB, compared to the 64 sols that were initially predicted.

## 6.2. Outstanding Questions

Perseverance's explorations of the crater floor have already answered some of the major questions posed for years in the Mars science community (Section 2.2). Most notably, observations from the rover's PS and RS instruments have shown that the Mááz and Séítah formations are unequivocally igneous in origin (Section 5.2.1), resolving a decade-long debate about the igneous or sedimentary origins of these units (Section 2.2). However, several questions remain unanswered and may only be addressed by the returned samples (Simon et al., 2023) or future exploration of the Jezero delta and beyond.

### 6.2.1. Relationship of the Crater Floor Units to the Jezero Delta

The relationships of the crater floor units to other units within and outside of Jezero crater have also generated numerous science questions that may not be answered until Perseverance explores these other units or samples from all units are returned to Earth. For example, the contact relationship between the Mááz formation and the delta is an important and debated one with implications for the age of the delta (Section 2.2.2), but such a contact has not been observed in Perseverance's remote images. Future in situ searches for this contact will rely on subsurface RIMFAX data or the contact being unobscured by regolith, which has been a challenge during the crater floor campaign.

### 6.2.2. Relationship of the Crater Floor Units to the Regional Olivine-Bearing Unit and Mafic Cap Unit

Another outstanding question is the regional extent of the Mááz and Séítah formations, both of which have been hypothesized to be related to other units located on the Jezero crater wall (i.e., the marginal deposits may be related to Séítah; Figure 1d), the crater rim, and in the broader circum-Isidis region (Nili Planum, Nili Fossae, Libya Montes) (Section 2.2). The regional mafic cap and olivine-bearing unit had previously been hypothesized to be volcanoclastic units based on their spatial extent and thin and continuous bedding across a wide range of elevations (Hundal et al., 2022; Kremer et al., 2019; Mandon et al., 2020; Sun & Stack, 2020). These interpretations for the regional units are incongruent with the extrusive and cumulate origin of the Mááz and Séítah formations, respectively (Section 2.2). It is possible that either (a) Jezero's crater floor units are not related to the regional units, or that (b) the regional units are actually emplaced in multiple events and/or via multiple processes, as has been observed on Earth, that produced units with similar orbital morphologies and compositions (Alwmark et al., 2023; Farley et al., 2022; Liu et al., 2022; Ravanis et al., 2022; Wiens et al., 2022). Future exploration of Jezero crater and Nili Planum may ascertain whether the regional units are indeed related to Mááz and Séítah, and if they are similar in origin.

### 6.2.3. Volcanic or Magmatic Source of Mááz and Séítah

Though observations show that the Mááz and Séítah formations are unequivocally igneous in origin, the source for these rocks is still uncertain (Farley et al., 2022). An unlikely hypothesis for the crater floor rocks is that they may result from differentiation of impact melt, but a sufficiently large impact event has yet to be identified, and the Isidis impact has been discounted as it would have predated Jezero crater and the emplacement of the rocks within (Section 2.2.1). If volcanic in origin, the Syrtis Major complex to the southwest of Jezero (Figure 1) may be a possible source, although no definite links to the crater floor units have been observed from orbital studies so far (Sun & Stack, 2020). Other possible volcanic sources include a hill on the southeast rim of Jezero crater which may be a volcanic construct (Figure 1b; Farley et al., 2022), but this remains hypothetical and may remain so until that structure is explored in situ, likely not by Perseverance.

### 6.2.4. Age Constraints From Returned Sample Science of Ch'at Samples

A main objective of the crater floor campaign was to collect samples from the crater-retaining part of the Mááz formation to enable calculations of absolute age for the Mááz formation that could then be related to crater-count ages for the unit (Section 3.1). Though this objective was accomplished, it is likely that any crater-count derived ages may reflect the exhumation age of Mááz, rather than the formation age of the unit (Quantin-Nataf

et al., 2021). Future absolute ages derived for the Ch'al samples will still be useful to reconstruct the timeline of events in Jezero crater, but the potential barrier to calibrating the absolute ages with the Mars crater chronology models is an inherent challenge.

#### 6.2.5. Nature of the Máaz-Séítah Contact

Despite traversing the length of Artuby ridge and imaging along the edges of the Máaz-Séítah contact near the rover traverse, a clear contact between the Máaz and Séítah units was never observed. The region between rocks of the Séítah formation and the Artuby/Rochette member rocks of the Máaz formation was always obscured by sand and regolith (Figure 18a), and the most precise constraints on the location of the contact are based on a few detections of olivine-bearing Séítah rocks in close proximity to Artuby ridge (Figure 12). The absence of an observable contact means that the emplacement relationship between Máaz and Séítah may never be fully understood, at least until samples are returned and analyzed in terrestrial laboratories to determine the ages and parental magmas of both units.

#### 6.2.6. Delta Remnants

An initial objective of the crater floor campaign was to make observations of the remnant mounds on the crater floor, especially Pilot Pinnacle, to determine if they may be distal remnants of the western delta (Section 2.2.4). Observations of sedimentary structures in these remnant mounds could have bolstered the hypothesis that they are indeed delta remnants, but no such structures were observed. Instead, even simple outcrop was difficult to identify in the remnant mounds, as most of their surfaces are smooth-textured, indicative of regolith cover (Figure 7). It is possible that Pilot Pinnacle and similar remnant mounds are composed of finer-grained materials that are more susceptible to erosion and less likely to form resistant outcrops, although it should be noted that fine-grained lacustrine rocks at Gale crater do form extensive outcrop exposures. Given the lack of substantial outcrop exposed at the surface of these distal remnant mounds, their relationship to the delta may forever remain an outstanding question. An exception to this is the Kodiak remnant, which did exhibit outcrop and sedimentary structures linking it to the delta (Mangold et al., 2021).

#### 6.2.7. Absence of Fracture Fill or Veins and Limited Alteration

An interesting outcome of the crater floor campaign was that no fracture fill or mineralized veins were observed in any of the Máaz or Séítah formation rocks, despite the general prevalence of fractures on the Jezero crater floor (Section 2.2.4). Any areas where fracture fill was hypothesized to exist were instead filled in by regolith, including at the Mont Rocheforte set of fractures which were removed from the campaign plan upon this realization (Figure 10). In the abrasion patches, alteration appears to form along cracks and voids in the rocks, but not to the extent where there are large domains of alteration products (Section 5.2.2). The absence of fracture fill is an equally important observation as if there were fracture fill present, as this indicates limited secondary processes in stark contrast to other Mars landing sites like Gale crater and Meridiani Planum where diagenetic features are abundant (e.g., Kronyak et al., 2019; Squyres et al., 2004; Sun et al., 2019). Other possible explanations are that it was simply the fractures that did not experience extended interaction with fluids, or that the fractures postdate the period of alteration. The lack of observed fracture fill is consistent with the general observation that although alteration minerals are detected all along the traverse, the crater floor rocks are overall not substantially altered and large domains of the primary igneous lithology, especially olivine, are still preserved (Clavé et al., 2023; Liu et al., 2022; Tice et al., 2022).

## 7. Summary and Conclusions

Between sols 100–379, the Mars 2020 Perseverance rover executed its first science campaign on the Jezero crater floor and explored its constituent Máaz and Séítah formations. In that time, Perseverance traversed more than 5 km of distance, analyzed seven abrasion patches, and acquired four paired samples and an atmospheric sample for a total of nine sample tubes filled (four from the Máaz formation, four from the Séítah formation, and one atmospheric sample).

- Five Máaz formation members (which may be distilled to two compositional groups, lower Máaz and upper Máaz) and at least two Séítah formation members were identified on the basis of key distinctions in texture,

morphology, composition, and stratigraphic position (Farley et al., 2022). Samples were acquired from the Rochette and Ch'al members, the latter in particular to help constrain the timing of the crater fill stratigraphy and Mars crater chronology. Abrasions were obtained on these two members as well as the Roubion and Artuby members. The two Séítah samples are both of the layered Bastide member, but represent different stratigraphic intervals of that member. The Séítah formation has been confirmed as stratigraphically underlying, and thus being likely older than, the Mááz formation. Earth-based geochronology studies of the samples will help to determine the age of emplacement of these igneous members relative to one another and to the Isidis basin and Jezero crater-forming events, as well as constraining the nature of Jezero resurfacing events and subsequent exhumation and erosion. The Mááz and Séítah formations are igneous in origin (e.g., Farley et al., 2022; Liu et al., 2022); Séítah represents an olivine-rich cumulate formed from differentiation of a large melt or magmatic body, and the Mááz formation likely represents a separate series of lava flows emplaced on top of Séítah, with possible minor contributions from pyroclastic or airfall deposits (Alwmark et al., 2023). Geochronology and geochemical analysis of the returned samples will help to refine the petrologic histories of the Séítah and Mááz formations.

- Both the Mááz and Séítah formation rocks show evidence for multiple distinct episodes of aqueous alteration, although not in an extensive open system. Secondary minerals including carbonate, Fe/Mg phyllosilicates, amorphous silicates, sulfates, perchlorate, and Fe-silicates were identified in the abrasion patches to various degrees. The carbonate likely formed through in situ alteration of existing olivine, and sulfates and perchlorates likely formed in more recent aqueous episodes. Other evidence for alteration exists as purple coatings on the natural surfaces of the Mááz and Séítah rocks, likely resulting from cementation of regolith by fluids and oxides. Earth-based analysis of the samples will enable detection of phases that may be present in the samples, but which are hard to detect or present below detection limits of the rover payload, and which are of astrobiological significance, such as borates and oxalates. This also applies to the presence and nature of organic compounds.
- After their emplacement, the Mááz and Séítah formations experienced physical modification as well. Yet unidentified processes tilted these rocks, especially in the regions where the two formations contact at the Artuby ridge, resulting in a 10° tilt to the southwest that is observable at the surface and in the subsurface. Erosion created the present-day topographic and morphologic differences observed between both formations and their members, and eroded olivine grains from the Séítah formation made their way into regolith on the Mááz formation.
- Organics have been detected at numerous sites via fluorescence peaks in the ~345–350 and ~270–285 nm regions. These bands are suggestive of aromatic molecules, but the possibility of mineral luminescence, at least for the shorter wavelength band, cannot be ruled out. Raman measurements have not yet corroborated the fluorescence measurements.
- Jezero crater is one of the most active aeolian sites ever visited on Mars, with observations of several gust lifting events, dust devils, wind gusts, and migrating megaripples amongst many other temporal observations.

## Data Availability Statement

All of the image data used in this manuscript are available at the Planetary Data System Imaging node (<https://pds-imaging.jpl.nasa.gov/volumes/mars2020.html>) and the Geosciences node (<https://pds-geosciences.wustl.edu/missions/mars2020/>): Mastcam-Z images (J. Bell & Maki, 2021), Supercam RMI images (Wiens & Maurice, 2021), WATSON images (Beegle & Bhartia, 2021), Navcam images (Maki et al., 2020c), Hazcam images (Maki et al., 2020b), and Cachecam images (Maki et al., 2020a).

## References

- Allwood, A. C., Wade, L. A., Foote, M. C., Elam, W. T., Hurowitz, J. A., Battel, S., et al. (2020). PIXL: Planetary instrument for X-ray lithochemistry. *Space Science Reviews*, 216(8), 134. <https://doi.org/10.1007/s11214-020-00767-7>
- Alwmark, S., Horgan, B., Udry, A., Bechtold, A., Fagents, S., Ravanis, E., et al. (2023). Diverse lava flow morphologies in the stratigraphy of the Jezero Crater Floor. *Journal of Geophysical Research: Planets*, e2022JE007446. <https://doi.org/10.1029/2022JE007446>
- Balaram, J., Aung, M., & Golombek, M. P. (2021). The ingenuity helicopter on the perseverance rover. *Space Science Reviews*, 217(4), 56. <https://doi.org/10.1007/s11214-021-00815-w>
- Beegle, L. W., & Bhartia, R. (2021). Mars 2020 SHERLOC bundle [Dataset]. NASA Planetary Data System. <https://doi.org/10.17189/1522643>

## Acknowledgments

We are grateful to the hundreds of people on the Mars 2020 science and engineering teams who operate the *Perseverance* rover on a daily basis, as well as the people who conceptualized, built, launched, and landed the rover during a global pandemic. We would also like to thank the JGR Planet editors, staff, and the guest editors for their help in organizing this special issue, and reviewers Chris Kremer and Larry Crumpler for their constructive comments on this manuscript. This research was carried out at the Jet Propulsion Laboratory, California Institute of Technology, under a contract with the National Aeronautics and Space Administration (80NM0018D0004). TF acknowledges the Italian Space Agency (ASI) grant agreement ASI/INAF n. 2017-48-H-0. SA acknowledges the Swedish Research Council (Grant 2017-06388). KK acknowledges the Carlsberg Foundation Grant CF19-0023. SS acknowledges Swedish National Space Board (contracts 137/19 and 2021-00092).

- Bell, J., Maki, J. N., Alwmark, S., Ehlmann, B. L., Fagents, S. A., Grotzinger, J. P., et al. (2022). Geological and meteorological imaging results from the Mars 2020 Perseverance rover in Jezero crater. *Science Advances*, 8, abo4856. <https://doi.org/10.1126/sciadv.abo4856>
- Bell, J., & Maki, J. (2021). Mars 2020 Mast Camera zoom bundle, from operations team, mosaic products [Dataset]. NASA Planetary Data System. <https://doi.org/10.17189/bmq-nm72>
- Bell, J. F., Maki, J. N., Mehall, G. L., Ravine, M. A., Caplinger, M. A., Bailey, Z. J., et al. (2021). The Mars 2020 perseverance rover Mast Camera zoom (Mastcam-Z) multispectral, stereoscopic imaging investigation. *Space Science Reviews*, 217(1), 24. <https://doi.org/10.1007/s11214-020-00755-x>
- Bhartia, R., Beegle, L. W., DeFlores, L., Abbey, W., Razzell Hollis, J., Uckert, K., et al. (2021). Perseverance's scanning habitable environments with Raman and luminescence for organics and chemicals (SHERLOC) investigation. *Space Science Reviews*, 217(4), 58. <https://doi.org/10.1007/s11214-021-00812-z>
- Bibring, J.-P., Langevin, Y., Mustard, J. F., Poulet, F., Arvidson, R., Gendrin, A., et al. (2006). Global mineralogical and aqueous Mars history derived from OMEGA/Mars express data. *Science*, 312(5772), 400–404. <https://doi.org/10.1126/science.1122659>
- Bramble, M. S., Mustard, J. F., & Salvatore, M. R. (2017). The geological history of northeast Syrtis major, Mars. *Icarus*, 293, 66–93. <https://doi.org/10.1016/j.icarus.2017.03.030>
- Calef, F. J., III, Soliman, T., & Abarca, H. E. (2020). Multi-mission geographic information system: Updates and Mars science operations status. In *51st lunar and planetary science conference, abstract #2689*.
- Carr, M. H., & Clow, G. D. (1981). Martian channels and valleys: Their characteristics, distribution, and age. *Icarus*, 48(1), 91–117. [https://doi.org/10.1016/0019-1035\(81\)90156-1](https://doi.org/10.1016/0019-1035(81)90156-1)
- Clavé, E., Benzerara, K., Meslin, P.-Y., Forni, O., Royer, C., Mandon, L., et al. (2023). Carbonate detection with SuperCam in igneous rocks on the floor of Jezero Crater, Mars. *Journal of Geophysical Research: Planets*, e2022JE007463. <https://doi.org/10.1029/2022JE007463>
- Corpolongo, A., Jakubek, R. S., Burton, A. S., Brown, A. J., Yanchilina, A., Czaja, A. D., et al. (2023). SHERLOC Raman mineral class detections of the Mars 2020 Crater Floor Campaign. *Journal of Geophysical Research: Planets*, 128(3), e2022JE007455. <https://doi.org/10.1029/2022JE007455>
- Crumpler, L. S., Horgan, B., Simon, J., Stack, K., Alwmark, S., Gilles, D., et al. (2023). In situ geologic context mapping transect on the floor of Jezero Crater from Mars 2020 perseverance rover observations. *Journal of Geophysical Research: Planets*, e2022JE007444. <https://doi.org/10.1029/2022JE007444>
- Day, M., & Dorn, T. (2019). Wind in Jezero Crater, Mars. *Geophysical Research Letters*, 46(6), 3099–3107. <https://doi.org/10.1029/2019GL022118>
- Ehlmann, B. L., & Mustard, J. F. (2012). An in-situ record of major environmental transitions on early Mars at Northeast Syrtis Major. *Geophysical Research Letters*, 39(11), 11202. <https://doi.org/10.1029/2012GL051594>
- Ehlmann, B. L., Mustard, J. F., Murchie, S. L., Poulet, F., Bishop, J. L., Brown, A. J., et al. (2008). Orbital identification of carbonate-bearing rocks on Mars. *Science*, 322(5909), 1828–1832. <https://doi.org/10.1126/science.1164759>
- Ehlmann, B. L., Mustard, J. F., Swayze, G. A., Clark, R. N., Bishop, J. L., Poulet, F., et al. (2009). Identification of hydrated silicate minerals on Mars using MRO-CRISM: Geologic context near Nili Fossae and implications for aqueous alteration. *Journal of Geophysical Research*, 114(E2), E00D08. <https://doi.org/10.1029/2009JE003339>
- Farley, K. A., Stack, K. M., Shuster, D. L., Horgan, B. H. N., Hurowitz, J. A., Tarnas, J. D., et al. (2022). Aqueously altered igneous rocks sampled on the floor of Jezero crater, Mars. *Science*, 377(6614), eabo2196. <https://doi.org/10.1126/science.abo2196>
- Farley, K. A., Williford, K. H., Stack, K. M., Bhartia, R., Chen, A., de la Torre, M., et al. (2020). Mars 2020 mission overview. *Space Science Reviews*, 216(8), 142. <https://doi.org/10.1007/s11214-020-00762-y>
- Fassett, C. I., & Head, J. W. (2005). Fluvial sedimentary deposits on Mars: Ancient deltas in a crater lake in the Nili Fossae region. *Geophysical Research Letters*, 32(14), L14201. <https://doi.org/10.1029/2005GL023456>
- Fassett, C. I., & Head, J. W. (2008). The timing of Martian valley network activity: Constraints from buffered crater counting. *Icarus*, 195(1), 61–89. <https://doi.org/10.1016/j.icarus.2007.12.009>
- Fouchet, T., Reess, J.-M., Montmessin, F., Hassen-Khodja, R., Nguyen-Tuong, N., Humeau, O., et al. (2022). The SuperCam infrared spectrometer for the perseverance rover of the Mars2020 mission. *Icarus*, 373, 114773. <https://doi.org/10.1016/j.icarus.2021.114773>
- Fries, M. D., Lee, C., Bhartia, R., Razzell Hollis, J., Beegle, L. W., Uckert, K., et al. (2022). The SHERLOC calibration target on the Mars 2020 perseverance rover: Design, operations, outreach, and future human exploration functions. *Space Science Reviews*, 218(6), 46. <https://doi.org/10.1007/s11214-022-00907-1>
- Garczynski, B. J., Bell, J. F., III, Horgan, B. H. N., Johnson, J. R., Rice, M. S., Vaughan, A., et al. (2022). Perseverance and the purple coating: A Mastcam-Z multispectral story. In *Proceedings of the 53rd lunar and planetary science conference (LPSC)*. Lunar and Planetary Institute, United States of America.
- Gouge, T. A., Mustard, J. F., Head, J. W., Fassett, C. I., & Wiseman, S. M. (2015). Assessing the mineralogy of the watershed and fan deposits of the Jezero crater paleolake system, Mars. *Journal of Geophysical Research: Planets*, 120(4), 775–808. <https://doi.org/10.1002/2014JE004782>
- Greeley, R., & Guest, J. E. (1987). Geologic map of the eastern equatorial region of Mars (report no. 1802B). Retrieved from <http://pubs.er.usgs.gov/publication/i1802B>
- Hamilton, V. E., & Christensen, P. R. (2005). Evidence for extensive, olivine-rich bedrock on Mars. *Geology*, 33(6), 433–436. <https://doi.org/10.1130/G21258.1>
- Hamran, S.-E., Paige, D. A., Allwood, A., Amundsen, H. E. F., Berger, T., Brovoll, S., et al. (2022). Ground penetrating radar observations of subsurface structures in the floor of Jezero crater, Mars. *Science Advances*, 8(34), eabp8564. <https://doi.org/10.1126/sciadv.abp8564>
- Hamran, S.-E., Paige, D. A., Amundsen, H. E. F., Berger, T., Brovoll, S., Carter, L., et al. (2020). Radar imager for Mars' subsurface experiment—RIMFAX. *Space Science Reviews*, 216(8), 128. <https://doi.org/10.1007/s11214-020-00740-4>
- Hayes, A. G., Corlies, P., Tate, C., Barrington, M., Bell, J. F., Maki, J. N., et al. (2021). Pre-flight calibration of the Mars 2020 rover Mastcam zoom (Mastcam-Z) multispectral, stereoscopic imager. *Space Science Reviews*, 217(2), 29. <https://doi.org/10.1007/s11214-021-00795-x>
- Hecht, M., Hoffman, J., Rapp, D., McClean, J., SooHoo, J., Schaefer, R., et al. (2021). Mars oxygen ISRU experiment (MOXIE). *Space Science Reviews*, 217(1), 9. <https://doi.org/10.1007/s11214-020-00782-8>
- Herkenhoff, K. E., Sullivan, R. J., Newman, C. E., Paar, G., Baker, M., Viúdez-Moreiras, D., et al. (2023). Comparison of ventifact orientations and recent wind direction indicators on the floor of Jezero Crater, Mars. *Journal of Geophysical Research: Planets*, 128(3), e2022JE007599. <https://doi.org/10.1029/2022JE007599>
- Holm-Alwmark, S., Kinch, K. M., Hansen, M. D., Shahrzad, S., Svennevig, K., Abbey, W. J., et al. (2021). Stratigraphic relationships in Jezero Crater, Mars: Constraints on the timing of fluvial-lacustrine activity from orbital observations. *Journal of Geophysical Research: Planets*, 126(7), e2021JE006840. <https://doi.org/10.1029/2021JE006840>

- Horgan, B., Rice, M., Garczynski, B., Johnson, J., StackMorgan, K., Vaughan, A., et al. (2022). Mineralogy, morphology, and geochronological significance of the Mááz formation and the Jezero crater floor. In *Proceedings of the 53rd lunar and planetary science conference (LPSC)*. Lunar and Planetary Institute, United States of America.
- Horgan, B. H. N., Anderson, R. B., Dromart, G., Amador, E. S., & Rice, M. S. (2020). The mineral diversity of Jezero crater: Evidence for possible lacustrine carbonates on Mars. *Icarus*, 339, 113526. <https://doi.org/10.1016/j.icarus.2019.113526>
- Hueso, R., Newman, C. E., del Río-Gaztelurrutia, T., Munguira, A., Sánchez-Lavega, A., Toledo, D., et al. (2023). Convective vortices and dust devils detected and characterized by Mars 2020. *Journal of Geophysical Research: Planets*, 128(2), e2022JE007516. <https://doi.org/10.1029/2022JE007516>
- Hundal, C. B., Mustard, J. F., Kremer, C. H., Tarnas, J. D., & Pascuzzo, A. C. (2022). The circum-isisidus capping unit: An extensive regional ashfall deposit exposed in Jezero Crater. *Geophysical Research Letters*, 49(9), e2021GL096920. <https://doi.org/10.1029/2021GL096920>
- Ivanov, M. A., Hiesinger, H., Erkeling, G., Hielscher, F. J., & Reiss, D. (2012). Major episodes of geologic history of Isidis Planitia on Mars. *Icarus*, 218(1), 24–46. <https://doi.org/10.1016/j.icarus.2011.11.029>
- Kremer, C. H., Mustard, J. F., & Bramble, M. S. (2019). A widespread olivine-rich ash deposit on Mars. *Geology*, 47(7), 677–681. <https://doi.org/10.1130/G45563.1>
- Kronyak, R. E., Kah, L. C., Edgett, K. S., Van Bommel, S. J., Thompson, L. M., Wiens, R. C., et al. (2019). Mineral-filled fractures as indicators of multigenerational fluid flow in the Pahrump hills member of the Murray formation, Gale crater, Mars. *Earth and Space Science*, 6(2), 238–265. <https://doi.org/10.1029/2018EA000482>
- Lange, R., Walker, L., Lenda, M., Morantz, C., Zorn, T., Alibay, F., et al. (2022). Mars 2020 perseverance rover surface operations commissioning phase overview. In *2022 IEEE aerospace conference (AERO)* (pp. 1–20). <https://doi.org/10.1109/AERO53065.2022.9843314>
- Lemmon, M. T., Lorenz, R. D., Rabinovitch, J., Newman, C. E., Williams, N. R., Sullivan, R., et al. (2023). Dust, sand, and winds within an active Martian storm in Jezero Crater. *Journal of Geophysical Research: Planets*, 127(12), e2022GL100126. <https://doi.org/10.1029/2022JE007605>
- Liu, Y., Tice, M. M., Schmidt, M. E., Treiman, A. H., Kizovski, T. V., Hurowitz, J. A., et al. (2022). An olivine cumulate outcrop on the floor of Jezero crater, Mars. *Science*, 377(6614), 1513–1519. <https://doi.org/10.1126/science.aba2756>
- Maki, J. N. (2020a). Mars 2020 cache Cameras bundle, calibrated products [Dataset]. NASA Planetary Data System. <https://doi.org/10.17189/47kr-ta40>
- Maki, J. N. (2020b). Mars 2020 Hazard Cameras bundle, mosaic products [Dataset]. NASA Planetary Data System. <https://doi.org/10.17189/w93h-5w52>
- Maki, J. N. (2020c). Mars 2020 navigation Cameras bundle, mosaic products [Dataset]. NASA Planetary Data System. <https://doi.org/10.17189/0sxn-zb41>
- Maki, J. N., Gruel, D., McKinney, C., Ravine, M. A., Morales, M., Lee, D., et al. (2020). The Mars 2020 engineering Cameras and microphone on the perseverance rover: A next-generation imaging system for Mars exploration. *Space Science Reviews*, 216(8), 137. <https://doi.org/10.1007/s11214-020-00765-9>
- Mandon, L., Quantin-Nataf, C., Royer, C., Beck, P., Fouchet, T., Johnson, J. R., et al. (2023). Reflectance of Jezero crater floor: 2. Mineralogical interpretation. *Journal of Geophysical Research: Planets*, e2022JE007450. <https://doi.org/10.1029/2022JE007450>
- Mandon, L., Quantin-Nataf, C., Thollot, P., Mangold, N., Lozac'h, L., Dromart, G., et al. (2020). Refining the age, emplacement and alteration scenarios of the olivine-rich unit in the Nili Fossae region, Mars. *Icarus*, 336, 113436. <https://doi.org/10.1016/j.icarus.2019.113436>
- Mangold, N., Dromart, G., Ansan, V., Salese, F., Kleinhans, M. G., Massé, M., et al. (2020). Fluvial regimes, morphology, and age of Jezero crater paleolake inlet valleys and their exobiological significance for the 2020 Rover Mission Landing Site. *Astrobiology*, 20(8), 994–1013. <https://doi.org/10.1089/ast.2019.2132>
- Mangold, N., Gupta, S., Gasnault, O., Dromart, G., Tarnas, J. D., Sholes, S. F., et al. (2021). Perseverance rover reveals an ancient delta-lake system and flood deposits at Jezero crater, Mars. *Science*, 374(6568), 711–717. <https://doi.org/10.1126/science.aba4051>
- Mangold, N., Poulet, F., Mustard, J. F., Bibring, J.-P., Gondet, B., Langevin, Y., et al. (2007). Mineralogy of the Nili Fossae region with OMEGA/Mars express data: 2. Aqueous alteration of the crust. *Journal of Geophysical Research*, 112(E8), E08S04. <https://doi.org/10.1029/2006JE002835>
- Maurice, S., Wiens, R. C., Bernardi, P., Caïs, P., Robinson, S., Nelson, T., et al. (2021). The SuperCam instrument suite on the Mars 2020 rover: Science objectives and mast-unit description. *Space Science Reviews*, 217(3), 47. <https://doi.org/10.1007/s11214-021-00807-w>
- McMahon, S., Bosak, T., Grotzinger, J. P., Milliken, R. E., Summons, R. E., Daye, M., et al. (2018). A field guide to finding fossils on Mars. *Journal of Geophysical Research: Planets*, 123(5), 1012–1040. <https://doi.org/10.1029/2017JE005478>
- Milkovich, S. M., Stack, K. M., Sun, V. Z., Maxwell, K., Kronyak, R., Schnadt, S. L., et al. (2022). Balancing predictive and reactive science planning for Mars 2020 perseverance. In *2022 IEEE aerospace conference (AERO)* (pp. 1–12). <https://doi.org/10.1109/AERO53065.2022.9843572>
- Moeller, R. C., Jandura, L., Rosette, K., Robinson, M., Samuels, J., Silverman, M., et al. (2020). The sampling and caching subsystem (SCS) for the scientific exploration of Jezero Crater by the Mars 2020 perseverance rover. *Space Science Reviews*, 217(1), 5. <https://doi.org/10.1007/s11214-020-00783-7>
- Mustard, J. F., Ehlmann, B. L., Murchie, S. L., Poulet, F., Mangold, N., Head, J. W., et al. (2009). Composition, morphology, and stratigraphy of Noachian crust around the Isidis basin. *Journal of Geophysical Research*, 114(E2), E00D12. <https://doi.org/10.1029/2009JE003349>
- Mustard, J. F., Poulet, F., Head, J. W., Mangold, N., Bibring, J.-P., Pelkey, S. M., et al. (2007). Mineralogy of the Nili Fossae region with OMEGA/Mars express data: 1. Ancient impact melt in the Isidis basin and implications for the transition from the Noachian to Hesperian. *Journal of Geophysical Research*, 112(E8), E08S03. <https://doi.org/10.1029/2006JE002834>
- Newman, C. E., de la Torre Juárez, M., Pla-García, J., Wilson, R. J., Lewis, S. R., Neary, L., et al. (2021). Multi-model meteorological and aeolian predictions for Mars 2020 and the Jezero Crater region. *Space Science Reviews*, 217(1), 20. <https://doi.org/10.1007/s11214-020-00788-2>
- Newman, C. E., Hueso, R., Lemmon, M. T., Munguira, A., Vicente-Retortillo, Á., Apestigue, V., et al. (2022). The dynamic atmospheric and aeolian environment of Jezero crater, Mars. *Science Advances*, 8(21), eabn3783. <https://doi.org/10.1126/sciadv.abn3783>
- Nimmo, F., & Tanaka, K. (2005). Early crustal evolution of Mars. *Annual Review of Earth and Planetary Sciences*, 33(1), 133–161. <https://doi.org/10.1146/annurev.earth.33.092203.122637>
- Pascuzzo, A. C., Mustard, J. F., Kremer, C. H., & Ebinger, E. (2019). The formation of irregular polygonal ridge networks, Nili Fossae, Mars: Implications for extensive subsurface channelized fluid flow in the Noachian. *Icarus*, 319, 852–868. <https://doi.org/10.1016/j.icarus.2018.10.020>
- Pieri, D. C. (1980). Martian valleys: Morphology, distribution, age, and origin. *Science*, 210(4472), 895–897. <https://doi.org/10.1126/science.210.4472.895>
- Quantin-Nataf, C., Holm-Alwmark, S., Lasue, J., Calef, F. J., Shuster, D., Kinch, K. M., et al. (2021). The complex exhumation history of Jezero Crater floor unit. In *52nd lunar and planetary science conference, held virtually, 15–19 March, 2021. LPI contribution no. 2548*.
- Ravanis, E., Fagents, S., Newman, C., Brown, A., Holm-Alwmark, S., Horgan, B., & Zorzano, M.-P. (2022). Evaluating the role of pyroclastic fall processes in the origin of the Nili Fossae olivine-bearing unit on Mars from ash dispersal modeling. In *Presented at the 44th COSPAR scientific assembly. Held 16–24 July* (Vol. 44, p. 389)



- Razzell Hollis, J., Moore, K. R., Sharma, S., Beegle, L., Grotzinger, J. P., Allwood, A., et al. (2022). The power of paired proximity science observations: Co-Located data from SHERLOC and PIXL on Mars. *Icarus*, 387, 115179. <https://doi.org/10.1016/j.icarus.2022.115179>
- Rice, M. S., Johnson, J. R., Million, C. C., St. Clair, M., Horgan, B. N., Vaughan, A., et al. (2023). Spectral variability of rocks and soils on the Jezero crater floor: A summary of multispectral observations from Perseverance's mastcam-Z instrument. *Journal of Geophysical Research: Planets*, e2022JE007548. <https://doi.org/10.1029/2022JE007548>
- Rodriguez-Manfredi, J. A., de la Torre Juárez, M., Alonso, A., Apéstigue, V., Arruero, I., Atienza, T., et al. (2021). The Mars environmental dynamics analyzer, MEDA. A suite of environmental sensors for the Mars 2020 mission. *Space Science Reviews*, 217(3), 48. <https://doi.org/10.1007/s11214-021-00816-9>
- Rogers, A. D., Warner, N. H., Golombek, M. P., Head, J. W., III, & Cowart, J. C. (2018). Areally extensive surface bedrock exposures on Mars: Many are clastic rocks, not lavas. *Geophysical Research Letters*, 45(4), 1767–1777. <https://doi.org/10.1002/2018GL077030>
- Ruff, S. W., Hamilton, V. E., Rogers, A. D., Edwards, C. S., & Horgan, B. H. N. (2022). Olivine and carbonate-rich bedrock in Gusev crater and the Nili Fossae region of Mars may be altered ignimbrite deposits. *Icarus*, 380, 114974. <https://doi.org/10.1016/j.icarus.2022.114974>
- Salese, F., Kleinhans, M. G., Mangold, N., Ansan, V., McMahon, W., de Haas, T., & Dromart, G. (2020). Estimated minimum life span of the Jezero fluvial delta (Mars). *Astrobiology*, 20(8), 977–993. <https://doi.org/10.1089/ast.2020.2228>
- Salvatore, M. R., Goudge, T. A., Bramble, M. S., Edwards, C. S., Bandfield, J. L., Amador, E. S., et al. (2018). Bulk mineralogy of the NE Syrtis and Jezero crater regions of Mars derived through thermal infrared spectral analyses. *Icarus*, 301, 76–96. <https://doi.org/10.1016/j.icarus.2017.09.019>
- Saper, L., & Mustard, J. F. (2013). Extensive linear ridge networks in Nili Fossae and Nilosyrtis, Mars: Implications for fluid flow in the ancient crust. *Geophysical Research Letters*, 40(2), 245–249. <https://doi.org/10.1002/grl.50106>
- Scheller, E. L., & Ehlmann, B. L. (2020). Composition, stratigraphy, and geological history of the Noachian basement surrounding the Isidis impact basin. *Journal of Geophysical Research: Planets*, 125(7), e2019JE006190. <https://doi.org/10.1029/2019JE006190>
- Scheller, E. L., Hollis, J. R., Cardarelli, E. L., Steele, A., Beegle, L. W., Bhartia, R., et al. (2022). First-results from the Perseverance SHERLOC investigation: Aqueous alteration processes and implications for organic geochemistry in Jezero crater, Mars. In *Proceedings of the 53rd lunar and planetary science conference (LPSC)*. Lunar and Planetary Institute.
- Schmidt, M., Allwood, A., Clark, B., Elam, W., Heirwegh, C., & Henley, T. (2021). Naltsos Abstract for Fall AGU 2021.v2.docx. Retrieved from <https://evsserver1.jpl.nasa.gov/EnterpriseVault/Search/htmlview.aspx?VaultId=13EE8A0F7D1720843BBFF8ABD57AD6F64110000evsserver1&SaveSetId=202201212763380~202107211725160000~Z~7099C9D740389A3D458D7270499E10A1&AttachmentId=1>
- Schon, S. C., Head, J. W., & Fassett, C. I. (2012). An overfilled lacustrine system and progradational delta in Jezero crater, Mars: Implications for Noachian climate. *Planetary and Space Science*, 67(1), 28–45. <https://doi.org/10.1016/j.pss.2012.02.003>
- Schultz, R. A., & Frey, H. V. (1990). A new survey of multiring impact basins on Mars. *Journal of Geophysical Research*, 95(B9), 14175–14189. <https://doi.org/10.1029/JB095iB09p14175>
- Scott, D. H., & Carr, M. H. (1978). *Geologic map of Mars*. IMAP. <https://doi.org/10.3133/i1083>
- Shahrazad, S., Kinch, K. M., Goudge, T. A., Fassett, C. I., Needham, D. H., Quantin-Nataf, C., & Knudsen, C. P. (2019). Crater statistics on the dark-toned, mafic floor unit in Jezero Crater, Mars. *Geophysical Research Letters*, 46(5), 2408–2416. <https://doi.org/10.1029/2018GL081402>
- Sharma, S., Murphy, A., Beegle, L. W., Bhartia, R., Steele, A., Hollis, J. R., et al. (2022). Mapping organic-mineral associations in Jezero crater. In *Presented at the AGU fall conference, chicago, IL*. Retrieved from <https://ntrs.nasa.gov/citations/20220011715>
- Simon, J. I., Hickman-Lewis, K., Cohen, B. A., Mayhew, L. E., Shuster, D. L., Debaille, V., et al. (2023). Samples collected from the floor of Jezero Crater with the Mars 2020 perseverance rover. *Journal of Geophysical Research: Planets*, e2022JE007474. <https://doi.org/10.1029/2022JE007474>
- Squyres, S. W., Grotzinger, J. P., Arvidson, R. E., Bell, J. F., Calvin, W., Christensen, P. R., et al. (2004). In situ evidence for an ancient aqueous environment at Meridiani Planum, Mars. *Science*, 306(5702), 1709–1714. <https://doi.org/10.1126/science.1104559>
- Squyres, S. W., & Kasting, J. F. (1994). Early Mars: How warm and how wet? *Science*, 265(5173), 744–749. <https://doi.org/10.1126/science.265.5173.744>
- Stack, K. M., Williams, N. R., Calef, F., Sun, V. Z., Williford, K. H., Farley, K. A., et al. (2020). Photogeologic map of the perseverance rover field site in Jezero Crater constructed by the Mars 2020 science team. *Space Science Reviews*, 216(8), 127. <https://doi.org/10.1007/s11214-020-00739-x>
- Sullivan, R., Baker, M., Golombek, M., Herkenhoff, K., Newman, C., & Tate, C. (2022). Enigmatic large bedforms on the floor of Jezero crater. In *53rd lunar and planetary science conference, abstract 2887*.
- Sun, V. Z., & Stack, K. M. (2020). Geologic map of Jezero crater and the Nili Planum region, Mars (USGS numbered series no. 3464). In *Geologic map of Jezero Crater and the Nili Planum region, Mars* (Vol. 3464). U.S. Geological Survey. <https://doi.org/10.3133/sim3464>
- Sun, V. Z., Stack, K. M., Kah, L. C., Thompson, L., Fischer, W., Williams, A. J., et al. (2019). Late-stage diagenetic concretions in the Murray formation, Gale crater, Mars. *Icarus*, 321, 866–890. <https://doi.org/10.1016/j.icarus.2018.12.030>
- Tice, M. M., Hurowitz, J. A., Allwood, A. C., Jones, M. W. M., Orenstein, B. J., Davidoff, S., et al. (2022). Alteration history of Séítah formation rocks inferred by PIXL X-ray fluorescence, X-ray diffraction, and multispectral imaging on Mars. *Science Advances*, 8(47), eabp9084. <https://doi.org/10.1126/sciadv.abp9084>
- Tornabene, L. L., Moersch, J. E., McSween, H. Y., Hamilton, V. E., Piatek, J. L., & Christensen, P. R. (2008). Surface and crater-exposed lithologic units of the Isidis Basin as mapped by coanalysis of THEMIS and TES derived data products. *Journal of Geophysical Research*, 113(E10), E10001. <https://doi.org/10.1029/2007JE002988>
- Udry, A., Ostwald, A., Sautter, V., Cousin, A., Beyssac, O., Forni, O., et al. (2023). A Mars 2020 perseverance SuperCam perspective on the igneous nature of the Mááz formation at Jezero crater and link with Séítah, Mars. *Journal of Geophysical Research: Planets*, e2022JE007440. <https://doi.org/10.1029/2022JE007440>
- Vasavada, A. R., Grotzinger, J. P., Arvidson, R. E., Calef, F. J., Crisp, J. A., Gupta, S., et al. (2014). Overview of the Mars science laboratory mission: Bradbury landing to Yellowknife Bay and beyond. *Journal of Geophysical Research: Planets*, 119(6), 1134–1161. <https://doi.org/10.1002/2014JE004622>
- Vaughan, A., Minitti, M. E., Cardarelli, E. L., Johnson, J. R., Kah, L. C., Pilleri, P., et al. (2023). Regolith of the Crater Floor units, Jezero Crater, Mars: Textures, composition, and implications for provenance. *Journal of Geophysical Research: Planets*, 128(3), e2022JE007437. <https://doi.org/10.1029/2022JE007437>
- Verma, V., Hartman, F., Rankin, A., Maimone, M., Del Sesto, T., Toupet, O., et al. (2022). First 210 solar days of Mars 2020 perseverance robotic operations—Mobility, robotic arm, sampling, and helicopter. In *2022 IEEE Aerospace Conference (AERO)* (pp. 1–20). <https://doi.org/10.1109/AERO53065.2022.9843204>
- Vicente-Retortillo, A., Lemmon, M. T., Martinez, G. M., Toledo, D., Apestigue, V., Arruero, I., et al. (2023). Dust accumulation from MEDA measurements at Jezero crater, Mars. In *54th lunar and planetary science conference, abstract 1969*.

- Werner, S. C. (2009). The global Martian volcanic evolutionary history. *Icarus*, *201*(1), 44–68. <https://doi.org/10.1016/j.icarus.2008.12.019>
- Wiens, R. C., Maurice, S., Robinson, S. H., Nelson, A. E., Cais, P., Bernardi, P., et al. (2020). The SuperCam instrument suite on the NASA Mars 2020 rover: Body unit and combined system tests. *Space Science Reviews*, *217*(1), 4. <https://doi.org/10.1007/s11214-020-00777-5>
- Wiens, R. C., & Maurice, S. A. (2021). Mars 2020 SuperCam bundle [Dataset]. NASA Planetary Data System. <https://doi.org/10.17189/1522646>
- Wiens, R. C., Udry, A., Beyssac, O., Quantin-Nataf, C., Mangold, N., Cousin, A., et al. (2022). Compositionally and density stratified igneous terrain in Jezero crater, Mars. *Science Advances*, *8*(34), eabo3399. <https://doi.org/10.1126/sciadv.abo3399>
- Yingst, R. A., Berger, J., Cohen, B. A., Hynes, B., & Schmidt, M. E. (2017). Determining best practices in reconnoitering sites for habitability potential on Mars using a semi-autonomous rover: A GeoHeuristic operational strategies test. *Acta Astronautica*, *132*, 268–281. <https://doi.org/10.1016/j.actaastro.2016.12.018>

## References From the Supporting Information

- Paar, G., Ortner, T., Tate, C., Deen, R. G., Abercrombie, P., Vona, M., et al. (2023). Three-dimensional data preparation and immersive mission-spanning visualization and analysis of Mars 2020 Mastcam-Z stereo image sequences. *Earth and Space Science*, *10*(3), e2022EA002532. <https://doi.org/10.1029/2022EA002532>
- Pla-García, J., Rafkin, S. C. R., Martínez, G. M., Vicente-Retortillo, Á., Newman, C. E., Savijärvi, H., et al. (2020). Meteorological predictions for Mars 2020 perseverance rover landing site at Jezero Crater. *Space Science Reviews*, *216*(8), 148. <https://doi.org/10.1007/s11214-020-00763-x>
- Steele, A., Benning, L. G., Wirth, R., Schreiber, A., Araki, T., McCubbin, F. M., et al. (2022). Organic synthesis associated with serpentinization and carbonation on early Mars. *Science*, *375*(6577), 172–177. <https://doi.org/10.1126/science.abg7905>